

9-15-2011

Effect of Storm Enhanced Densities on Geo-Location Accuracy Over CONUS

Lindon H. Steadman

Follow this and additional works at: <https://scholar.afit.edu/etd>

Part of the [Atmospheric Sciences Commons](#), and the [Engineering Physics Commons](#)

Recommended Citation

Steadman, Lindon H., "Effect of Storm Enhanced Densities on Geo-Location Accuracy Over CONUS" (2011). *Theses and Dissertations*. 1474.
<https://scholar.afit.edu/etd/1474>

This Thesis is brought to you for free and open access by the Student Graduate Works at AFIT Scholar. It has been accepted for inclusion in Theses and Dissertations by an authorized administrator of AFIT Scholar. For more information, please contact richard.mansfield@afit.edu.



**EFFECTS OF STORM ENHANCED
DENSITIES ON GEO-LOCATION
ACCURACY OVER CONUS**

THESIS

Lindon H. Steadman, Captain, USAF
AFIT/GAP/ENP/11-S03

**DEPARTMENT OF THE AIR FORCE
AIR UNIVERSITY**

AIR FORCE INSTITUTE OF TECHNOLOGY

Wright-Patterson Air Force Base, Ohio

DISTRIBUTION STATEMENT A
APPROVED FOR PUBLIC RELEASE; DISTRIBUTION UNLIMITED.

The views expressed in this thesis are those of the author and do not reflect the official policy or position of the United States Air Force, Department of Defense, or the United States Government. This material is declared a work of the U.S. Government and is not subject to copyright protection in the United States.

AFIT/GAP/ENP/11-S03

EFFECTS OF STORM ENHANCED DENSITIES ON GEO-LOCATION
ACCURACY OVER CONUS

THESIS

Presented to the Faculty
Department of Engineering Physics
Graduate School of Engineering and Management
Air Force Institute of Technology
Air University
Air Education and Training Command
in Partial Fulfillment of the Requirements for the
Degree of Master of Science in Applied Physics

Lindon H. Steadman, BS
Captain, USAF

September 2011

DISTRIBUTION STATEMENT A
APPROVED FOR PUBLIC RELEASE; DISTRIBUTION UNLIMITED.

EFFECTS OF STORM ENHANCED DENSITIES ON GEO-LOCATION
ACCURACY OVER CONUS

Lindon H. Steadman, BS
Captain, USAF

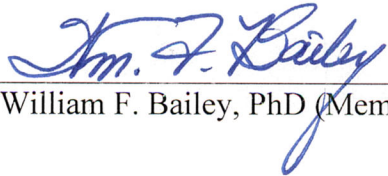
Approved:



Lt Col Ariel O. Acebal (Chairman)

26 JUL 2011

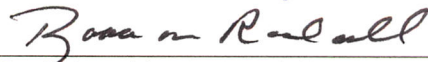
Date



William F. Bailey, PhD (Member)

26 July 2011

Date



Lt Col Robb M. Randall (Member)

26 Jul 2011

Date

Abstract

Storm enhanced densities (SEDs) are ionospheric plasma enhancements that disrupt radio communications in the near-Earth space environment, degrading the Global Positioning System (GPS) and other key technologies. Accurate GPS/total electron content (TEC) correction maps produced by ionosphere models can mitigate degradations from SEDs. An artificial SED was created and ingested via slant TEC measurements into the Global Assimilation of Ionospheric Measurements Gauss-Markov Kalman Filter Model to determine how many ground GPS receivers are needed to produce reliable GPS/TEC correction maps over the continental United States during geomagnetic storming. It was found that 110 well-positioned GPS receivers produced the best overall TEC accuracy, although significantly improved accuracy was still achieved if 40 or more receivers were used. Furthermore, receiver positioning had a greater impact on TEC accuracy than the number of receivers used. It was also found that TEC accuracy for the SED region increased at the expense of TEC accuracy everywhere else on the map.

Acknowledgements

First, I am very grateful to God for blessing me with the opportunity to serve my country and giving me the ability to complete this challenging project.

Next I would like to thank my wife for motivating and supporting me, and for essentially raising our children by herself while I was neck-deep in this research. She definitely deserves 21 months of her life back.

I would also like to thank my research advisor, Lt Col Ariel Acebal, for his high expectations and great example as an officer. I don't think anyone could have taught me Space Weather better than he did. His mentorship has helped me to become both a better student and leader.

Likewise I extend thanks to my thesis committee members, Dr. William Bailey, and Lt Col Robb Randall, as well as to the amazingly smart scientists at Utah State University: Drs. Robert Schunk, Larry Gardner, Ludger Scherliess and Lie Zhu. Their guidance, insight, and willingness to help at a moment's notice were invaluable. Additionally I would like to thank Dr. Don Thompson for sharing his technical expertise and donating much personal time to help get this project underway.

I also want to thank my classmates who helped me along the way: Captains Ken Fenton, Janelle Jenniges, Omar Nava, and Lt Paul Domm. In the words of a Quaker proverb, "Thee lift me, and me lift thee, and together we'll ascend to heaven."

Lastly I express gratitude to my parents for their continual encouragement and support, and for treating my successes as if they were there own.

Lindon H. Steadman

Table of Contents

	Page
Abstract	iv
Acknowledgements	v
List of Figures	viii
List of Tables	xi
I. Introduction	1
1.1 Motivation and Background	1
1.2 Research Objective	3
1.3 Document Structure	3
II. Background	4
2.1 Chapter Overview	4
2.2 The Ionosphere	4
2.3 Geomagnetic Storms	7
2.4 Storm Enhanced Density (SED)	10
2.5 GAIM-GM Kalman Filter Model	13
2.5.1 Ionospheric Forecast Model (IFM)	14
2.5.2 GAIM-GM Output and Resolution	16
2.5.3 Gauss-Markov Kalman Filter	16
2.5.4 Assimilation of GPS Slant TEC	18
III. Methodology	21
3.1 Chapter Overview	21
3.2 IFM Density Backgrounds	21
3.3 Modeling the SED	23
3.4 Creating GPS Ground Station Distributions	29
3.5 Taking Slant TEC Measurements	33
3.6 Running GAIM-GM	37
3.7 Analysis Techniques	40
3.8 Data Visualization	43
IV. Results and Analysis	45
4.1 Chapter Overview	45
4.2 Baseline Run with Zero GPS Ground Stations	45
4.3 Case 1: Normal GAIM-GM and CORS Grids	46
4.4 Case 2: Modified GAIM-GM and CORS Grids	53

	Page
4.5 Case 3: Modified GAIM-GM and Ideal Grids	57
4.6 Case 4: High-Altitude SED	60
4.7 Case 5: Reduced Time Constant	64
4.8 Case 6: Simulated Bad Data at One Station	66
4.9 Case 7: Reversed Ideal 21 Grid	70
4.10 Case 8: Normal GAIM-GM with Depleted IFM	72
4.11 Case 9: Reduced Time Constant with Depleted IFM	76
4.12 Case 10: Elevation Mask Raised to 45°	77
V. Conclusions and Recommendations	81
5.1 Chapter Overview	81
5.2 Conclusions	81
5.3 Recommendations for Future Work	85
Appendix A. The Global Positioning System (GPS)	87
Appendix B. AFWA 12th Station	91
Appendix C. Slant TEC Assimilation Per Time Step in GAIM-GM	94
Bibliography	96
Vita	99

List of Figures

Figure		Page
1.	Chapman layer	5
2.	Vertical profile of the ionosphere	6
3.	Geomagnetic storm a_p and Dst profiles	9
4.	SAPS electric field	11
5.	SED plume during the 31 March 2001 geomagnetic storm	12
6.	GAIM-GM data sources	14
7.	IFM TEC and electron density	15
8.	GAIM-GM resolutions for global and regional output	17
9.	Plasmasphere contribution to slant TEC	20
10.	IFM TEC for $K_p = 1$ and $K_p = 6$	23
11.	IFM interpolation to GAIM-GM resolution	25
12.	20 November 2003 SED	26
13.	GAIM-GM recreation of the 20 November 2003 SED	26
14.	Synthetic SED profile in the IFM	27
15.	Synthetic SED trajectory	28
16.	CORS grids	31
17.	Station density for the AFWA+400 grid	32
18.	Ideal grids	33
19.	Vertical TEC measurement errors	36
20.	GAIM-GM model run flowchart	39
21.	GAIM-GM with zero data assimilation vs. the IFM	47
22.	Case 1: GAIM-GM TEC	48

Figure	Page
23.	Case 1: GAIM-GM electron density vertical profiles 49
24.	Case 1: GAIM-GM minus IFM TEC difference 50
25.	Case 1: Skill score map for the AFWA+30 grid 51
26.	Case 1: Skill score graphs for the SED period 52
27.	Case 2: GAIM-GM TEC 54
28.	Case 2: GAIM-GM minus IFM TEC difference 55
29.	Case 2: Skill score graphs for the SED period 56
30.	Case 3: GAIM-GM TEC 59
31.	Case 3: GAIM-GM minus IFM TEC difference 60
32.	Case 3: Skill score graphs for the SED period 61
33.	Case 5: Electron density difference 63
34.	Case 4: High altitude SED vertical profile 64
35.	Case 5: Reduced Time Constant TEC difference 65
36.	Case 5: Skill score graph for the SED period 66
37.	Case 6: TEC difference from one bad station 68
38.	Case 6: Skill score graph for the SED period 68
39.	Case 6: Skill score maps for the AFWA+100 grid 69
40.	Case 7: GAIM-GM TEC 71
41.	Case 7: Skill score graph for the SED period 71
42.	Case 8: GAIM-GM TEC 73
43.	Case 8: Electron density vertical profiles 74
44.	Case 8: Skill score graph for the SED period 75
45.	Case 9: TEC difference from changing the Time Constant 77
46.	Case 10: GAIM-GM TEC and electron density profile 79

Figure		Page
47.	Skill score summary	82
48.	GPS satellite orbital tracks	88
49.	CORS network	89
50.	Real SED in GAIM-GM vs. synthetic SED in the IFM	92
51.	TEC differences due to the 12th AFWA station	93
52.	Slant TEC paths using the AFWA grid	94

List of Tables

Table		Page
1.	SED properties	10
2.	IFM input parameters	22
3.	IFM and GAIM-GM resolution	24
4.	Synthetic vs. real SED properties	28
5.	AFWA GPS stations	30
6.	Distance between GPS ground stations	34
7.	Slant TEC uncertainty	37
8.	Complete list of GAIM-GM runs	44
9.	Case 1 skill scores	53
10.	Case 2 skill scores	57
11.	Case 3 skill scores	60
12.	Case 5 skill scores	66
13.	Case 6 skill scores	70
14.	Case 7 skill scores	72
15.	Case 8 skill scores	76
16.	Case 9 MAE	77
17.	Case 10 MAE	78
18.	Slant TEC assimilation for 45° and 15° Elevation Masks	80
19.	Slant TEC equation constants	90
20.	Slant TEC assimilation totals per station distribution	95

EFFECTS OF STORM ENHANCED DENSITIES ON GEO-LOCATION ACCURACY OVER CONUS

I. Introduction

1.1 Motivation and Background

In recent years society has greatly benefitted from advances in spaced-based communication and navigation technology. Civilian, military, and government institutions alike have thrived on the conveniences offered by these systems and have come to rely on them daily. The Global Positioning System (GPS) is one such modern convenience that has brought enormous improvements to navigation and geo-location since its creation in the late 1970's.

As with other platforms that dwell in the near-Earth environment, GPS satellites broadcast signals to Earth via electromagnetic transmissions that must pass through a deep atmospheric layer known as the ionosphere. The ionosphere is the layer of the Earth's atmosphere consisting of free thermal electrons and ions, as well as some neutral species. It extends from about 50 – 1500 *km* and then transitions into the plasmasphere (*Schunk and Nagy, 2009*). Several regions exist within the ionosphere, the characteristics of which are highly dependent on time of day, season, solar cycle, geographic location, and geomagnetic activity.

The ionosphere has significant spatial and temporal variations that can enhance, degrade, or completely disrupt electromagnetic transmissions. Because of society's increased dependence on GPS and other systems that employ electromagnetic propagation through the ionosphere, the need for accurate ionospheric forecasts has also

increased. Reliable space weather forecasts can help mitigate degradation to important military, government, and civil platforms caused by ionospheric disturbances.

Geomagnetic storming typically causes large disturbances in the ionosphere that may last for several days (*Prolss, 2004*). Although the most active periods of geomagnetic storming occur during the peak of the 11-year solar cycle, storming can happen at solar minimum as well due to solar phenomena like coronal mass ejections (CMEs) and corotating interactive regions (*Schunk and Nagy, 2009*).

Regions of increased plasma density known as storm enhanced densities (SEDs) are regularly observed during geomagnetic storms and can seriously degrade geolocation accuracy by interfering with GPS signals. One system prone to geo-location disruption due to SEDs is the Federal Aviation Administration's Wide Area Augmentation System (WAAS). This air navigation aid augments GPS accuracy and enables precision approaches to any airport within its coverage area (*Federal Aviation Administration, 2011*). For example, a halo CME on 3 April 2010 and ensuing geomagnetic storm caused especially poor satellite tracking at several WAAS sites in Alaska, resulting in a 34-minute Precision Approach service outage (*Rosen, 2010*). Such outages could prove dangerous for major airports during hours of heavy air traffic.

Ionosphere models reduce the effects of geomagnetic storming on geolocation accuracy by providing GPS/Total Electron Content (TEC) correction maps, enabling GPS receivers to correct for ionospheric enhancements that alter GPS signals. The model used operationally by the Air Force Weather Agency (AFWA) is the Global Assimilation of Ionosphere Measurements Gauss-Markov (GAIM-GM) Kalman Filter Model, developed by Dr. Robert Schunk and his team at Utah State University (USU). This model uses the physics-based Ionospheric Forecast Model (IFM) and data assimilation from a variety of sources to create accurate specifications of the ionosphere. By ingesting real observations of the ionosphere, GAIM-GM has been

shown to create TEC maps that significantly improve the comparison to independent TEC observations [(*Thompson et al.*, 2005) (*Scherliess et al.*, 2006), (*Zhu et al.*, 2006), (*Decker and McNamara*, 2007), (*Schunk et al.*, 2010)].

1.2 Research Objective

The objective of this research is to determine how many ground GPS receivers (i.e. ground stations) are needed in the continental United States (CONUS) in order to have reliable GPS/TEC correction maps during geomagnetic storming. This is done by imposing an artificial SED on an electron density background and then taking slant TEC measurements through that background via simulated GPS satellites and several different distributions of GPS ground stations. GAIM-GM ingests these data and produces TEC maps that differ in accuracy according to the number of GPS ground stations used. By varying the number of available ground stations and comparing the model output, a clearer picture emerges of how many ground GPS receivers are needed for reliable TEC maps.

1.3 Document Structure

This document is organized into five chapters. Chapter II provides background information on the ionosphere and SEDs caused by geomagnetic storming. It also gives an overview of the GAIM-GM model. Chapter III explains the methodology used to conduct this research and outlines the selection of model parameters, designing the synthetic SED, piercing the SED with slant TEC measurements, running GAIM-GM, and data comparison techniques. Chapter IV presents the results of assimilating slant TEC data into GAIM-GM for varying GPS ground station distributions and gives skill score analyses. A summary of the results, final conclusions, and recommendations for future work are given lastly in Chapter V.

II. Background

2.1 Chapter Overview

This chapter provides background information on the ionosphere and geomagnetic storms, and details how these storms impact the GPS. The basic structure of the ionosphere and the processes by which it is formed are described, followed by an overview of ionospheric disturbances known as SEDs and their effects on human activity. The two ionosphere models used in this research are also described, namely, the IFM and the GAIM-GM Kalman Filter Model.

2.2 The Ionosphere

The ionosphere is the region of the Earth's atmosphere where there are enough free thermal electrons and ions to create a plasma dense enough to affect radio wave propagation. Some of these ions and free electrons are produced by high latitude particle precipitation but the majority result from photoionization of neutral species in the upper atmosphere (above 50 km) by solar and stellar irradiance in the extreme ultraviolet (EUV) and x-ray wavelength range.

The photoionization rate in Earth's atmosphere can be represented by the highly simplified Chapman production function:

$$P(z, \chi) = I(z, \chi)\eta\sigma^a n(z) \tag{1}$$

In this equation P is the *ion production rate*, I is the *photon flux* as a function of height z and *solar zenith angle* χ , η is the *probability of photon absorption* (resulting in the production of an electron-ion pair), σ^a is the *absorption cross-section*, and $n(z)$ is the *neutral species density* as a function of height (*Schunk and Nagy, 2009*).

Figure 1 illustrates the relationship between neutral density and solar irradiance in determining the height of maximum photoionization, known as a Chapman layer.

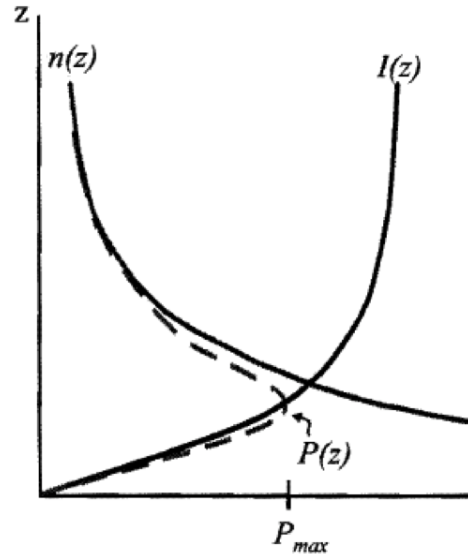


Figure 1. Chapman layer and ionization curve (dashed line). Decreasing neutral densities ($n(z)$) and increasing solar irradiance ($I(z)$) with altitude form an ionization peak known as a Chapman layer

As plasma is produced it gets transported throughout the atmosphere via different mechanisms such as electromagnetic forces, gravitational force, the pressure gradient, and collisions with neutral particles (*Ondoh and Marubashi, 2001*). Combined with ion/neutral production and loss processes through chemical reactions, several distinct layers of the ionosphere are formed: 1) the D region; 2) the E region; 3) the F region; and 4) the topside ionosphere, which transitions into the plasmasphere at about 1500 *km*. The vertical profile of these regions are illustrated in Figure 2, which also includes typical ion composition and electron density values for each region.

The lowest layer of the ionosphere, the D region, is found between 50 – 90 *km*. It is the most complex of all four regions and here ion production and loss are dominated by chemical processes occurring in the relatively dense neutral atmosphere.

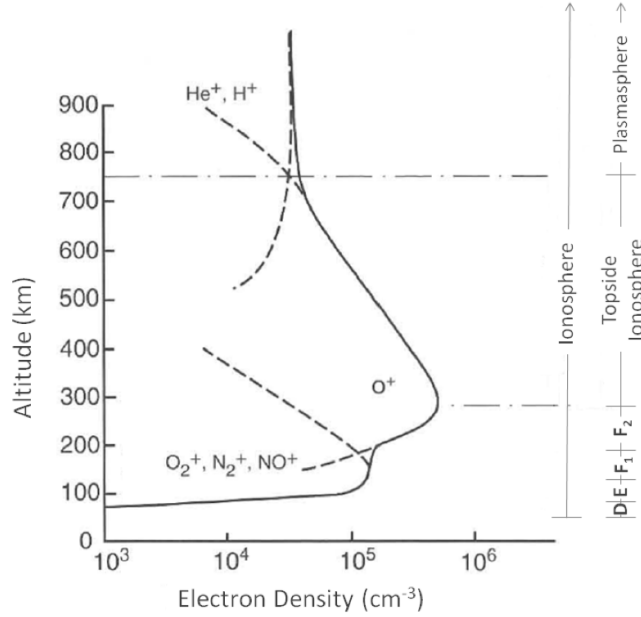


Figure 2. Vertical profile of the ionosphere. Densities consisting mainly of O^+ reach maximum values near the F_2 peak, seen at about 300 km in this figure. Additionally, a smaller peak consisting of several ion species is found in the E region near 130 km (Adapted from *Schunk and Nagy (2009)*)

Molecular ions are most abundant in this region and there also exist negative ions which contribute significantly to total plasma density. Above this layer, the E region spans from about $90 - 150\text{ km}$. Its dominant ions, NO^+ and O_2^+ , are formed from direct ionization of O_2 , as well as from chemical processes. High electron densities in this region do not occur because of an increased rate of ion recombination reactions.

Above the E region is the F region, which consists of three sub-regions: 1) F_1 region; 2) F_2 region; and 3) upper F region or topside ionosphere. Transport processes in the F region, some of which are very complex, are more dominant than those in the D and E regions and govern much of the ion production and loss. The F_1 region is found between approximately $150 - 250\text{ km}$. Plasma transport in the F_1 region leads to higher electron densities here than in lower regions and these densities continue to increase until peaking in the F_2 region. This region spans from about $250 - 600\text{ km}$ and contains the highest electron densities of the ionosphere. The F_2 peak can be

seen in Figure 2 near the 300 *km* height where electron densities approach 10^6 cm^{-3} . Above the F₂ region, the layer extending from about 600 – 1500 *km* is referred to as the topside ionosphere. The region of dominant H⁺ ions above the topside ionosphere is called the plasmasphere (or protonosphere) (*Schunk and Nagy, 2009*).

The ionosphere is often measured in terms of TEC where one TEC unit equals $10^{16} \text{ electrons/m}^2$. It represents the amount of free electrons present along a path between two points (typically the surface of the Earth and the top of the ionosphere). TEC analyses can easily be overlaid onto world or regional map projections, providing a fast way to visualize the ionosphere’s density. A more detailed explanation of how TEC can be derived using GPS satellites is given in Appendix 1.

All regions of the ionosphere are subject to variation as a function of latitude, longitude, universal time, season, solar cycle, and geomagnetic activity. As a result, the ionosphere is typically considered to have two states: a background or climatological state and a disturbed or storm state (*Schunk and Scherliess, 2004*). Both states can affect electromagnetic wave propagation, although the disturbed state tends to cause greater disruptions due to the effect of geomagnetic storming on plasma densities.

2.3 Geomagnetic Storms

Geomagnetic storms are events of strongly enhanced dissipation of solar wind energy into the near-Earth space environment. During these storms, the rate of energy transfer to the magnetosphere can be many times greater than the quiet condition energy transfer rate from the solar wind. The effects of this impulsive energy transfer – which usually lasts for 1 – 3 days – disturb the magnetosphere, thermosphere, ionosphere, auroral ovals, and the numerous current systems which couple these regions together (*Prolss, 2004*). Most periods of geomagnetic storming occur during solar maximum (i.e., the peak of the 11-year solar cycle), although

storms can happen during solar minimum as well (*Schunk and Nagy, 2009*).

Solar phenomena typically responsible for geomagnetic storming are CMEs and corotating interactive regions. A CME is the expulsion of a large amount ($10^{12} - 10^{13}$ kg) of gaseous solar mass into interplanetary space. These clouds of plasma are associated with strong magnetic fields that can be either northward (\mathbf{B}_z positive) or southward-oriented (\mathbf{B}_z negative). If the field is \mathbf{B}_z negative, reconnection with the Earth's northward-oriented magnetic field allows solar wind particles to more easily penetrate into the inner magnetosphere. CMEs with \mathbf{B}_z negative magnetic fields that reach Earth have been frequently associated with the onset of geomagnetic storms. In the case of corotating interactive regions, fast solar wind from a coronal hole interacts with the slower, surrounding solar wind and leads to compression of the interplanetary magnetic field (IMF). If the ambient IMF already possesses a \mathbf{B}_z negative component, it can be intensified to the point where a geomagnetic storm occurs as the region passes the Earth (*Prolss, 2004*).

There are generally three phases in a geomagnetic storm: 1) initial; 2) main; and 3) recovery. The initial phase begins with magnetospheric compression caused by a shock in the IMF (from a CME, etc.). During the main phase, energetic plasma from the magnetotail is injected into the inner magnetosphere, intensifying the ring current and inducing a magnetic field opposed to the Earth's own field at the surface – most notably at equatorial latitudes. This causes the Earth's magnetic field to weaken at the surface. The recovery phase entails a gradual return of the Earth's magnetic field to pre-storm levels. This can last up to several days while the enhanced ring current subsides and excess particles are lost through various mechanisms. Large storms can significantly modify the composition, density, and circulation of the ionosphere-plasmasphere system on a global scale. These changes can persist for several more days after the geomagnetic storming ceases (*Schunk and Nagy, 2009*).

A variety of geomagnetic indices have been devised to quantify variations in the Earth’s magnetic field and current systems during geomagnetic storms. Some commonly used indices are the K_p , a_p , and Dst indices. A typical fluctuation profile for some of these indices during a major geomagnetic storm is shown in Figure 3.

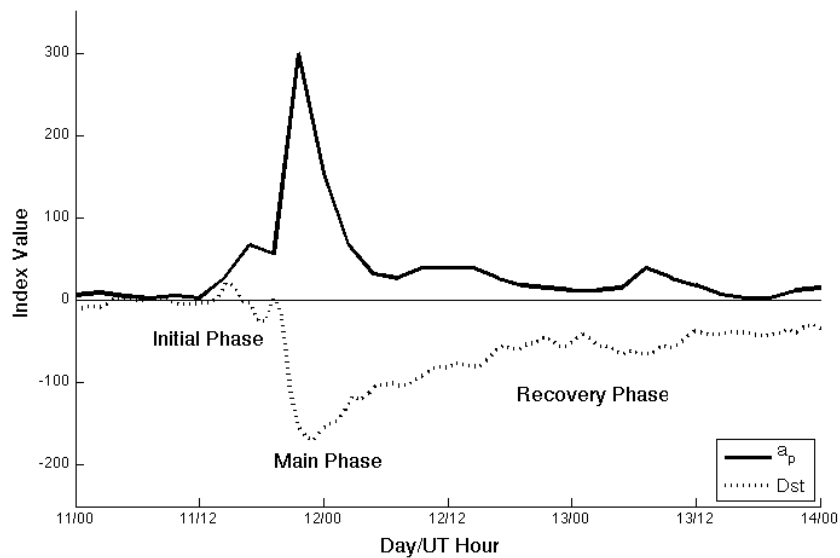


Figure 3. Profile of a_p and Dst indices during the 10 November 1986 geomagnetic storm. The linearly scaled, 3-hourly a_p index is simply a derivation of the quasi-logarithmic-scaled K_p index

The Dst index is given in nano teslas (nT) and indicates disturbances to the Earth’s magnetic field due to both ring current enhancements and increased solar wind pressure on the magnetosphere. The K_p and a_p indices are planetary measurements representing the strength the Earth’s magnetic field at the surface, relative to an assumed quiet-day curve. The K_p index uses a quasi-logarithmic scale while the a_p index is derived from the K_p index and uses a linear scale [(Perrone and De Franceschi, 1998), (National Geophysical Data Center, 2011)]. In Figure 3 both a_p and Dst indices increased during the initial storm phase, followed by a sharper increase in a_p and a simultaneous drop in Dst during the main phase. The recovery phase for this

storm lasted about two days as energetic particles which enhanced the ring current precipitated out of the magnetosphere and both indices returned to normal values.

2.4 Storm Enhanced Density (SED)

During the early stages of geomagnetic storms, regions of increased plasma density are regularly observed equatorward of the auroral oval in the pre-midnight ionosphere. These SEDs consist of ionization plumes of enhanced F region plasma where TEC can be two to four times greater than background TEC values (*Foster, 1993*). SEDs are prevalent over North America during high geomagnetic activity. A list of the defining SED characteristics and their values are presented in Table 1.

Table 1. SED properties

Property	Typical value	Source
Duration	2 – 5 hours	(<i>Coster et al., 2001</i>), (<i>Foster et al., 2004</i>)
Peak time	1730 – 2000 UT	(<i>Foster, 1993</i>), (<i>Coster et al., 2001</i>), (<i>Foster et al., 2005</i>), (<i>Foster et al., 2006</i>)
H_mF_2	> 500 km	(<i>Foster et al., 2005</i>)
Altitude extent	300 – 500 km	(<i>Foster, 1993</i>), (<i>Foster et al., 2004</i>)
Width	600 – 1000 km	(<i>Foster et al., 2004</i>), (<i>Kelley et al., 2004</i>)
Velocity	0.5 – 1 km/s	(<i>Foster, 1993</i>), (<i>Coster et al., 2001</i>), (<i>Foster et al., 2002</i>), (<i>Foster et al., 2005</i>)
N_mF_2	$1 - 3 \times 10^{12} m^{-3}$	(<i>Foster et al., 2004</i>), (<i>Foster et al., 2005</i>)
TEC increase	2 – 4 times	(<i>Foster, 1993</i>), (<i>Coster et al., 2001</i>)

Figure 4 illustrates the storm-time convection that sets up to form SEDs. The plasma found within SEDs actually originates in the sunlit equatorial ionosphere. Early in the geomagnetic storm a strong, eastward electric field at low latitudes drives plasma upward into the plasmasphere via an $\mathbf{E} \times \mathbf{B}$ drift so fast that it cannot dissociatively recombine with free electrons. From high altitudes it diffuses down geomagnetic field lines to lower-mid latitudes. At this point a poleward-oriented

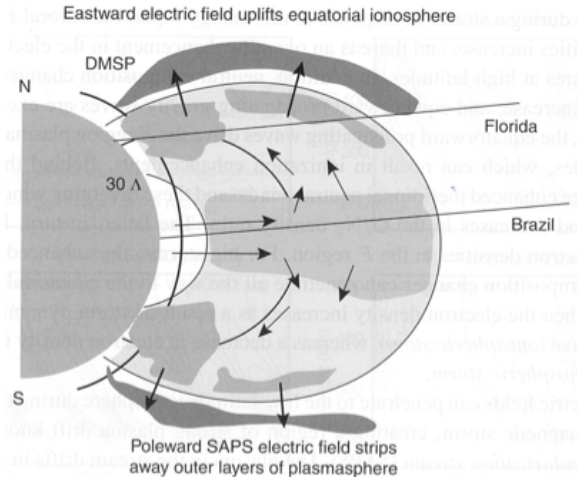


Figure 4. Plasma convection pattern during geomagnetic storming that leads to SED formation. Enhanced electric fields drive equatorial plasma (light grey patches) high into the plasmasphere, where it diffuses down magnetic field lines. At lower mid-latitudes an enhanced polarizing electric field then erodes the plasma from the plasmasphere and transports it poleward (dark grey patches) in the Sub-Auroral Polarization Stream (SAPS). (Adapted from *Schunk and Nagy (2009)*)

electric field convects the plasma both downward in altitude and towards the poles. This electric field arises during disturbed conditions and exists to close the circuit in the region of low conductivity between field aligned currents in the nighttime sub-auroral zone. Across this zone a region of strong plasma drift known as the sub-auroral polarization stream (SAPS) is formed and SEDs in the stream drift in a northwest direction across the U. S. (*Foster et al., 2002*).

Figure 5 shows the TEC characteristics of a SED plume over North America during a severe geomagnetic storm on 31 March 2001. This plot was created using ionosphere TEC values collected from more than 120 GPS ground stations (*Foster et al., 2002*). In typical cases such as this, high conductivities on the dayside prevent the poleward field from extending deep into the sunlit sector and flow stagnates, causing plasma to build up in a narrow channel along the dusk terminator (*Kelley et al., 2004*).

SEDs and strong geomagnetic activity in general cause a wide variety of societal and economic impacts. Much of the technical infrastructure, space-based assets, and

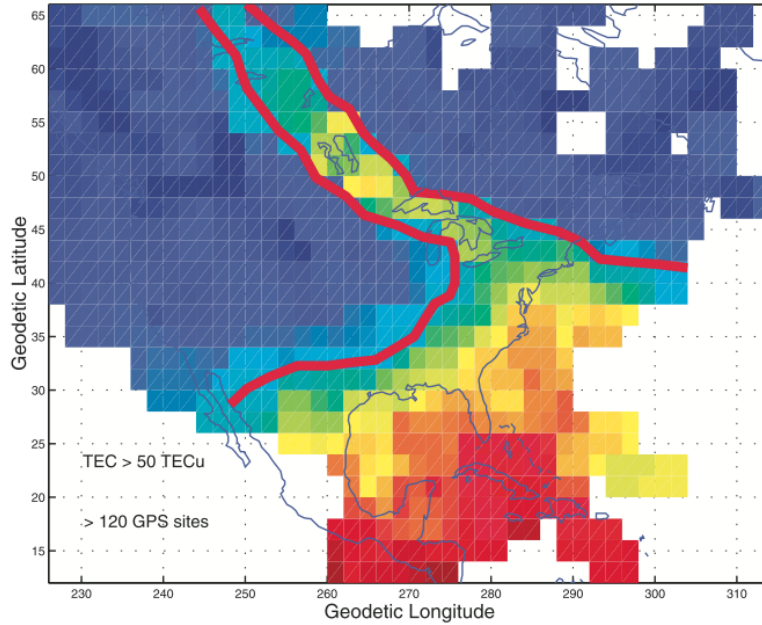


Figure 5. SED plume over the northern U.S. at 1930 UT during the 31 March 2001 geomagnetic storm. The 50 TEC unit contour is outlined in red and shows the position of the SED. Data from over 120 GPS ground stations were used to reconstruct this TEC map. (Adapted from *Foster* (2002))

enabling technology of the U.S. and world is frequently vulnerable to degradation and occasionally to damage during geomagnetic storming (*Baker et al.*, 2008). Impacted areas include, but are not limited to: 1) navigation and surveying using the GPS system; 2) high-frequency communications; 3) satellite tracking; 4) satellite lifetime; 5) surveillance; 6) pipeline integrity; 7) electrical power grids; and 8) over-the-horizon radar. Taking into consideration ground induced currents on U.S. power grids alone, it is estimated that a major blackout similar in size to the 14 August 2003 northeastern U.S./Canada blackout could cost \$4 to \$10 billion in economic loss (*U.S.–Canada Power System Outage Task Force*, 2004).

Ionospheric disturbances due to geomagnetic storming pose a particular threat to military objectives on both the strategic and tactical level. For example, capabilities such as satellite uplink for forward-deployed units and GPS-guided munitions have improved the effectiveness of military operations in recent years. As decision makers

rely more on technological and information superiority, the risk of degradation to key navigation, communication, and weapon systems during geomagnetic storming becomes greater. To mitigate these risks, advanced computer models that can accurately specify and forecast the ionosphere have been developed and will continue to play a vital role in the civilian, government, and military arena.

2.5 GAIM-GM Kalman Filter Model

The ionosphere model of interest for this research is the GAIM-GM Kalman Filter Model, developed by Dr. Robert Schunk and his team at USU and used operationally at AFWA. It may also be run on-demand for research studies through the NASA Community Coordinated Modeling Center. GAIM-GM creates a three-dimensional, time-dependent evolution of the global ionosphere from 90 – 1400 *km*. In recent years the accuracy of the model has been validated against a variety of independent observations for varying geophysical conditions [(*Thompson et al.*, 2005) (*Scherliess et al.*, 2006), (*Zhu et al.*, 2006), (*Decker and McNamara*, 2007), (*Schunk et al.*, 2010)].

GAIM-GM’s strength as an ionospheric model comes from its ability to assimilate ionospheric measurements from several sources, which include: 1) bottomside electron density profiles from a variable number of ionosondes; 2) *in situ* electron density from four Defense Meteorological Satellite Program (DMSP) satellites; 3) nighttime line-of-sight ultraviolet radiances measured by satellites; and 4) slant TEC from a variable number of GPS satellites (*Scherliess et al.*, 2006). A schematic diagram of these data sources are shown in Figure 6.

GAIM-GM is based on the global, physics-based Ionosphere Forecast Model (IFM) and a Gauss-Markov Kalman filter data assimilation algorithm. The IFM is used as an initial background from which ionospheric densities are taken, and then perturbations are superimposed on that background by the Kalman filter, based on available data

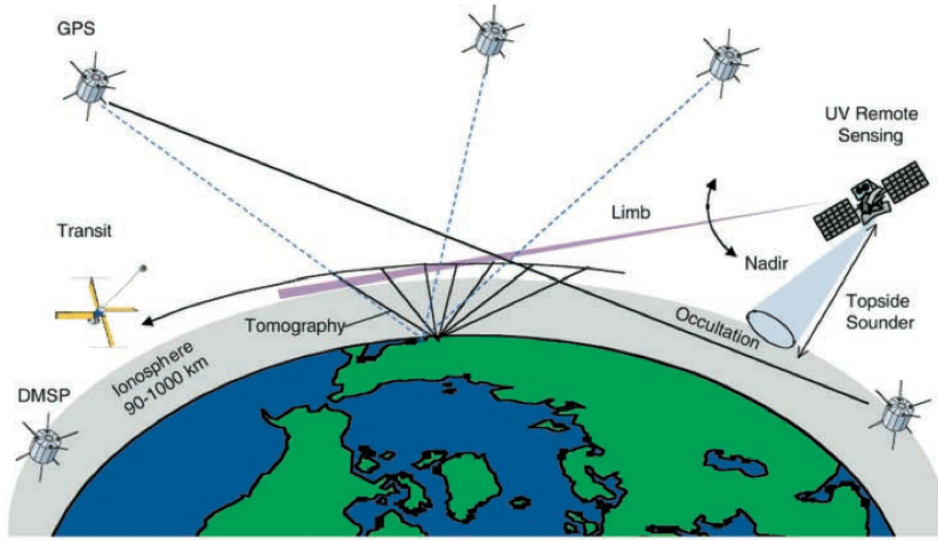


Figure 6. Portrayal of some of the data sources that are available for assimilation into GAIM-GM. (Adapted from Schunk (2004))

and their errors. A brief overview of the IFM and how it operates is given in the next section.

2.5.1 Ionospheric Forecast Model (IFM).

The IFM is a numerical, physics-based model that provides the three-dimensional, time-dependent evolution of the global ionosphere from 90 – 1600 *km*. It provides the density distributions of four major ions (NO^+ , O_2^+ , N_2^+ , O^+) at E region altitudes, two major (NO^+ , O^+) and two minor (N_2^+ , O_2^+) ions at F region altitudes, TEC, and also ion and electron temperatures at both E and F region altitudes. The IFM also calculates H^+ densities in the F region and topside ionosphere, as well as the density of the E and F region peaks and their altitudes. These peaks are easily resolved by the model's vertical resolution of 4 *km* in the E region and 20 *km* in the F region (Schunk *et al.*, 1997). The latitude and longitude resolutions are 3° and 7.5° , respectively, and the output can be in either geographic or geomagnetic coordinates (Schunk and Scherliess, 2004). Figure 7 gives an example of an IFM specification

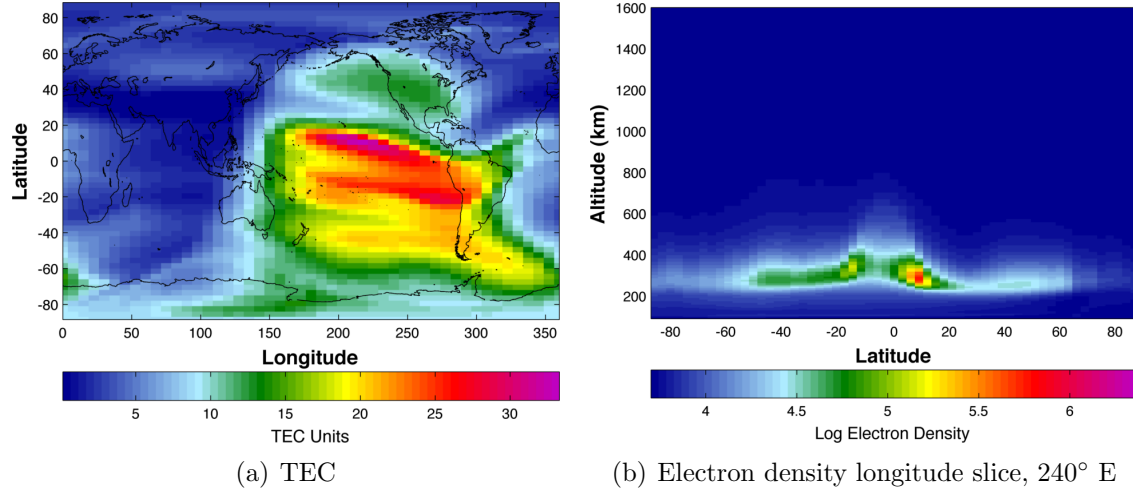


Figure 7. IFM specification during solar minimum (Year 2007, Day 355, 2200 UT). Note how the model output captures the equatorial Appleton Anomaly, or fountain effect, in the 240° E longitude slice (b)

for the winter solstice during solar minimum. The TEC at 2200 UT is shown in 7(a) while an electron density vertical profile at 240° E longitude for the same time is shown in 7(b). Note how the IFM captures the equatorial Appleton Anomaly.

The IFM uses the $F10.7$, Kp , and Ap indices as solar and geomagnetic inputs. These values are in turn used to compute neutral densities, winds, temperatures, and the plasma convection and precipitation patterns via integrated empirical models (*Space Environment Corporation, 2002*).

The most important chemical and physical processes of the ionosphere are accounted for in the IFM's numerical solution. This solution is based on: 1) field-aligned plasma diffusion; 2) cross-field electrodynamic drifts governed by magnetospheric and dynamo electric fields; 3) thermospheric winds; 4) exchange fluxes in the protonosphere; 5) energy-dependent chemical reactions; 6) electron thermal conduction; 7) numerous ion production sources (photoionization from solar EUV radiation, auroral particle precipitation, backscattered solar radiation, and starlight); 8) neutral composition changes; and 9) a variety of local heating and cooling processes (*Schunk and*

Scherliess, 2004). Validations of the IFM against observations for different parameters have been performed by *Scherliess et al.* (2006), *Zhu et al.* (2006), *Decker and McNamara* (2007), *Thompson et al.* (2006), and others.

2.5.2 GAIM-GM Output and Resolution.

The output from GAIM-GM is a continuous, time-varying, three-dimensional reconstruction of the electron density distribution from 92 – 1400 *km*. The model also produces auxiliary parameters including the heights and densities of the F₂ region peak, the heights and densities of the E region peak, and TEC. GAIM-GM also provides global distributions for the ionospheric drivers, which include magnetospheric and equatorial electric fields, electron precipitation patterns, and neutral winds (*Schunk and Scherliess*, 2004).

There are two modes for running the model: global and regional. Figure 8 shows the latitudinal and longitudinal resolutions of both modes. The global mode has a typical resolution of 4.6° latitude by 15° longitude, while the regional mode is user-adjustable and can resolve up to 1° latitude by 3.75° longitude, based on data coverage and the computational environment. The vertical resolution of the output is 4 *km* in the E region and 20 *km* in the F region and above, for both global and regional modes (*Scherliess et al.*, 2006).

2.5.3 Gauss-Markov Kalman Filter.

GAIM-GM operates by using a Kalman filter to superimpose density perturbations onto background IFM density field, based on available data and their errors. These perturbations and errors then evolve over time with a statistical model (the Gauss-Markov process). The *total electron density* at each grid point is expressed as:

$$N = N_{IFM} + N_{pert} \tag{2}$$

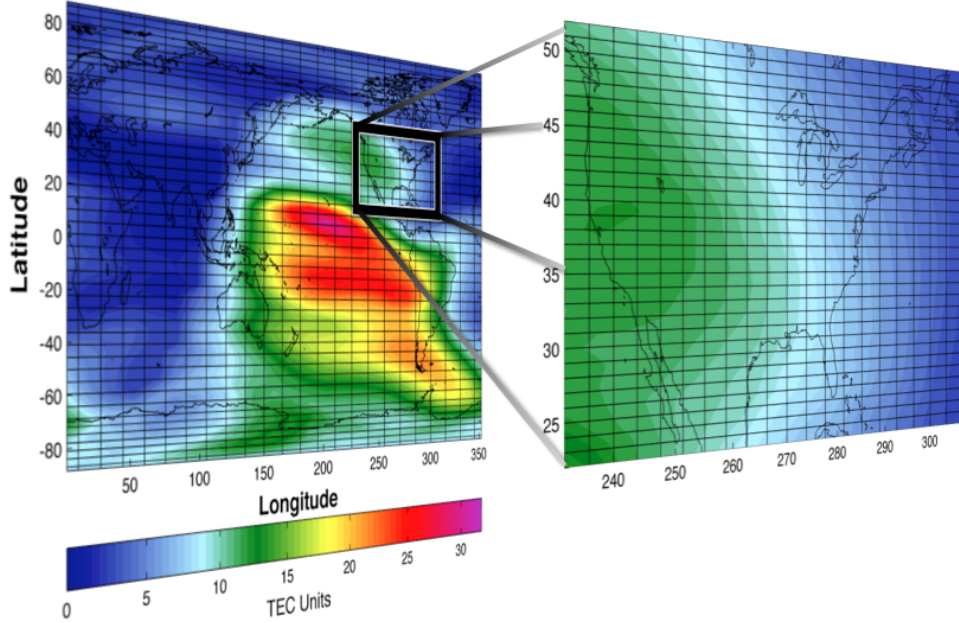


Figure 8. GAIM-GM model output for global and regional modes. Global mode resolution is typically 4.6° latitude by 15° longitude, while resolution as high as 1° latitude by 3.75° longitude can be obtained in regional mode

where N_{IFM} is the *electron density* from the IFM background and N_{pert} is the *perturbation density* derived by the Kalman filter. The density N_{pert} is given in a geographic frame and evolves over each 15-minute assimilation time step through the following formula:

$$N_{pert}^{t+1} = \mathbf{L}N_{pert}^t \quad (3)$$

where \mathbf{L} is a transition matrix, the product of a translation matrix \mathbf{L}_1 and a diagonal matrix \mathbf{L}_2 . The matrix \mathbf{L}_1 moves the perturbation density field at each time step in a sun-synchronous magnetic frame while the diagonal matrix \mathbf{L}_2 relaxes the perturbations to zero if there is no data present. The *relaxation time* τ is set to $\tau = 5$ hours by default, but can be adjusted to better capture changing geophysical conditions (Scherliess *et al.*, 2006).

The Gauss-Markov Kalman filter uses an error covariance matrix that evolves with the same transition matrix \mathbf{L} as the electron density perturbations. Included in

the error covariance matrix are the uncertainties of the \mathbf{L} , which were obtained from 1107 individual 2-day runs of the IFM with varying external forcing parameters and a wide range of climatological variations. In the absence of assimilation data (GPS, DMSP, etc.) the model error covariances are given by these uncertainties. For this reason, GAIM-GM will not exactly reproduce the IFM density background even if no observational data are assimilated.

Quality control is performed on the observations assimilated by the Kalman filter. Obviously wrong observations are rejected and appropriate data errors are assigned to remaining data. These errors consist in an observational error associated with the instrument taking the measurements, and an error associated with the representativeness of the observation. All data errors are assumed to have a Gaussian distribution and to be uncorrelated with one another (*Scherliess et al., 2006*). A problem can arise when closely spaced measurements are assimilated, such as those from a dense grid of GPS ground stations. The error of representativeness becomes highly correlated and the TEC measurements are trusted too much. The solution available to the user is to reduce the data density, either by: 1) increasing the model grid density via running GAIM-GM in regional mode with higher resolution; or 2) maintaining the same resolution but simply using less data. Increasing the number of ground stations without raising grid resolution does not improve the TEC result and can actually degrade the F_2 region peak density results (*Thompson et al., 2005*).

2.5.4 Assimilation of GPS Slant TEC.

Among the many data types that GAIM-GM can ingest, GPS slant TEC measurements are some of the most readily available. For a 15-minute sampling cadence, a single GPS ground station located within CONUS can produce between 35 – 45 slant TEC measurements per hour, yielding about 1000 measurements per day. This

becomes a truly vast reservoir of data for GAIM-GM when multiplied by the number of available GPS ground stations.

The Gauss-Markov Kalman filter makes an important adjustment to slant TEC data during the assimilation process. Recall that slant TEC measurements consist of integrated electron densities along the paths from GPS satellites to ground stations. These satellites orbit near 20,200 *km* and thus slant TEC paths include electron contributions from both the ionosphere and plasmasphere (see Figure 9). When satellites are not directly overhead, slant paths can be considerably larger, causing a significant amount of plasmasphere electrons to be integrated into the total slant path. Since the upper bounds of GAIM-GM extend no higher than 1400 *km*, the plasmaspheric contribution to GPS slant TEC measurements (1400 – 20,200 *km*) must be accounted for and discarded. This is done through an internal representation of the plasmasphere which estimates the plasmasphere TEC contribution and subtracts it during the data assimilation process. Even this simple representation of the plasmasphere provides significantly better distributions of F₂ peak density and TEC, compared to results where the plasmasphere contribution is ignored (*Thompson et al.*, 2009).

After the slant TEC data have been adjusted for plasmasphere contributions, the Kalman filter assigns errors to the observations. One of these errors is the phase TEC error. This results from inherent fluctuations in the slant TEC estimate due to bandwidth limitation precision, multipath errors, receiver noise, and other effects (*Dyrud et al.*, 2008). Fortunately the phase TEC error values are normally given separately in slant TEC observations, enabling the Kalman filter to appropriately weigh ingested data when constructing the perturbation density matrix N_{pert} .

Additionally, the Kalman filter assigns errors according to instrument biases in both GPS satellite and receiver sensors. These so-called differential code biases (DCBs) are caused by delay and dispersion of GPS signals traveling through ana-

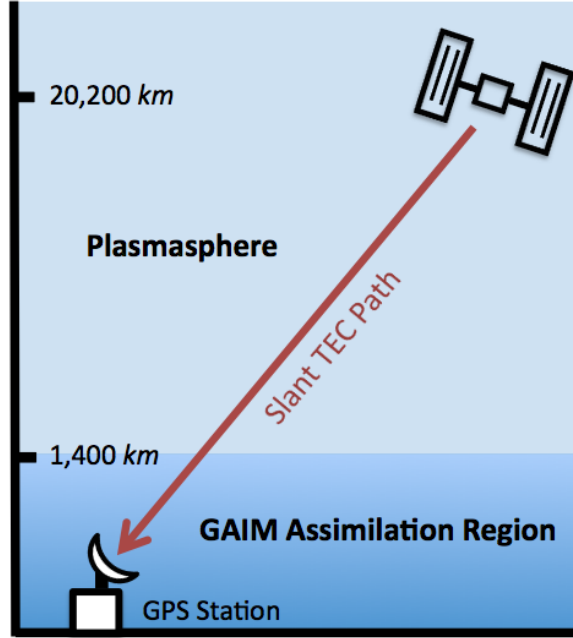


Figure 9. Plasmaspheric contribution to slant TEC path between a GPS ground station and GPS satellite. The GAIM-GM Kalman filter uses an internal algorithm to discard all extra slant TEC above the data assimilation region of 1400 km

log circuits and filters in satellites and receivers, and therefore DCBs are unique to each piece of equipment. DCBs cause significant errors in TEC estimates and must be addressed before the data can be reliably used for ionospheric reconstruction. Fortunately, the International Global Navigational Satellite System Service (IGS) compiles a daily list of corresponding satellite-to-receiver DCBs for many stations worldwide (Dyrud *et al.*, 2008). GAIM-GM ingests these lists from the Internet and provides the DCBs to the Kalman filter. If GPS DCBs are not available for a given ground station the Kalman filter solves internally for the missing bias (Scherliess *et al.*, 2006).

By assimilating slant TEC from available of ground GPS receivers, GAIM-GM can significantly improve its ionosphere specification compared to independent measures of vertical TEC and thus create more reliable ionosphere reconstructions (Schunk *et al.*, 2010). This will lead to better ionosphere correction maps and reduced degradation to military, government, and civil navigation and communication systems.

III. Methodology

3.1 Chapter Overview

This chapter describes the methods used to perform this study and is broken into seven sections. First it details how the IFM density backgrounds were created, followed by a section that describes how the synthetic SED was modeled and imposed onto the IFM background. The GPS ground station distributions and the methods for creating them will be examined, followed by a description of how slant TEC measurements were cut through the IFM background and prepared for assimilation into GAIM-GM. This leads directly into an outline of procedures for running the GAIM-GM model. Additionally, the methods used to analyze and visualize model output are presented.

3.2 IFM Density Backgrounds

The first objective was to obtain IFM electron density background maps. These served two purposes: 1) provide the initial, background ionosphere specification for the GAIM-GM model; and 2) provide a background observation onto which a synthetic SED could be imposed. The day chosen for the IFM backgrounds was 21 June 2001 (day 172 of the year), which corresponded to the summer solstice during the peak of solar cycle 23. This was a logical choice because geomagnetic storming occurs most often during solar maximum. Slant TEC measurements of the IFM backgrounds with the imposed SED could then be cut between GPS satellites and several different distribution of GPS ground stations. These slant TEC measurements were the only data ingested by GAIM-GM.

When running GAIM-GM, two days of IFM output are needed to produce a one-day GAIM-GM specification if output from a previous IFM run is not available. This

is because the IFM is initiated using the empirical International Reference Ionosphere model (IRI) (*Space Environment Corporation*, 2002). In such cases the IFM output is degraded, so it is necessary to run IFM for two warm-up days, followed by two good days in order to arrive at a steady-state specification of the ionosphere. The IFM input parameters for the two good days (171 and 172) are listed in Table 2. The input parameters for the two warm-up days (169 and 170) used the same parameters as day 171. Note that only the K_p and A_p indices changed between days 171 and 172. The $F10.7$ (10.7 cm wavelength solar radio flux) and $F10.7A$ (90-day average $F10.7$) indices were taken from historical observations and reflect solar maximum conditions during early 2001.

Table 2. IFM input parameters

Parameter	Day before storm	Day of storm
Year	2001	2001
Day	171	172
K_p	3	6
A_p	14	83
$F10.7$	205	205
$F10.7A$	153	153

A K_p of 3 was used on day 171 to reflect a relatively quiet, pre-storm ionosphere state. As the K_p index increased to 6 on day 172, the IFM output gave significantly higher TEC values, as shown in Figure 10. While higher TEC is often seen during geomagnetic storming, IFM TEC associated with elevated K_p indices tends to be erroneously high due to missing physics in the IFM. With enough assimilated data, GAIM-GM is able to overcome this shortcoming in the IFM background (*Schunk et al.*, 2010).

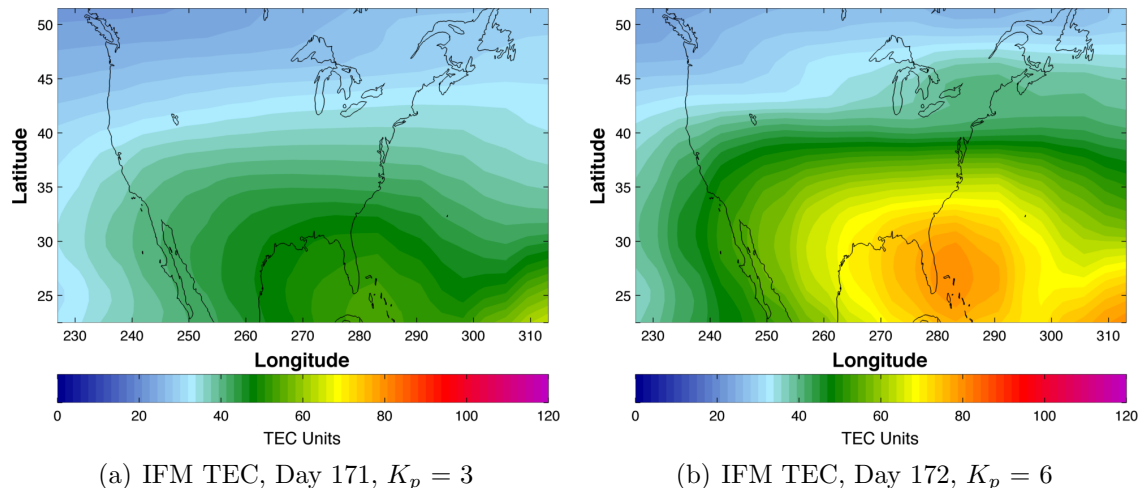


Figure 10. IFM background TEC maps at 1700 UT for days 171 (a) and 172 (b) of year 2001. Much larger TEC values were modeled by IFM on day 172 due to higher K_p levels. Unlike Figure 7, contour smoothing was applied to these images to remove the pixelated appearance

3.3 Modeling the SED

Once the IFM runs for days 171 and 172 were completed, the output was downloaded from USU servers via Secure File Transfer Protocol (SFTP) as Network Common Data Form (NetCDF) files. These files were then opened and manipulated in MATLAB[®]. An IFM NetCDF file contains one simulated day's worth of output in 28 different variables. Only two variables were used during the process of modeling the SED: 1) three-dimensional electron density; and 2) TEC.

The entire process of imposing a synthetic SED was accomplished in the MATLAB[®] utility called *Storm.m*. This and all other MATLAB[®] program used during this project were designed by the author at the Air Force Institute of Technology (AFIT). Copies of these programs and their operating instructions may be requested from the author.

Storm.m first made two adjustments to the IFM output electron density array. The first adjustment was to shave exactly 3.75° longitude worth of data from both

edges of the world grid. IFM has a native resolution of 3° latitude by 7.5° longitude and gives its output in arrays of size 30×49 . The 1st and 49th longitude indices (corresponding to 0° and 360° longitude) are duplicates, which means that there is an extra 3.75° of longitude at the eastern and western edges of the world map. These two strips of data ran from pole to pole and had to be removed so that the IFM would fit exactly within the boundaries of a world map.

The second adjustment was to increase IFM's grid resolution to match GAIM-GM in regional mode, so that IFM output could be directly compared to GAIM-GM output at a later point. This was done via the MATLAB[®]*imresize* function which uses Lanczos filtering, a simple and attractive method of interpolating between sampled data (*Duchon, 1979*). The Lanczos filter is the product of two *sinc* functions, where the resulting function is used as a convolution kernel to resample the input field.

An example of IFM TEC output before and after interpolation is shown in Figure 11. The IFM output in 11(a) is in the native resolution while the output in 11(b) has been interpolated and resized to match GAIM-GM's resolution. Table 3 compares the scale and resolution of IFM global output to GAIM-GM regional mode output.

Table 3. IFM output size and resolution, compared to GAIM-GM regional mode size and resolution. The IFM had to be resized and interpolated to match GAIM-GM dimensions so that direct comparisons over CONUS could be performed

Parameter	IFM	GAIM-GM
Latitude Resolution	3°	1°
Longitude Resolution	7.5°	3.75°
Western Boundary	0° E	225° E
Eastern Boundary	360° E	315° E
Northern Boundary	90° N	52° N
Southern Boundary	90° S	22° N

The most important component of *Storm.m* is the matrix which contains the synthetic SED profile. This profile was patterned after the behavior of real SEDs,

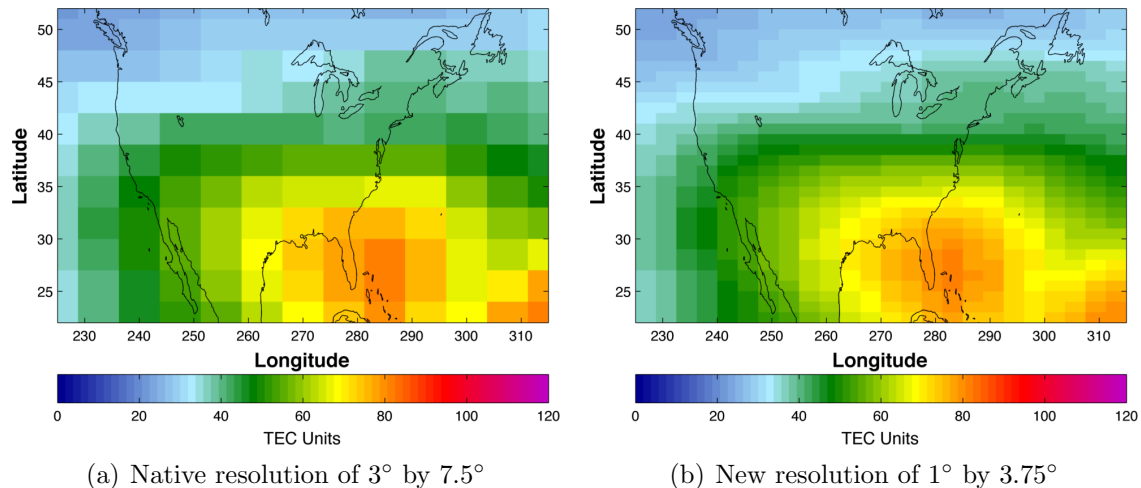


Figure 11. Interpolation of IFM TEC output to the finer GAIM-GM resolution for year 2001, day 172, time 1700 UT, via Lanczos filtering in Matlab[®]. Contour smoothing was not applied to these images, hence the digitized appearance

several of which have been well-documented in the past decade. Ultimately the 20 November 2003 SED analyzed by *Foster* (2005) was chosen as the basic template for the synthetic SED. Figure 12 shows GPS TEC observations over CONUS at the 1945 UT height of the storm, taken from about 450 North American GPS sites. Additional insight on the SED’s movement was gained by running GAIM-GM and ingesting historical slant TEC data from the day of the storm to replicate the SED features. Using 89 North American GPS sites, GAIM-GM produced the TEC map and electron density distribution shown in Figure 13.

For simplicity and efficiency, the basic SED properties were captured using Figure 12, Figure 13, and Table 1. Focus was placed on depicting the northwestward movement of a plasma parcel within the broad tongue of ionization, which in Figure 12 extends from the U.S. East Coast to the central Canada. The finalized synthetic SED is shown in Figure 14 in terms of TEC and vertical electron density profile.

A schematic diagram of the synthetic SED’s trajectory is given in Figure 15, identifying its precise location during its three-hour transit of CONUS. It must be

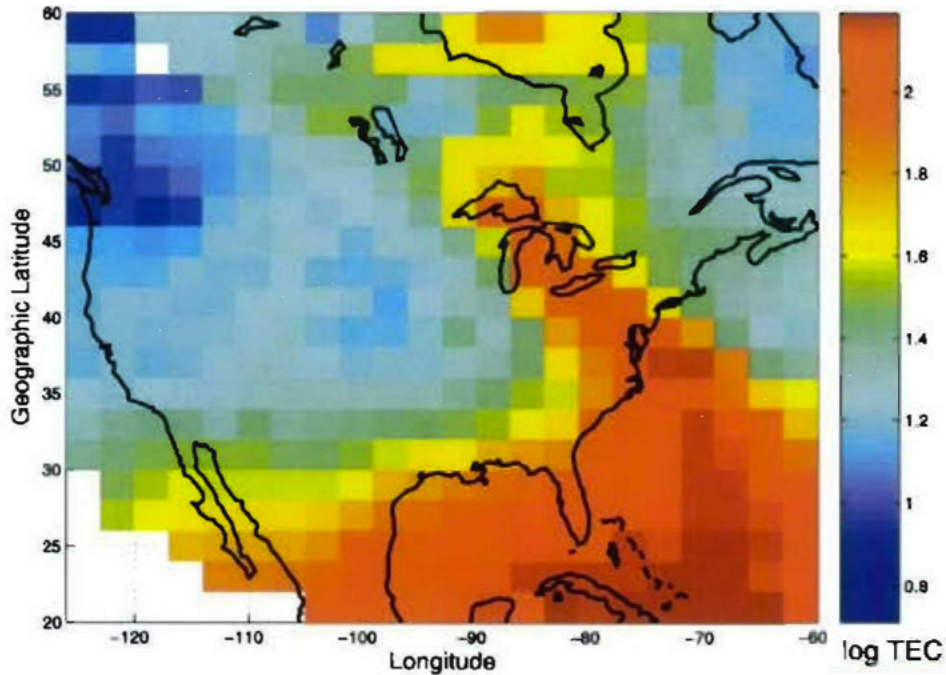


Figure 12. GPS vertical TEC observations over the U.S. at 1945 UT during the height of the 20 November 2003 geomagnetic storm. The SED is the tongue of ionization extending from the Mid-Atlantic coast to the Great Lakes. 450 GPS receivers provided vertical TEC data to create this image (Adapted from *Foster (2005)*)

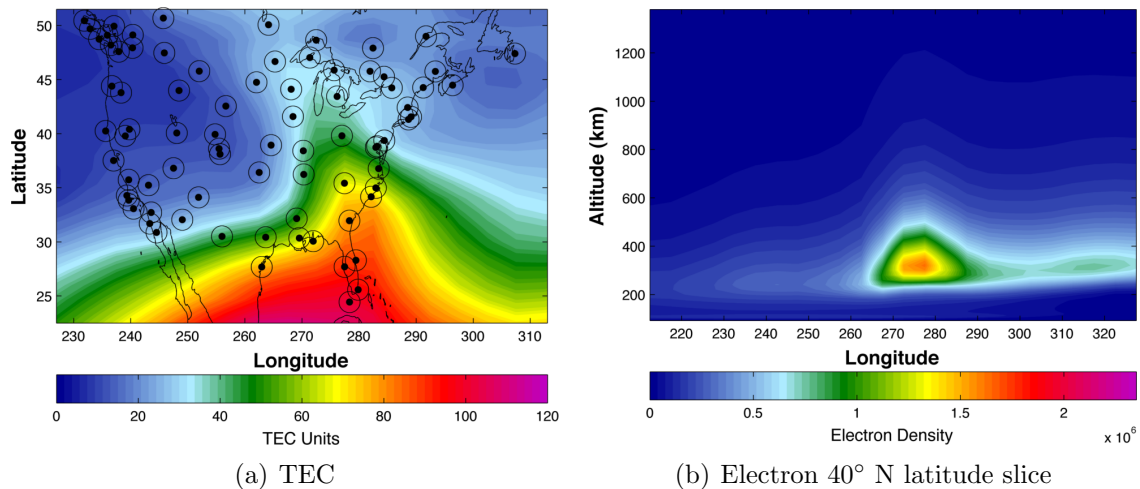


Figure 13. GAIM-GM recreation of the 20 November 2003 geomagnetic storm at 1945 UT. Historical slant TEC data from 89 North American GPS sites (overlaid as black circles) were ingested into the model. (a) shows TEC during the height of the storm while (b) is a vertical cross-section of electron density, taken at 40° N latitude. The model resolution at the time was 1.333° latitude by 5° longitude

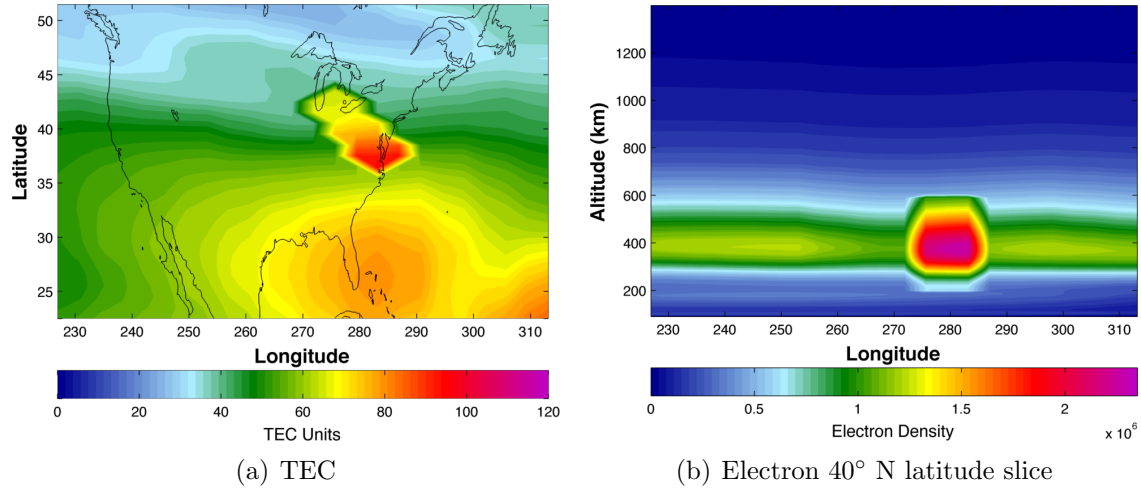


Figure 14. Synthetic SED in an IFM background at 1945 UT. The IFM was run for year 2001, day 172, with a K_p of 6 and the the SED was superimposed by multiplying background densities between 200 – 600 km by a factor of 2. (a) shows TEC while (b) is a vertical cross-section of electron density, taken at 40° N latitude. The model grid resolution is 1° latitude by 3.75° longitude

stressed that real SEDs consist of an entire plume of high density plasma extending across CONUS, in which plasma flows northwestward within the plume. The synthetic SED in this research is a much more basic construct that only models a parcel of high density plasma moving along the path that the plume would normally outline. However, the properties of the synthetic SED itself closely match those of real SEDs, as can be verified in Table 4, which compares the properties of both SED types.

Storm.m imposed the synthetic SED by first extracting the IFM three-dimensional electron density output at each time step for the target day (year 2001, day 172) from the NetCDF file and loading it into a four-dimensional read-only array. This array consisted of latitude, longitude, altitude, and time dimensions. *Storm.m* then multiplied all background electron densities found within the volumetric boundary of the SED region by a factor of 2 and wrote them to a new four-dimensional storm density array. At the next time step, the SED boundaries were propagated exactly 2° latitude to the north and 3.75° longitude to the west and the IFM background electron

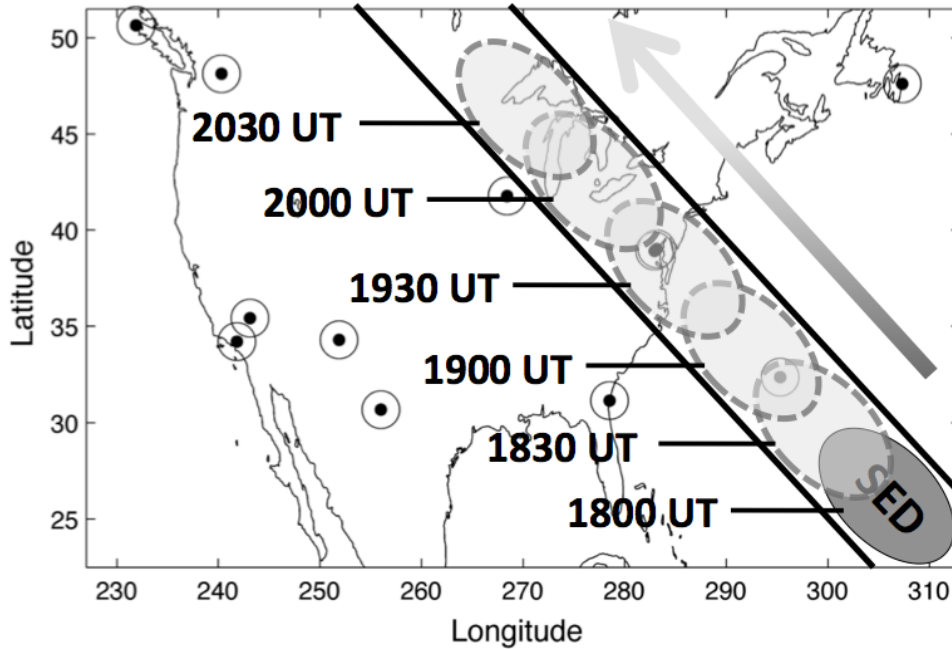


Figure 15. Trajectory of synthetic SED across CONUS. The feature originates at 22° N over the Atlantic Ocean at 1800 UT and travels in a northwestward direction at about 0.5 km/s until disappearing at 2100 UT at 52° N over lower Manitoba, Canada

Table 4. Synthetic vs. real SED properties

Property	Synthetic SED	Real SED
Duration	3 hours	2 – 5 hours
Peak time	1800 – 2100 UT	1730 – 2000 UT
$H_m F_2$	400 km	> 500 km
Base elevation	200 km	Variable
Ceiling elevation	600 km	Variable
Altitude extent	400 km	300 – 500 km
Length	1500 km	> 3000 km
Width	700 km	600 – 1000 km
Velocity	0.5 km/s	0.5 – 1 km/s
$N_m F_2$	$1 - 4 \times 10^{12} m^{-3}$	$1 - 3 \times 10^{12} m^{-3}$
TEC increase	1.7 times	2 – 4 times

densities within the SED volume (from the read-only array) were again doubled. By taking densities from the read-only array and writing them to the new storm density array, densities within the SED were prevented from being doubled repeatedly. After the SED was fully inserted, *Storm.m* used an algorithm developed by Capt Janelle Jenniges to transform the 73-layer, three-dimensional electron density arrays into new TEC maps for each time step (Jenniges, 2011). The TEC maps were retained for later comparison to GAIM-GM output while the four-dimensional electron density arrays served as backgrounds through which slant TEC measurements were taken.

3.4 Creating GPS Ground Station Distributions

Having obtained the IFM specifications and imposed the synthetic SED, the next step was to acquire several distributions of GPS ground stations. Two types of ground station grids were created: 1) grids of real GPS ground stations taken from the Continuously Operating Reference Station (CORS) network, hereafter referred to as CORS grids; and 2) grids of evenly spaced and ideally located, artificial ground stations, hereafter referred to as Ideal grids.

In the CORS grids there were five different GPS ground station distributions. The first distribution was taken from a list of 11 GPS ground stations that the operational GAIM-GM at AFWA had routinely ingested during February 2011. It was found that the synthetic SED's trajectory put the AFWA station distribution at an unreasonable disadvantage for detecting and replicating the storm feature, so a GPS ground station located in the state of Georgia was added to the AFWA list, bringing the total number of stations to 12 (see Table 5). Justification for the addition of this 12th station and its impact on the results of this research are given in Appendix B.

Using this modified 12-station AFWA grid as the baseline distribution, additional stations were added in increments of 30, 100, 200, and 400, to create a total of five

Table 5. AFWA GPS stations

Site	ID	Latitude ($^{\circ}$ N)	Longitude ($^{\circ}$ E)	Ellip. height (m)
McDonald, TX	MDO1	30.674	255.991	2005
Brunswick, GA ^a	GABK	31.150	278.508	-13
Bermuda	BRMU	32.368	295.308	-10
Pasadena, CA	JPLM	34.202	241.829	424
Pie Town, NM	PIE1	34.300	251.881	2348
Goldstone, CA	GOLD	35.421	243.113	987
Washington, DC	USN3	38.920	282.930	58
Greenbelt, MD	GODE	39.019	283.177	15
North Liberty, IA	NLIB	41.769	268.428	208
St. John, Canada	STJO	47.600	307.320	153
Brewster, WA	BREW	48.125	240.323	239
Holberg, Canada	HOLB	50.640	231.870	560

^a Brunswick was not part of the original 11-station AFWA list. Appendix B explains why it was added as the 12th station

CORS grids. The first 30 stations added to the AFWA grid were hand-picked to maximize even placement, while a MATLAB[®] utility called *StationSort.m* selected the 100, 200, and 400 additional stations via a special filter that maximized uniform spacing. Figure 16 shows the locations of GPS ground stations for each CORS grid. It is important to emphasize that the each grid builds upon the previous one, such that only 412 stations were used overall.

Attaining a perfectly uniform distribution was impossible for any CORS grid because of limitations in the CORS network layout. All ~ 1900 CORS occupy only 259 of the GAIM-GM regional mode grid squares (there are 720 total grid squares in the model), creating large data gaps over oceans and highly saturated areas of ground stations over land. Although the AFWA+400 grid was distributed as evenly as possible, 59% of station-hosting model grid squares contain two GPS ground stations and one square contains three (see Figure 17). This is an important point since closely spaced GPS receivers are problematic in GAIM-GM, as TEC measurements become highly-correlated and are overly trusted by the Kalman filter (*Thompson et al.*, 2005).

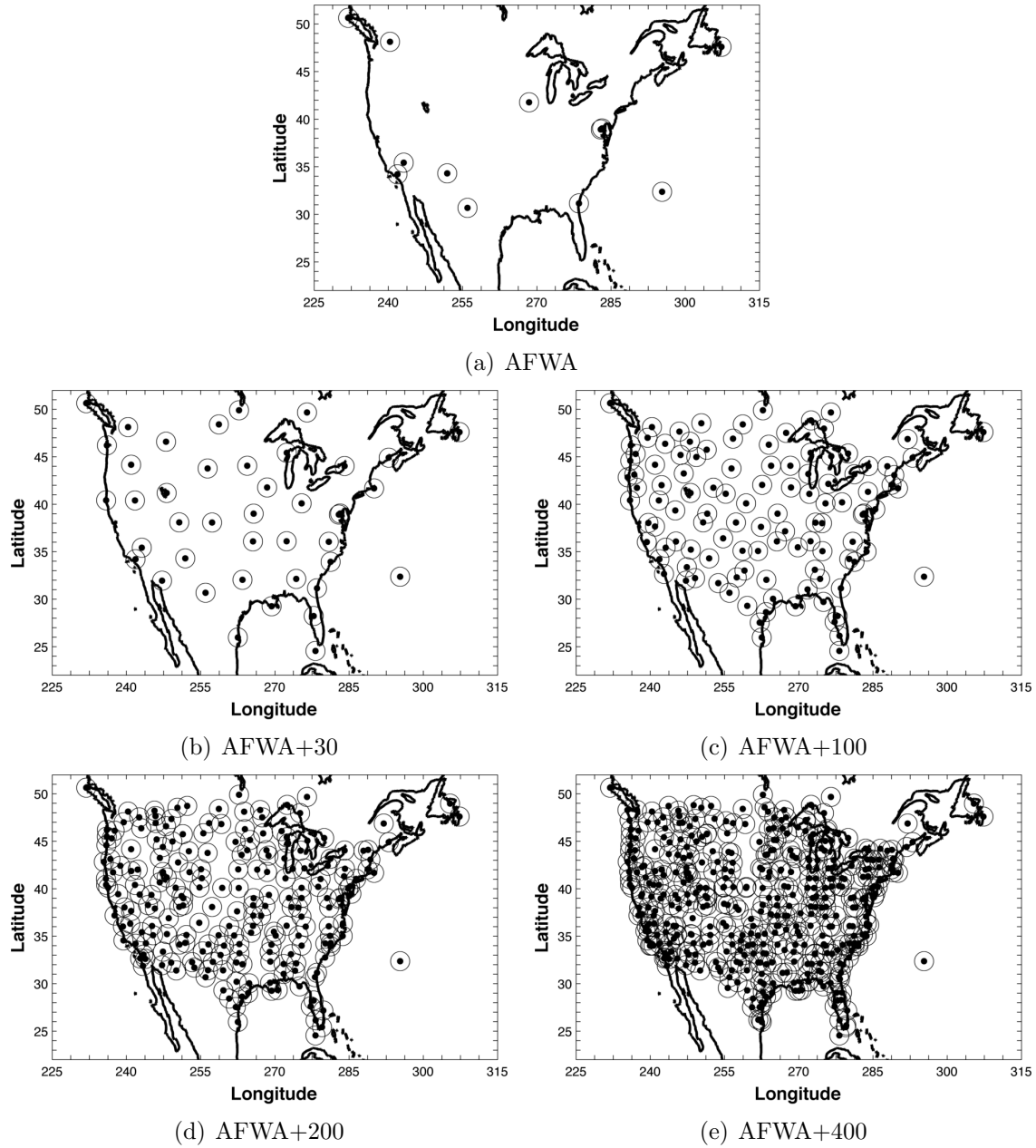


Figure 16. CORs grids of GPS ground stations. These grids use actual station locations from the CORS network

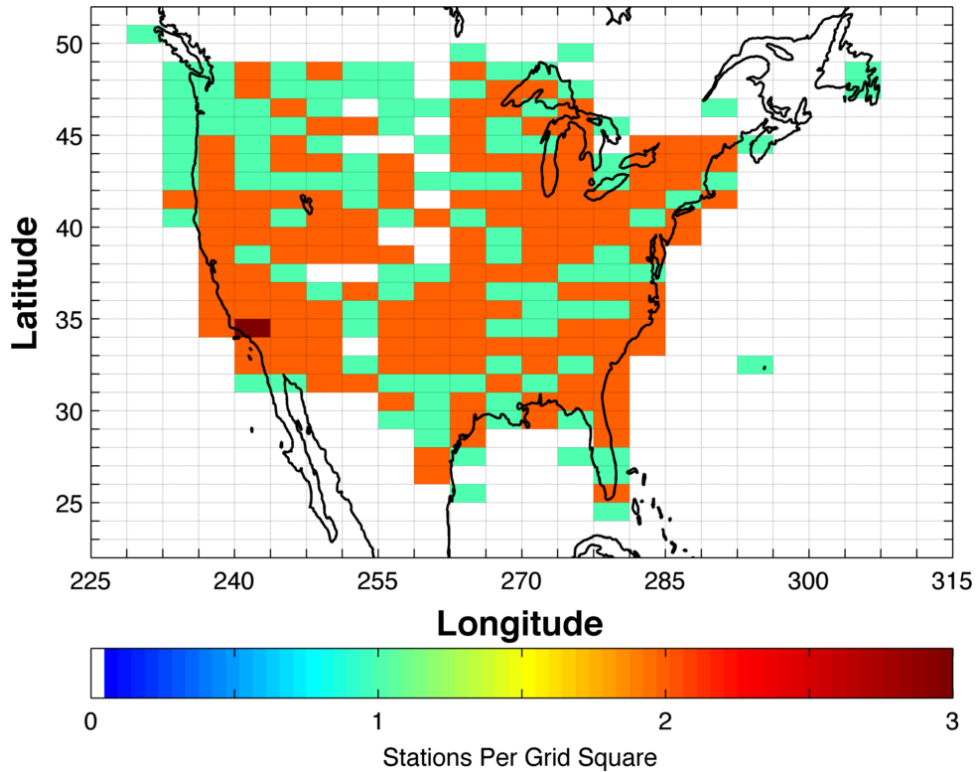


Figure 17. GPS ground station density per model grid square for the AFWA+400 grid. 106 model grid squares have only one station, 152 model grid squares have two stations, and one model grid square over southern California has three stations. GAIM-GM resolution was set to 1° latitude by 3.75° longitude

The Ideal grids were designed to test how geo-location accuracy over CONUS improves when optimal GPS ground station spacing is applied, completely unrestricted by oceans and terrain. Figure 18 shows the four Ideal grids, which were created using 21, 90, 360, and 720 artificial ground stations. Each grid builds upon the last in the same manner as the CORS grids. The main differences between the Ideal grids and the CORS grids are: 1) the Ideal grids' ground stations are artificial; and 2) the Ideal grids have only one station per model grid square.

For both the CORS and Ideal grids, the average and median distances separating nearest neighbor stations are listed in Table 6. The median distance is a more reasonable value because, unlike the average distance, it is not skewed by contributions

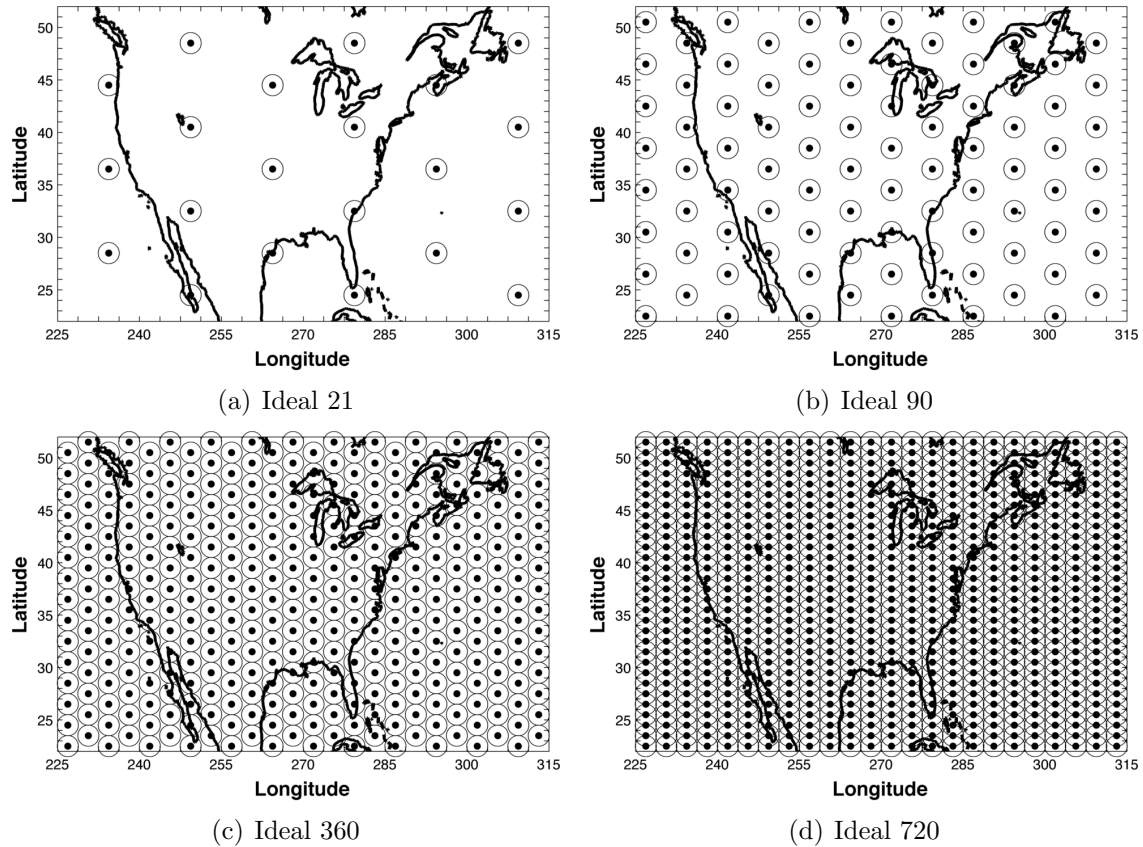


Figure 18. Ideal grids of GPS ground stations. These grids represent optimized distributions of ground stations and do not exist in reality

from geographically isolated stations such as Bermuda. Note that even though Ideal 720 grid has more stations than the AFWA+400 grid, the distances between stations are still greater because the stations are able to spread out over the oceans.

3.5 Taking Slant TEC Measurements

Slant TEC measurements are derived from phase differences introduced into a GPS satellite's signal as it penetrates the ionosphere. Unlike simple, single-channel GPS devices sold commercially, ground receivers at official GPS monitoring stations are dual-channel and can receive both the L1 and L2 signals broadcast by GPS satellites. Precise measurement of the time delay difference between these two signals allows

Table 6. Distance between GPS ground station nearest neighbors

Distribution	# Stations	Average (<i>km</i>)	Median (<i>km</i>)	Standard Dev. (<i>km</i>)
AFWA	12	1580	1321	720
AFWA+30	42	749	686	275
AFWA+100	112	418	362	213
AFWA+200	212	289	252	166
AFWA+400	412	198	171	134
Ideal 21	21	1325	1250	204
Ideal 90	90	659	621	135
Ideal 360	360	324	308	90
Ideal 720	720	257	247	86

the TEC along the signal slant path to be calculated (see Appendix A for further details).

The GPS satellites used in this research were simulated, but their time-dependent position came from actual archived GPS ephemerides. These archived data sets from the past decade to the present are available from NASA’s Crustal Dynamics Data Information System (CDDIS) in the form of .sp3 files and can be downloaded via FTP (*Crustal Dynamics Data Information System*, 2011). GPS constellation ephemerides from 2 October 2010 were selected to represent the GPS constellation, making this research more relative to present day capabilities. A useful diagram of these satellites’ positions over the course of a 24-hour period is presented in Appendix A, Figure 48.

With the GPS ground stations, IFM background, and simulated GPS constellation in place, the slant TEC measurements were taken using a MATLAB[®] utility called *SlantTEC.m*. This program required three data sets in order to operate: 1) the time-dependent IFM density background with the imposed SED; 2) a list of GPS ground station coordinates and elliptical elevations; and 3) a .sp3 file containing GPS satellite ephemerides. *SlantTEC.m* used a 15-minute sampling cadence in order to match GAIM-GM’s data assimilation rate, as well as a 15° Elevation Mask so that slant TEC measurement were only taken from satellites at least 15° above the horizon

in a GPS station's field of view. The output from *SlantTEC.m* was one specially formatted text file per station, per simulated hour, that could be uploaded directly to USU servers and assimilated by GAIM-GM. To put this into perspective, using 720 GPS ground stations meant that 17,280 text files were produced to capture slant TEC measurements for one day. These files were then uploaded to GAIM-GM via SFTP.

The portion of *SlantTEC.m* that actually calculated the slant TEC was adapted from a program written by USU. A copy of USU's original slant TEC calculation code in FORTRAN can be obtained by contacting the Center for Atmospheric and Space Sciences. Their code derives the TEC between two points given in Earth-centered, Earth-fixed coordinates by dividing the slant path into fixed increments and linearly interpolating the electron densities. Each interpolated density is multiplied by the fixed incremental distance in order to determine the TEC for the slant path segment. The TEC values are then totaled to produce the slant TEC value for the entire slant path (*Nava, 2011*).

To ensure the accuracy of the USU slant TEC code and quantify the error its density interpolation scheme introduced, a simple validation was performed. In MATLAB[®], 720 simulated, non-moving GPS satellites were held fixed over an interpolated IFM density background's 720 model grid squares. These simulated satellites then took vertical TEC measurements at each 15-minute time step for all 24 hours of IFM year 2001, day 172 output (without the imposed SED). The vertical slant TEC piercings from every grid square were then compared to actual IFM TEC values, as taken directly from the IFM's NetCDF output files. Figure 19 shows the average difference for each grid square over the 24-hour period. Dark shades of blue and red mark locations where the largest differences (i.e. errors) occurred, while white grid squares indicate locations with very small errors. The average TEC difference for the entire

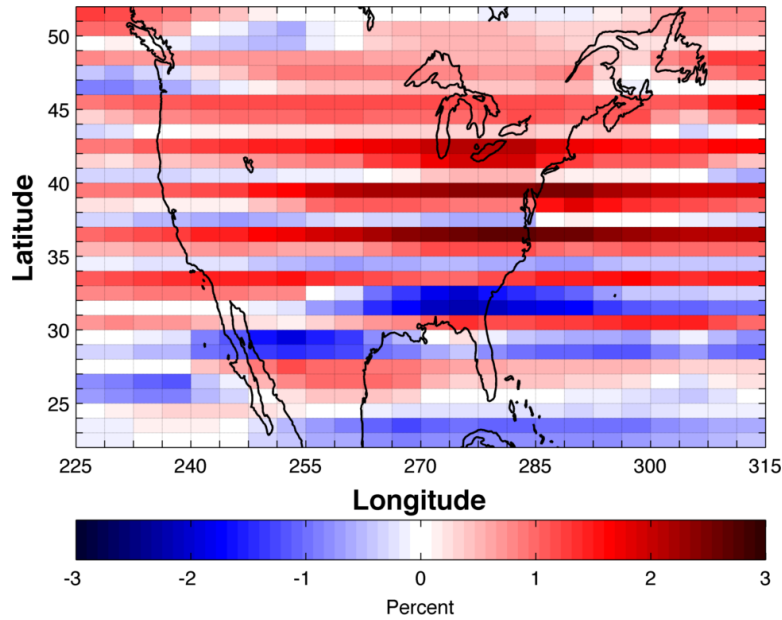


Figure 19. Average vertical slant TEC error per grid square over a 24-hour period, taken for year 2001, day 172. Vertical piercings of the IFM density background were performed at every 15-minute time step and compared to actual TEC values. The mean absolute difference for all vertical slant TEC measurements was 2.7%

map was 2.7% while the maximum difference of any single grid square, for all time steps, was 3.2%. The greatest slant TEC errors generally occurred in areas of strong TEC gradients, such as along the northern edge of the equatorial anomaly.

The average uncertainty in GAIM-GM output was 5.7%, based solely on the 3.0 TEC unit Phase TEC error assigned to each slant TEC data. Although there was no actual Phase TEC error in this research because all measurements were simulated, there were two other errors types that needed to be accounted for by GAIM-GM (see Table 7). For simplification purposes, the Phase TEC error was retained as a proxy for the other two error types, which were due to 1) Slant TEC pierce point averaging; and 2) IFM/GAIM-GM ceiling difference.

Slant TEC pierce point averaging error caused an average of 2.7% uncertainty and occurred as *SlantTEC.m* took the mean density of all model grid squares adjacent to the pierce grid square, at every path increment. This localized interpolation helped

Table 7. Average uncertainty in GAIM-GM output due to slant TEC measurements. The sub-types stem from methods used in this research and are accounted for by the Phase TEC error

Type	Amount	Explanation
Phase TEC error	5.7%	Derived from the 3.0 TEC unit error assigned to every synthetic slant TEC measurement (a typical value for real slant TEC)
Sub-type	Amount	Explanation
Slant TEC pierce point averaging	2.7%	See Figure 19. USU slant TEC code takes the mean density of all grid squares adjacent to the pierced grid square, for every path increment. This is done to represent the continuous distribution of densities in the real ionosphere
IFM/GAIM-GM ceiling difference	1.4%	Average amount of TEC that the 1400 – 1600 <i>km</i> layer of the IFM background contributes to slant TEC measurements. GAIM-GM only has a ceiling of 1400 <i>km</i> but still assimilates the full slant TEC value taken from the IFM background

represent the continuous distribution of densities in the real ionosphere – unlike the discontinuous, pixelated densities in the IFM. The IFM/GAIM-GM ceiling difference error produced an average of 1.4% uncertainty. This occurred because the IFM extends 200 *km* higher than GAIM-GM and extra topside ionosphere plasma was integrated into slant TEC measurements. GAIM-GM accepted this extra fraction of TEC and applied it towards its 90 – 1400 *km* model region. Combined, these two error sources did not amount to the 5.7% reported Phase TEC error, but the higher 5.7% value was nonetheless kept because it represents the amount of error expected in real world slant TEC data.

3.6 Running GAIM-GM

GAIM-GM is a highly sophisticated computer model and detailed instructions regarding its operation are contained in the User’s Guide, which may be requested from USU. However, the basic process for using GAIM-GM to assimilate slant TEC and

replicate the synthetic SED are shown in a flowchart in Figure 20. The shaded right half of the flowchart depicts the operations performed physically at AFIT, while the unshaded left half of the flowchart depicts operations that occurred at USU. Arrows flowing across shaded regions represent SFTP actions. Dark grey ovals represent different inputs and light grey boxes depict the computer programs which utilized those inputs. After all data were assimilated and GAIM-GM produced its solution in NetCDF file format, those output files were downloaded and a variety of MATLAB[®] analysis utilities processed the raw numeric results into useful figures and plots.

A total of 10 cases were performed under varying model configurations, SED characteristics, and GPS ground station distributions, for 26 runs in all. Table 8 gives a complete list of these runs and their variations. More details on each run will be presented in the next chapter.

The GAIM-GM model used in this research was based on version 2.8.1 that AFWA uses operationally, but with three slight adjustments. First, the GPS ground station and satellite biases were deactivated because the simulated GPS ground stations and satellite constellation had no biases. Second, GAIM-GM's internal algorithm that subtracts out the plasmaspheric contribution to TEC was deactivated. Aside from the minor GAIM-GM/IFM ceiling difference described in Table 7, the IFM density background had precisely known values and there was no extra plasmasphere layer. Third, Cases 2 through 7 were run using a special version of GAIM-GM that assigned a high amount of trust, or heavier weight, to assimilated data. While this was useful for testing GAIM-GM's capabilities to resolve a relatively small storm feature, there are hazards in placing too much trust in observations, especially if the data is erroneous. Case 6 illustrates this point by reducing all slant TEC measurements at the Freeport, Ohio GPS station by a factor of 4 to simulate bad data, which in reality could be caused by instrument malfunction or improper calibration.

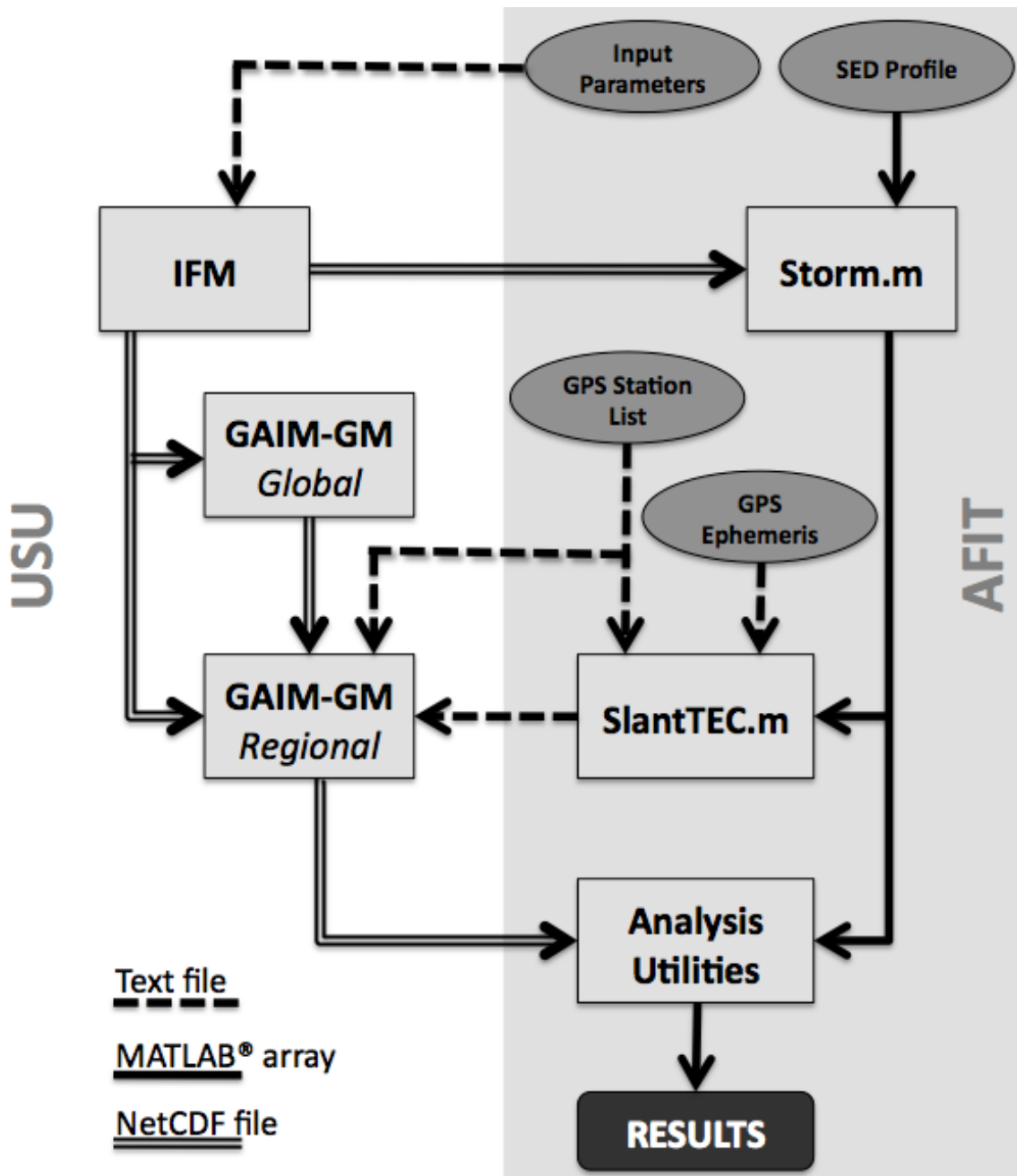


Figure 20. GAIM-GM model run flowchart

3.7 Analysis Techniques

Several analysis methods were applied to extract useful results from the GAIM-GM output. The statistics derived from these methods were expressed in: 1) differences (for TEC and electron density); 2) percentage differences; 3) mean absolute errors (MAEs); and 4) skill scores.

Difference plots are self-explanatory and provide a fast way to visualize the differences between two model runs. Two-dimensional latitude by longitude plots were used to compare TEC, while two-dimensional longitude by altitude electron density plots were used to identify differences in electron density vertical profiles. The difference at a single grid square is simply the value of first output minus the second output. The percentage difference at a single grid square, $DIFF_m$, is:

$$DIFF_m = \left(\frac{SPECI_m - REF_m}{SPECI_m} \right) \times 100 \quad (4)$$

where $SPECI_m$ is the GAIM-GM specification of interest and REF_m is a reference that can be either a GAIM-GM or IFM specification.

MAE is an accuracy measure that is sometimes used instead of root mean square error (RMSE) because it is not as sensitive to outlying data (*Hyndman and Koehler, 2005*). For these results, MAE applied only to TEC output and was used to measure how much the entire GAIM-GM map differed from the IFM background at a given time step. One value is generated for each time step, according to the formula:

$$MAE = \frac{1}{N} \sum |TEC_{GAIM}^{Grid} - TEC_{IFM}| \quad (5)$$

where TEC_{IFM} is the IFM TEC value and TEC_{GAIM}^{Grid} is the GAIM-GM TEC value for a given GPS ground station grid.

Skill scores are commonly used by meteorologists but can easily be applied to space

weather applications. These scores are generally defined as measures of the relative accuracy of forecasts produced by two forecasting systems, one of which is a reference system – such as climatology. Positive skill (in other words, favorable differences in accuracy) typically represents a minimal level of acceptable performance for a set of forecasts. A forecast receives a positive skill score if it matches observations more accurately than the climatology; if it is less accurate than the climatology, it receives a negative skill score (*Murphy, 1988*).

In the context of this research, skill scores measure how well a GAIM-GM model specification reproduces the IFM background with imposed SED, compared to a reference GAIM-GM specification that is also attempting to reproduce the IFM. The reference specification is the GAIM-GM AFWA grid solution, which represents AFWA’s current capabilities using its 12 GPS ground stations over the vicinity of CONUS. The formula for these skill scores was taken from a previous study that evaluated how well GAIM-GM and the IFM performed with respect to the IRI over Australia during 2004 (*Sojka et al., 2007*).

To find the skill score, first the RMSE scores are determined for the desired GAIM-GM grid specification and also for the GAIM-GM AFWA specification, given respectively as:

$$Score\ GAIM_{Grid} = \frac{1}{N} \sqrt{\sum (TEC_{IFM} - TEC_{GAIM}^{Grid})^2} \quad (6)$$

and

$$Score\ GAIM_{AFWA} = \frac{1}{N} \sqrt{\sum (TEC_{IFM} - TEC_{GAIM}^{AFWA})^2} \quad (7)$$

These scores are then combined to generate the *GAIM skill score*, which is:

$$GAIM_{SKILL}^{Grid} = \left(1.0 - \frac{Score\ GAIM_{Grid}}{Score\ GAIM_{AFWA}} \right) \times 100 \quad (8)$$

The skill scores are expressed as points and are positively bounded at 100 when

a GAIM-GM grid specification exactly matches the IFM background. Positive skill scores imply that the grid specification was more accurate than the reference AFWA specification, while negative scores indicate the AFWA specification was more accurate. Values of zero imply that both specifications were equivalent in reproducing the IFM background.

Although skill scores and MAEs are typically taken over an entire map, they can also be computed for just certain portions of the map. With careful coordinate indexing they can be customized to track a moving feature, or conversely everything except the moving feature, which is exactly what the MATLAB[®] utility *ScoreGAIM.m* did. It took the SED’s exact size and trajectory from matrices in *Storm.m* and created a sampling grid that moved with the SED (see Figure 15) and calculated skill scores and MAEs for just that area. It also derived skill scores and MAEs for everything except the SED by treating the moving sampling grid as a void in the map and scoring everything but that void. Developing statistics for these three domains (entire grid, the SED only, and everything but the SED) allowed for a more robust analysis of GAIM-GM’s accuracy.

In addition to the skill score and MAE plots, unique skill score maps were created to display scores over a two-dimensional latitude by longitude grid. The formula for each grid square on these maps is similar to Equation 8 except averages are not taken over the entire grid. Each grid square is scored as:

$$GAIM_{SKILL\ MAP}^{Grid} = \left(1.0 - \frac{(TEC_{IFM} - TEC_{GAIM}^{Grid})^2}{(TEC_{IFM} - TEC_{GAIM}^{AFWA})^2} \right) \times 100 \quad (9)$$

As shown in the next chapter, these skill score maps use a 64-hue color scale, where green tones show positive scores and brown tones show negative scores. White areas represent zero values where the grid specification was equivalent to the AFWA specification.

3.8 Data Visualization

Just as skill score maps can provide more insight than numbers alone, data visualization allows for quick and easy interpretation of the enormous amounts of data produced by GAIM-GM during this research. All data visualization products were created in MATLAB[®], to include: 1) GPS ground station maps; 2) GPS ground station density maps; 3) TEC maps; 4) TEC difference maps; 5) electron density latitude slices; 6) electron density difference profiles; 7) MAE plots; 8) skill score graphs; and 9) skill score maps.

The GPS ground station and density maps were relatively easy to create, requiring nothing but a spreadsheet of 4-digit station identifiers and coordinates as input. The TEC and electron density maps were a more difficult chore to produce and required extracting thousands of two-dimensional and three-dimensional arrays from NetCDF output files and loading them into four-dimensional arrays under a stringent system of bookkeeping. Although massive in size, the four-dimensional arrays dramatically reduced the number of variables required to contain the 24 hours worth of TEC and electron density specifications for each individual model run. The tradeoff for ease of use was higher computational demands. Workstations lacking 64-bit operating systems and at least 4 gigabytes of random access memory were incapable of running some of the MATLAB[®]utilities. Copies of the MATLAB[®]utilities from this project with concise operating instructions instructions may be requested from the author.

Table 8. Complete list of GAIM-GM regional mode runs

Case	GAIM-GM	GPS Grid	IFM	Variations
0 ^a	Normal	None	Normal	
1-A	Normal	AFWA	Normal	
1-B	Normal	AFWA+30	Normal	
1-C	Normal	AFWA+100	Normal	
1-D	Normal	AFWA+200	Normal	
1-E	Normal	AFWA+400	Normal	
2-A ^b	Modified	AFWA	Normal	
2-B	Modified	AFWA+30	Normal	
2-C	Modified	AFWA+100	Normal	
2-D	Modified	AFWA+200	Normal	
2-E	Modified	AFWA+400	Normal	
3-A	Modified	Ideal 21	Normal	
3-B	Modified	Ideal 90	Normal	
3-C	Modified	Ideal 360	Normal	
3-D	Modified	Ideal 720	Normal	
4	Modified	AFWA+100	Normal	SED raised up in altitude
5	Modified	AFWA+400	Normal	Time Constant reduced to 1
6	Modified	AFWA+100	Normal	One GPS station gave bad data
7	Modified	Ideal 21	Normal	GPS station grid reversed left-right
8-A ^c	Normal	AFWA	Depleted	
8-B	Normal	AFWA+30	Depleted	
8-C	Normal	AFWA+100	Depleted	
8-D	Normal	AFWA+200	Depleted	
8-E	Normal	AFWA+400	Depleted	
9	Normal	AFWA	Depleted	Time Constant reduced to 1
10	Normal	AFWA	Depleted	Elevation Mask raised to 45°

^a Zero station baseline run. Since there was no data assimilation, the version of GAIM-GM used and GPS station grid type had no effect on the output

^b Cases 2-A through 7 were not run in GAIM-GM 2.8.1, but a modified version of GAIM-GM that assigns more trust to assimilated data

^c Cases 8-A through 10 took all slant TEC measurements though an IFM background where all densities north of 30° N latitude (excluding the SED) were depleted by a factor of 4 during the storm period, 1800 - 2045 UT

IV. Results and Analysis

4.1 Chapter Overview

The objective of this research is to quantify how many ground GPS receivers are needed in CONUS to provide GAIM-GM with sufficient data to create reliable GPS/TEC correction maps during geomagnetic storms. The results presented in this chapter will show how varying the number of GPS ground stations, under several different scenarios, affected the accuracy of TEC maps. Ten separate cases were examined and each case comprises one section of this chapter.

Sections 1 and 2 discuss using the CORS grids to reproduce the synthetic SED in the normal and modified versions of GAIM-GM, respectively, while Section 3 discusses applying the Ideal grids to modified GAIM-GM. Sections 4 through 7 examine the following unique situations: 4) modeling a high-altitude synthetic SED; 5) reducing the Time Constant from 5 down to 1; 6) introducing simulated erroneous data into GAIM-GM via one bad station; and 7) reversing the layout of the 21-station Ideal grid. The 8th section discusses the results of depleting the IFM background around the SED to simulate the real SED from 20 Nov 2003 (see Figure 12). Lastly, Sections 9 and 10 examine the effects of reducing the Time Constant from 5 to 1 and raising the Elevation Mask from 15° to 45° in the depleted IFM environment.

4.2 Baseline Run with Zero GPS Ground Stations

The baseline run was simply the default output from GAIM-GM when no slant TEC measurements were assimilated. It is important to understand how GAIM-GM performs in the absence of data, using only the internal IFM background and error covariance matrix to build a solution (see Section 2.5.3). First note that because of the error covariance matrix, which contains an IFM climatology from 1107 model

runs, GAIM-GM does not make an exact replica of the IFM density background in the absence of external data. Rather, the Kalman filter imposes perturbations from the error covariance matrix onto the IFM background densities, yielding a slightly modified solution.

Figure 21 illustrates this by comparing IFM TEC output to GAIM-GM TEC output with no data assimilation for year 2001, day 172, at 1945 UT. The IFM’s geophysical input parameters were listed previously in Table 2 and are the same for every model run in this project. Note in 21(b) how GAIM-GM has lower TEC values than the IFM, by an average of 3.8 TEC units. The IFM tends to produce erroneously high TEC values during geomagnetic activity (*Schunk et al.*, 2010), and so even without ingesting data GAIM-GM provided a specification with slightly lower TEC values than the IFM.

4.3 Case 1: Normal GAIM-GM and CORS Grids

This case examined GAIM-GM’s ability to reproduce the synthetic SED using the five different CORS grids. Figure 22 shows the IFM TEC background compared to the GAIM-GM TEC specifications at 1945 UT. The GAIM-GM specifications visually showed increasing improvement in matching the IFM background as GPS ground stations were added to the existing AFWA grid, due to more slant TEC measurements.

The vertical electron density profiles at 40° N latitude for each model run also improved as the station count increased. Adding 30 ground stations to the AFWA list caused the most visible improvement from one run to the next, as seen in Figure 23. The unit for these density plots is *electrons/cm⁻³*. The highest density obtained in the AFWA grid (see Figure 23(a)) was 1.35×10^6 *electrons/cm⁻³*, compared to 1.69×10^6 *electrons/cm⁻³* in the AFWA+30 grid (see Figure 23(b)). Clearly more

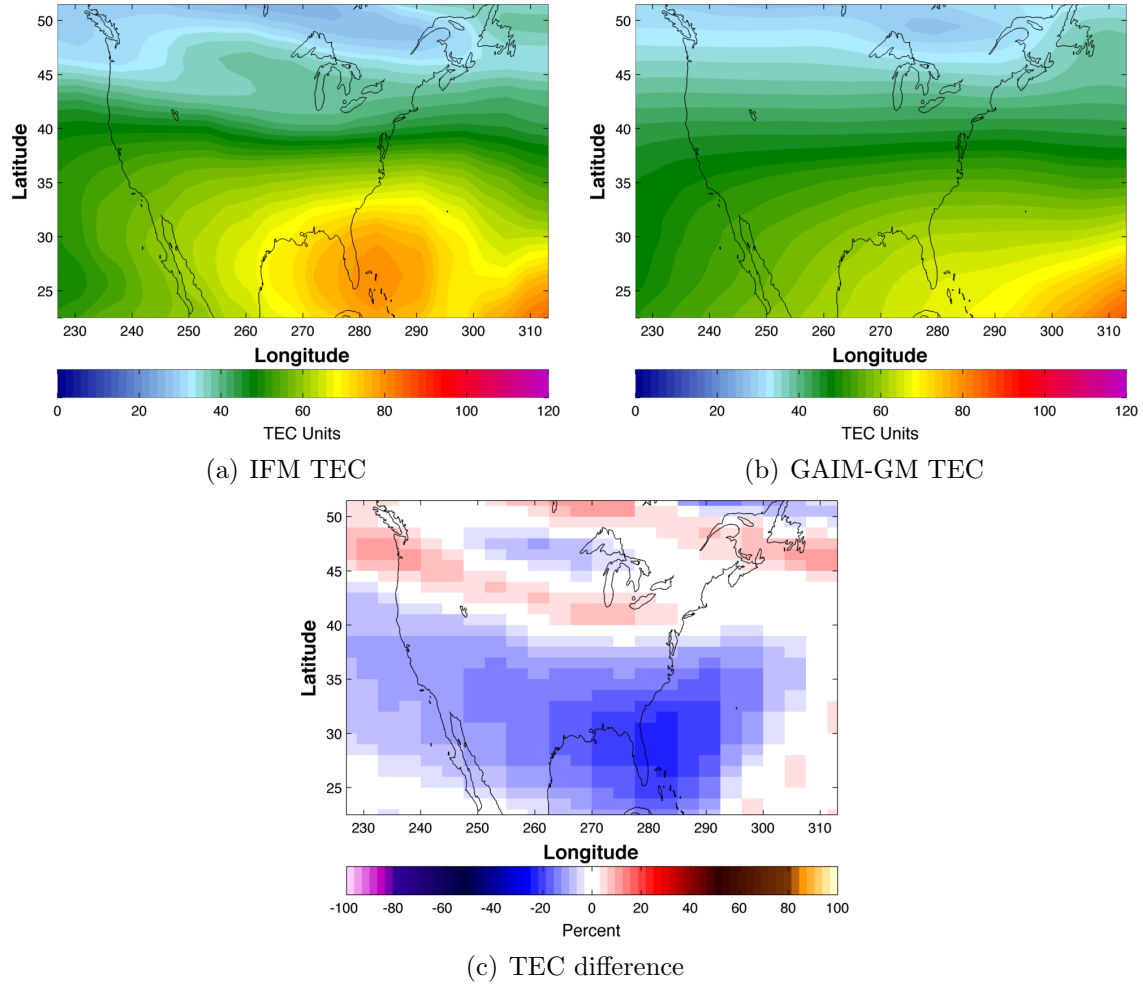


Figure 21. Comparison of IFM and GAIM-GM TEC specifications using zero GPS ground stations at 1945 UT. The difference of (b) - (a) is given in (c). Even though GAIM-GM falls back on the IFM density background when no data is available, GAIM-GM's internal error covariance matrix adjusts the solution based on climatology from 1107 archived IFM runs (see Section 2.5.3), causing the output to vary from the IFM

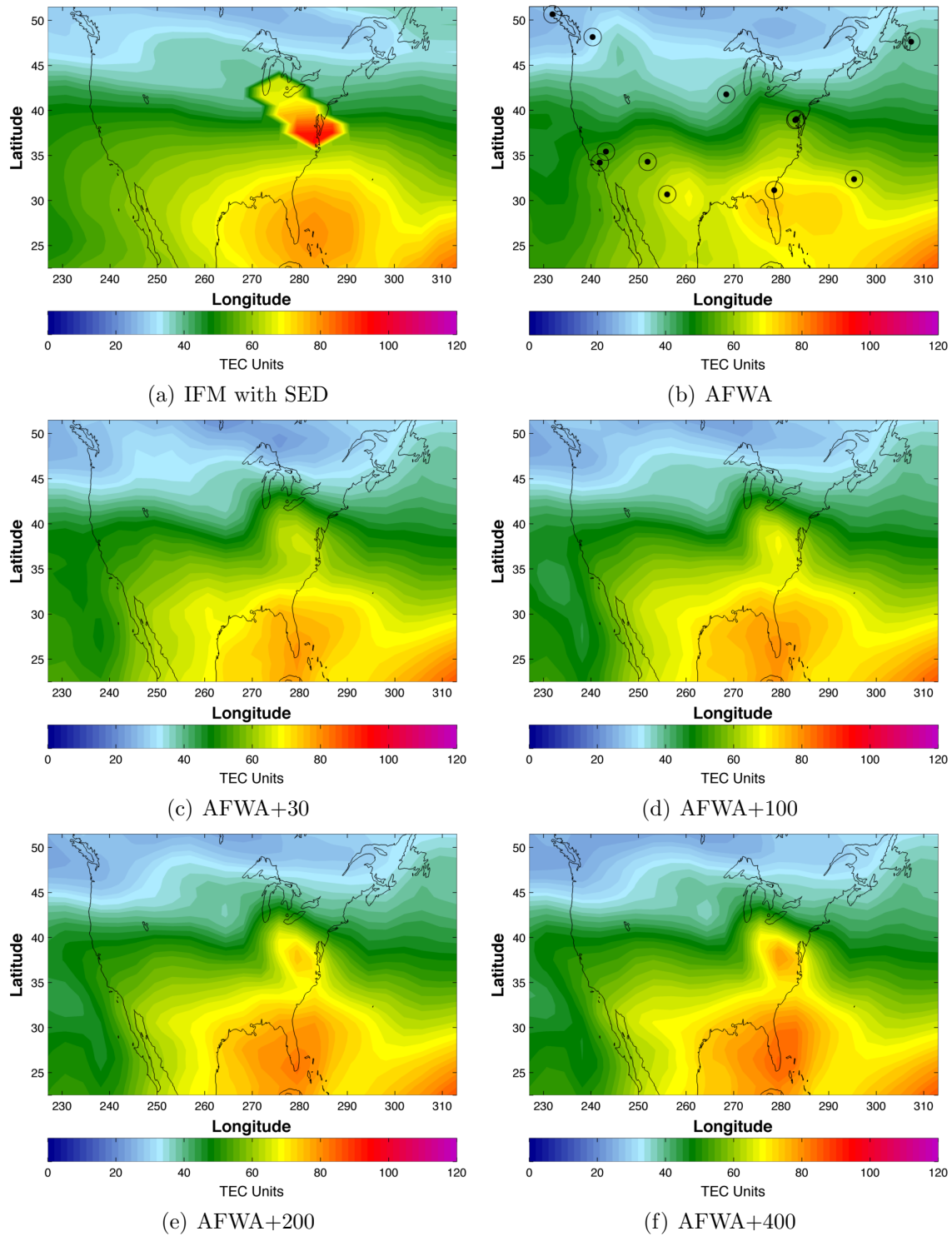


Figure 22. GAIM-GM TEC reproduction of the synthetic SED at 1945 UT, using slant TEC data from the CORS grids. The synthetic SED in the IFM background is shown in (a) as a reference and the locations of the 12 AFWA ground stations are shown as black double circles in (b). GAIM-GM resolution for this and all subsequent figures is 1° latitude by 3.75° longitude

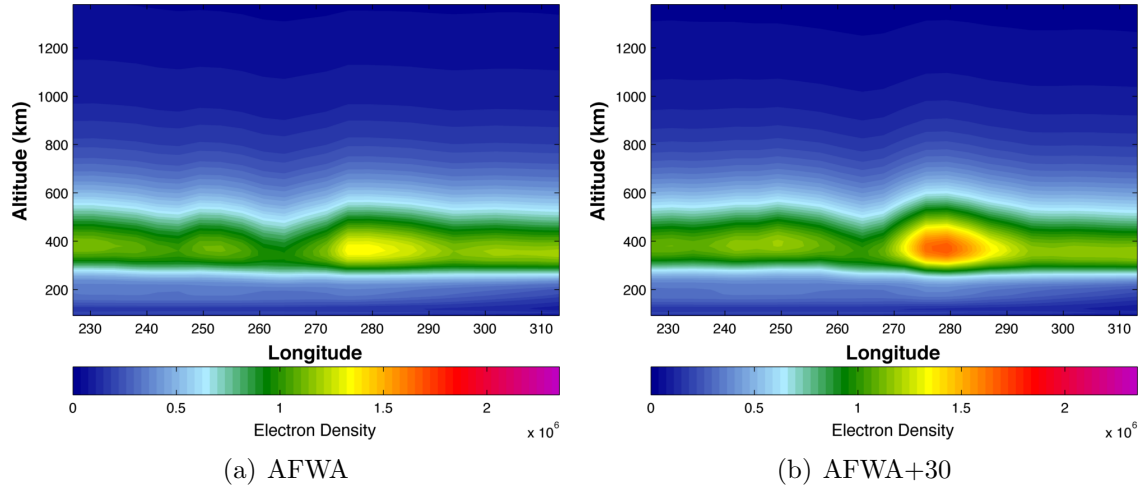


Figure 23. GAIM-GM electron density reproduction of the synthetic SED, using the CORS grid at 1945 UT. Latitude slices at 40° N are shown for the AFWA grid (a) and AFWA+30 grid (b). The high-density core of the SED is resolved much more accurately when 30 stations are added to the AFWA grid

slant TEC piercings from a denser ground station network allowed the AFWA+30 grid to take more cuts through the SED core, improving its solution. The actual IFM background density reached as high as 2.29×10^6 *electrons/cm⁻³* in the core of the IFM synthetic SED (not shown). Output from the AFWA+100, AFWA+200, and AFWA+400 runs appeared very similar to Figure 23(b) and are not presented.

A direct comparison of the GAIM-GM TEC to the IFM TEC for the AFWA and AFWA+30 grids is shown in Figure 24. This type of plot is useful for quickly identifying where GAIM-GM performed best at reproducing the IFM background. The AFWA+30 grid results in Figure 24(b) have much more white areas, indicating overall better IFM reproduction than the AFWA grid results. Note the red pixels (positive differences) immediately outside the SED area in Figure 24(b). Here GAIM-GM had difficulty resolving the sharp edge of the SED where IFM densities abruptly doubled, and instead smoothed the high TEC values over a broader area.

The percentage TEC difference between the AFWA and AFWA+30 GAIM-GM runs is shown in Figure 25(a). To the right, Figure 25(b) is a skill score map showing

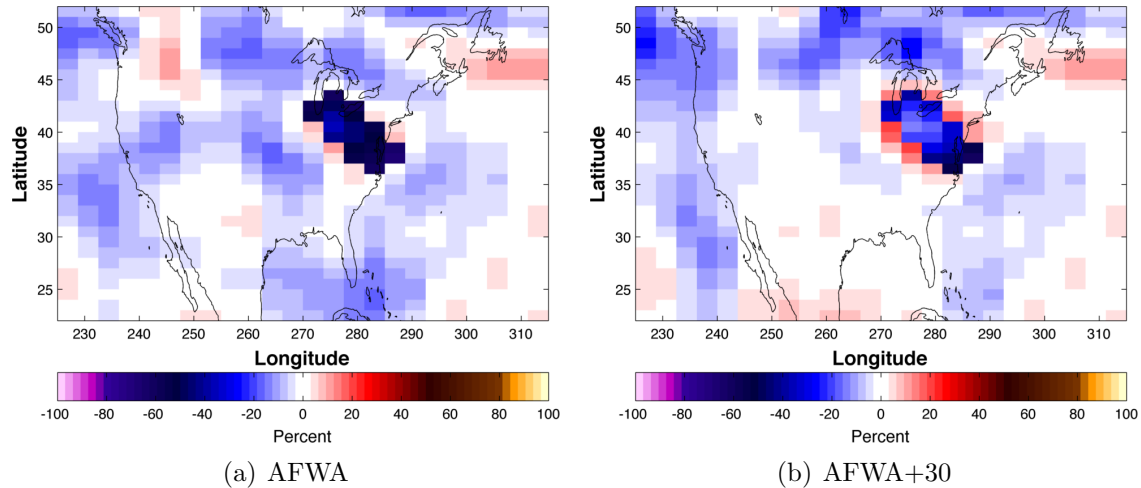


Figure 24. TEC difference between GAIM-GM and IFM background at 1945 UT. The IFM was subtracted from the GAIM-GM AFWA grid specification to create (a), while (b) shows the IFM subtracted from the GAIM-GM AFWA+30 grid specification. The SED’s location is clearly indicated by the dark blue patches where GAIM-GM differed most from the IFM. White regions indicate where GAIM-GM reproduced the IFM background with very little error

where the AFWA+30 grid improved over the AFWA grid in reproducing the IFM background. It is important to understand that TEC difference plots do not show accuracy improvement, whereas a skill score map does. Notice how the AFWA+30 grid had positive skill scores directly over the SED but negative skill scores around the SED periphery, due to the sharp gradient effect explained in the previous paragraph. Also notice how adding 30 stations to CONUS understandably did little to improve accuracy over the data sparse Atlantic Ocean, as indicated by the white area in the right side of Figure 25(b).

Average skill scores per time step for all five runs during the 1800 – 2045 UT storm period are presented in Figure 26. A plot of the SED’s trajectory is given in Figure 26(a) as a reference. For the SED-only domain, all scores were nearly identical until about 1900 UT because up to that time Bermuda was the only data source for all grids. As the SED neared the East Coast, the higher-density grids provided more slant TEC data, causing their skill scores to increase faster than the low density grids.

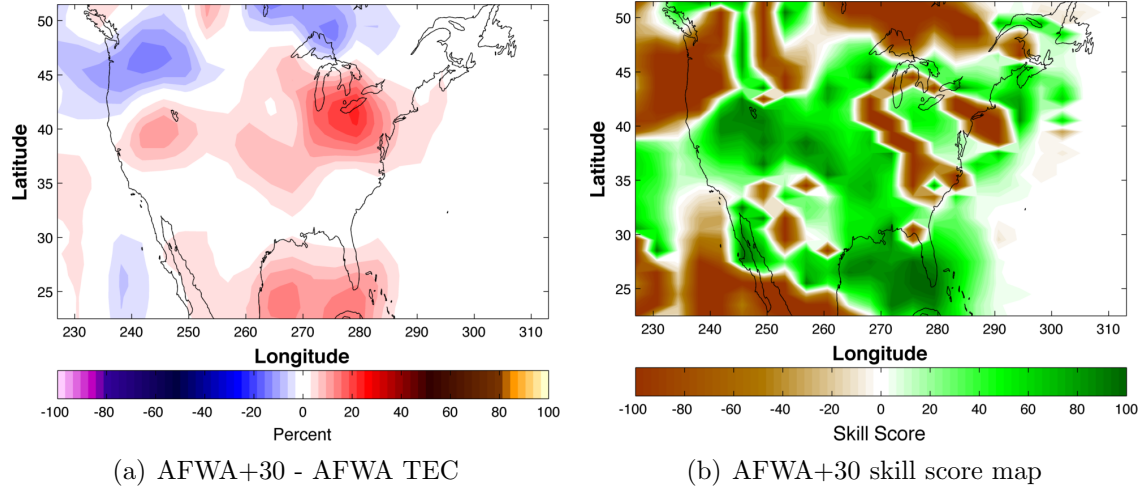


Figure 25. TEC difference and skill score map for the AFWA+30 grid at 1945 UT, compared to the AFWA grid. The AFWA grid TEC was subtracted from the AFWA+30 grid TEC to yield (a), while (b) is the AFWA+30 grid skill score. Greens in the skill score map show where the AFWA+30 grid was more accurate than the AFWA grid in reproducing the IFM background, while brown colors show where it was less accurate. Note that TEC difference maps cannot indicate areas of accuracy improvement over the AFWA grid, whereas skill score maps can

A different phenomenon was responsible for the skill score pattern seen in Figure 26(d), where scores for all areas outside the SED declined once the SED reached the mainland. Recall that the densely populated GPS station grids provided more slant TEC piercings through the SED than the sparsely populated grids. Because GAIM-GM could not resolve the sharp boundary of the SED, it spread high-density plasma perturbations from within the SED to areas outside of the SED. These errors accumulated with time as GAIM-GM’s default Time Constant setting of 5 hours held the high-density perturbations in the grid and propagated them downstream (i.e. to the west), causing skill scores outside the SED to decrease. By 2045 UT all skill scores had begun to improve, most likely because SED perturbations were less dense at higher latitudes and caused smaller TEC errors.

Table 9 gives an average of the time-dependent skill scores for each run over the 1800 – 2045 UT storm period. It must be noted that the skill scores for all

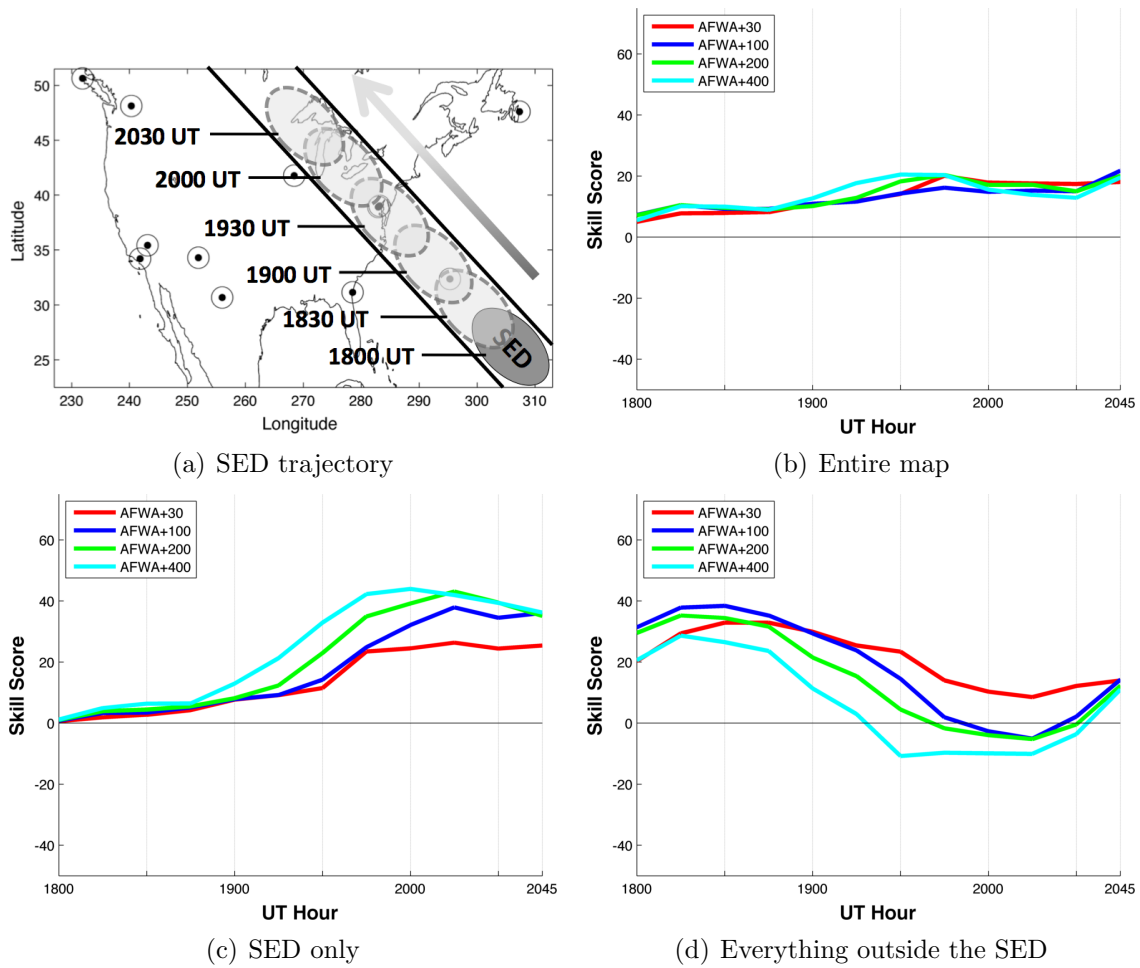


Figure 26. Skill scores for the CORS grids during the storm period from 1800 to 2045 UT. Compared are the accuracy improvement over the AFWA grid for three domains: (b) the entire map, (c) SED only, and (d) everything outside the SED. The trajectory of the SED is shown in (a) as a reference. Scores above zero indicate the grid was more accurate at reproducing the IFM background than the AFWA grid, while scores below zero indicate worse accuracy

results depended on the SED size and trajectory, as well as the specific combination of settings used in GAIM-GM. The zero station scores were all negative, indicating worse accuracy than that produced by the 12-station AFWA grid. Skill scores for the entire map stayed within 1 point for all five runs, while SED-only skill scores showed steady improvement as station counts increased. Conversely, scores for areas outside the SED, while better in all cases than the AFWA grid scores, actually decreased as the number of stations increased. The price for better accuracy in the SED-only domain was a reduction in accuracy everywhere else, but most notably in the region immediately surrounding the SED, as was shown in Figure 25(b). Because GAIM-GM could not resolve the SED’s sharp edges well, adding more GPS stations caused more erroneous density perturbations to accumulate around the SED periphery.

Table 9. Summary of Case 1 average skill scores. Standard deviations are given in parenthesis to the right of each score

Domain	No stations	AFWA +30	AFWA +100	AFWA +200	AFWA +400
Entire map	-19.0 (11.0)	13.1 (5.1)	13.0 (4.0)	13.9 (4.6)	14.0 (4.9)
SED only	-10.2 (7.5)	13.5 (10.5)	17.5 (14.4)	20.8 (16.6)	24.1 (16.9)
Outside SED	-39.1 (24.0)	21.1 (13.1)	18.4 (14.8)	14.4 (15.7)	6.7 (16.0)

4.4 Case 2: Modified GAIM-GM and CORS Grids

The same CORS grids from Case 1 were applied in Case 2, which used the modified version of GAIM-GM that assigns more weight to ingested data. Figure 27 shows the TEC results from the five model runs at 1945 UT, compared to the IFM background with imposed SED. In contrast to Figure 22, the SED was resolved more clearly. Notice there was very little change in TEC beyond the AFWA+30 grid.

Comparing GAIM-GM minus IFM difference plots at 1945 UT to those from Case 1 (see Figure 24), the modified GAIM-GM solution did better at reproducing

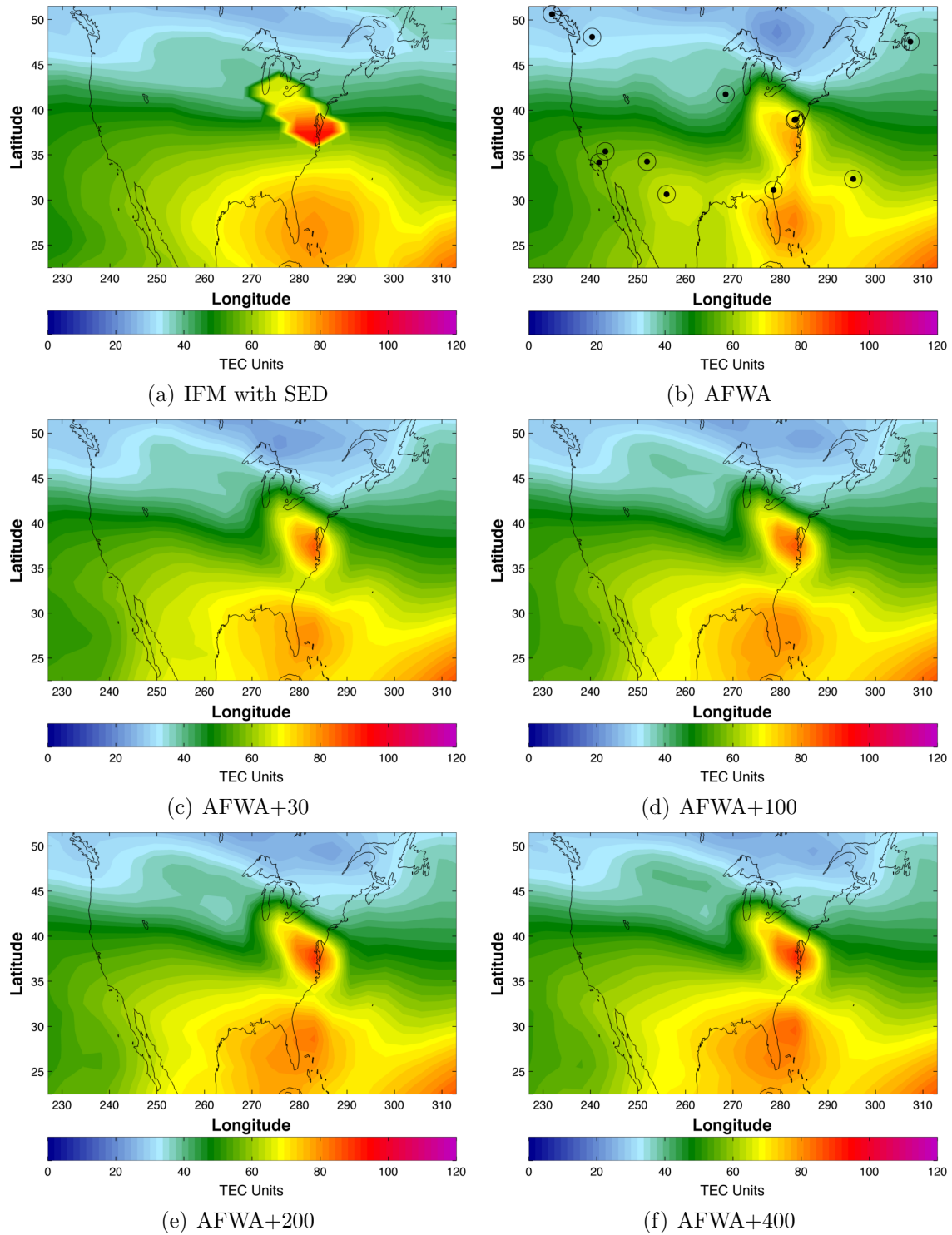


Figure 27. GAIM-GM TEC reproduction of the synthetic SED at 1945 UT, using GPS slant TEC data from the CORS grid. Note that the synthetic SED in the IFM background is shown in (a) as a reference and that the 12 AFWA ground stations are plotted in (b) as black circles

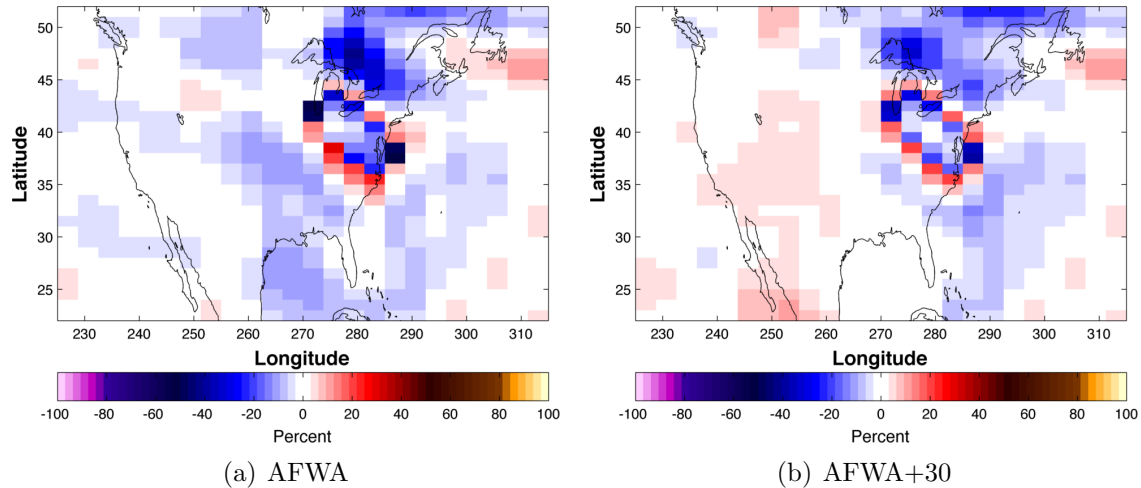


Figure 28. TEC difference between GAIM-GM and IFM background at 1945 UT. The IFM was subtracted from the GAIM-GM AFWA grid specification to create (a), while (b) shows the IFM subtracted from the GAIM-GM AFWA+30 grid specification. The SED’s location is clearly indicated by the dark blue patches where GAIM-GM differed most from the IFM. White regions indicate where GAIM-GM reproduced the IFM background with very little error

the IFM. In Figure 28(a) the white pixels within the SED indicate that GAIM-GM fully replicated some of the IFM TEC values using the 12 station AFWA grid. The GAIM-GM solution improved further in Figure 28(b) when 30 more stations were added, most notably over the the central U.S. and Gulf of Mexico.

The skill scores for Case 2 are given in Figure 29. The overall trends are similar to those for Case 1 but exhibit a more jagged appearance. Note that many of the sharp drops in skill score occurred when the SED was over one of the AFWA grid stations. At those times, the AFWA grid had direct vertical TEC measurements of the SED as it passed over GPS stations, resulting in lower errors for the SED-only domain. The CORs grids with additional stations did not necessarily perform poorly at those times, but rather the AFWA grid performed exceptionally well. For instance, whenever the SED passed over an AFWA station, the SED was measured well and the AFWA grid RMSEs decreased, which in turn lowered the skill scores for all other grids (see Equation 8). Also note in Figure 29(c) that skill scores for the SED-only

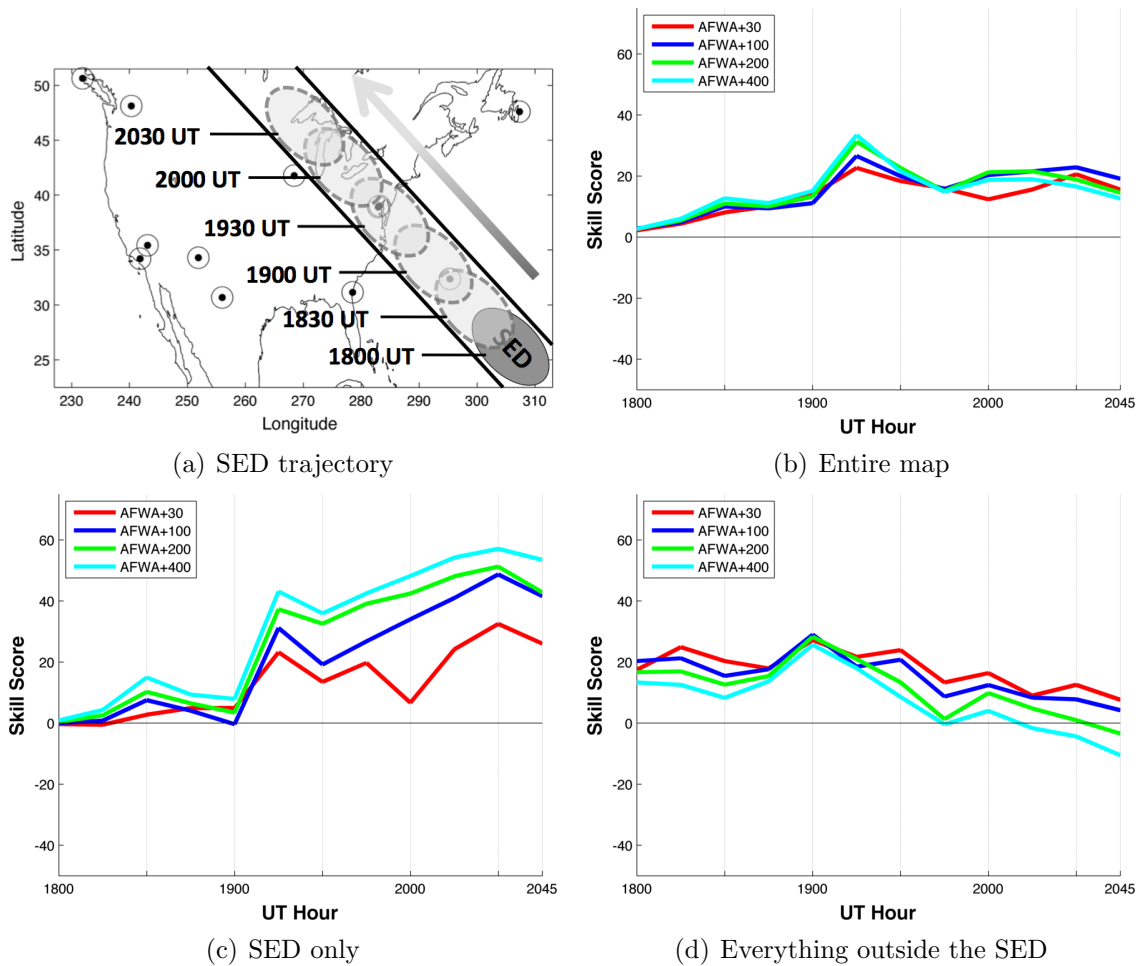


Figure 29. Skill scores for each of the CORS grids during the storm period from 1800 – 2045 UT. Compared are the accuracy improvement over the AFWA grid for three domains: (b) the entire map, (c) SED only, and (d) everything outside the SED. The trajectory of the SED is shown in (a) as a reference

domain increased as the number of stations increased, whereas in Figure 29(d) skill scores decreased for everything outside the SED as stations increased. This interesting relationship was also seen in Case 1.

Table 10 summarizes the skill scores for all five runs by averaging the time-dependent scores over the 1800 – 2045 UT storm period. For the domains of the entire map and SED only, these scores were an average of 10% and 21% higher, respectively, than the scores in Case 1. For the domain of outside the SED, they were

an average of 15% lower than Case 1. Again it appeared that the entire map domain saw little benefit from adding more than 30 stations to the AFWA grid, whereas the SED-only domain saw a steady increase in accuracy. All areas outside the SED had a steady decline in accuracy as stations increased. Note that the zero station solutions in all three domains were 50 – 60 skill score points below the AFWA grid (compared to 10 – 40 points below the AFWA grid for Case 1). This demonstrated the modified version of GAIM-GM’s impressive ability to reproduce the SED with smaller amounts of assimilated data.

Table 10. Summary of Case 2 average skill scores. Standard deviations are given in parenthesis to the right of each score

Domain	No stations	AFWA +30	AFWA +100	AFWA +200	AFWA +400
Entire map	-60.0 (19.1)	13.3 (6.2)	15.4 (7.6)	15.6 (8.0)	15.4 (7.8)
SED only	-64.2 (31.5)	13.1 (11.5)	21.2 (18.3)	26.4 (19.9)	31.0 (21.7)
Outside SED	-56.6 (41.0)	17.7 (8.3)	15.4 (7.3)	11.5 (7.0)	7.3 (7.9)

4.5 Case 3: Modified GAIM-GM and Ideal Grids

This section introduces results from the Ideal grids, comprising 21, 90, 360, and 720 evenly spaced, artificial GPS ground stations (see Figure 18). These grids were created with the goal of finding the best possible GPS receiver distribution over the CONUS area without the location restrictions of the current CORS network.

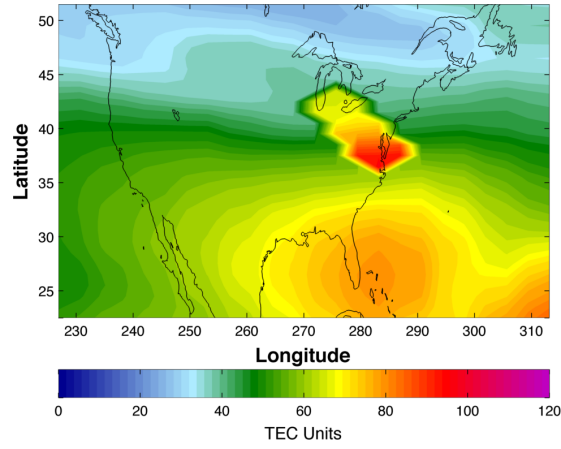
Figure 30 shows the TEC results from the four GAIM-GM model runs at 1945 UT, compared to the IFM background with imposed SED. At this time the highest TEC value in the IFM synthetic SED was 98.9 TEC units. The Ideal 21 grid reached a max of 75.7 TEC units within the SED, followed by 80.1, 87.6, and 88.1 TEC units for the Ideal 90, Ideal 360, and Ideal 720 grids, respectively. These values indicate that GAIM-GM’s accuracy in the SED-only domain improved as station count increased,

as expected. Nevertheless it was surprising that doubling the number of stations from 360 to 720 only yielded a 0.5 TEC unit increase in the maximum reproduced TEC value.

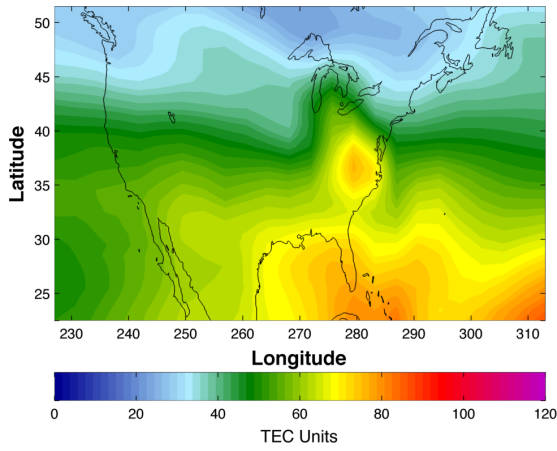
The greatest advantage the Ideal grids had over the CORS grid was the reduction of data sparse areas. This is illustrated in Figure 31, which gives differences between the GAIM-GM specifications and the IFM background for the AFWA grid (31(a)) and Ideal 90 grid (31(b)). Note particularly the Gulf of Mexico and Atlantic Ocean areas. The Ideal 90 grid had GPS receivers over these regions and was able to drastically improve its specification of the IFM background, as opposed to the CORS AFWA grid.

The skill score graphs against the AFWA grid are given in Figure 32. There are a three key features. First, since the Ideal grids covered the entire GAIM-GM model grid, their skill scores were not as dependent upon the SED's location as the scores for Cases 1 and 2 were. The Ideal 21 grid was an exception, since GPS stations were so widely separated that the SED's path over those stations had a strong effect on skill scores. More on that topic will be presented in Case 7. Second, the skill scores changed more drastically between the two least-dense Ideal grids than they did between the two least-dense CORS grids. This was likely due to the rapid decrease in average distance between stations (as shown in Table 6). Third, the Ideal 360 and Ideal 720 grids gave very similar results for the entire map and SED-only domains, in spite of the 2x difference in ground station density. This suggests that slant TEC data saturation in GAIM-GM may have occurred before each model grid square contained an observation.

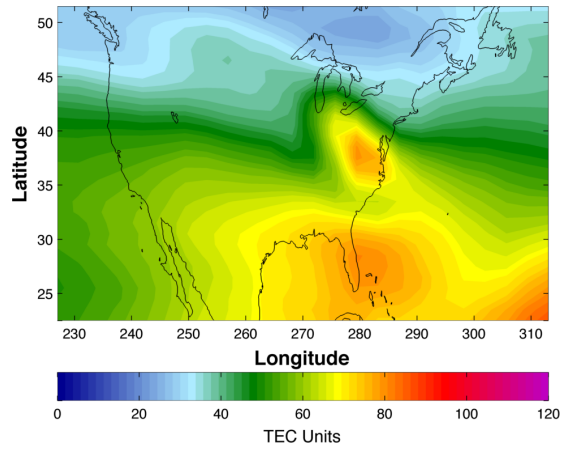
Table 11 lists the time-dependent skill scores averaged over the 1800 – 2045 UT storm period for all four Ideal grids. Owing to data sparsity, the Ideal 21 grid performed the worst with a 2.1 score for the entire map and -3.9 for the SED-only domain.



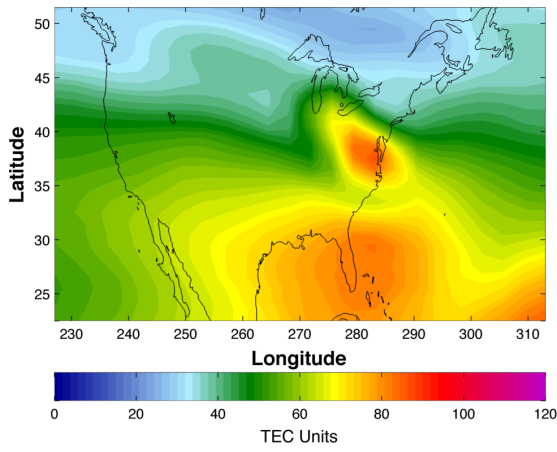
(a) IFM with SED



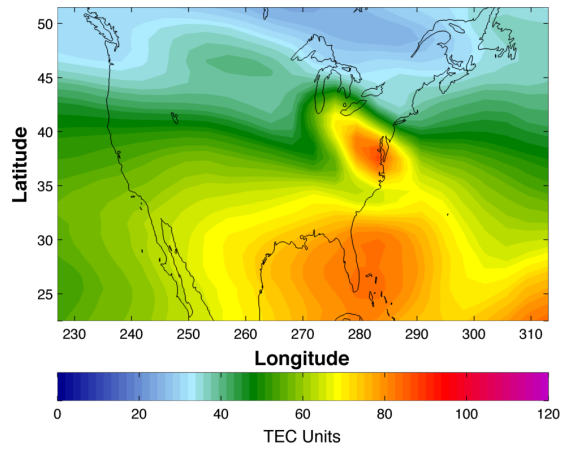
(b) Ideal 21



(c) Ideal 90



(d) Ideal 360



(e) Ideal 720

Figure 30. GAIM-GM TEC reproduction of the synthetic SED at 1945 UT, using GPS slant TEC data from the Ideal grids. The synthetic SED in the IFM background is shown in (a)

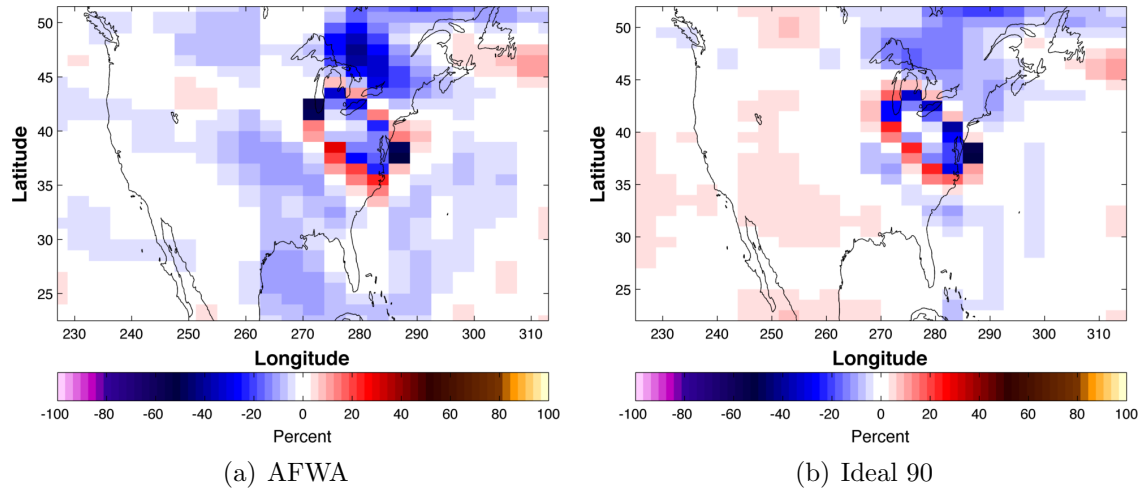


Figure 31. TEC difference between GAIM-GM and IFM background at 1945 UT. The IFM was subtracted from the GAIM-GM specification for the AFWA grid (a) and Ideal 90 grid (b). The SED’s location is clearly indicated by the dark blue patch where GAIM-GM differs most from the IFM. White regions indicate where GAIM-GM reproduced the IFM background with very little error

The Ideal 360 grid scored the highest for the entire map with 31.1 points. Skill scores for the SED-only domain steadily increased as GPS station counts increased, reaching a high of 47.0 with the Ideal 720 grid. However, the entire map domain had a lower score with 720 stations than with only 360 or 90 stations, indicating that errors outside the SED accumulated as station count increased.

Table 11. Summary of Case 3 average skill scores. Standard deviations are given in parenthesis to the right of each score

Domain	No stations	Ideal 21	Ideal 90	Ideal 360	Ideal 720
Entire map	-60.0 (19.1)	2.1 (15.5)	27.7 (7.0)	31.1 (5.8)	27.0 (8.9)
SED only	-64.2 (31.5)	-3.9 (25.4)	23.9 (12.1)	42.8 (6.8)	47.0 (6.9)
Outside SED	-56.6 (41.0)	8.7 (11.8)	31.8 (8.8)	18.1 (16.8)	6.4 (23.2)

4.6 Case 4: High-Altitude SED

Cases 4 through 7 are one-run scenarios (see Table 8 for descriptions), unlike the previous cases which were sets of runs using 4 – 5 different GPS station distributions.

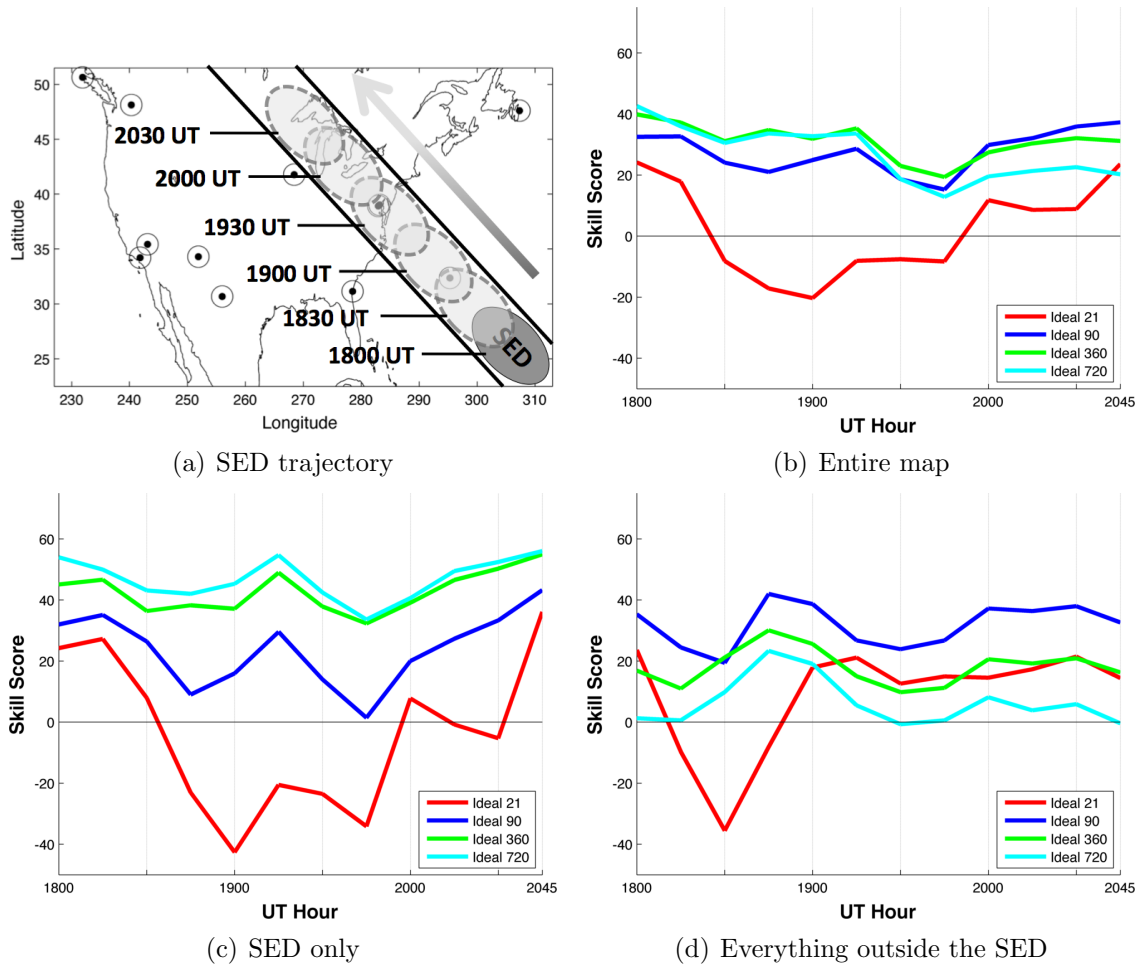


Figure 32. Skill scores for each of the Ideal grids during the storm period from 1800 – 2045 UT. Compared are the accuracy improvement over the AFWA grid for three domains: (b) the entire map, (c) SED only, and (d) everything outside the SED. The trajectory of the SED is shown in (a) as a reference

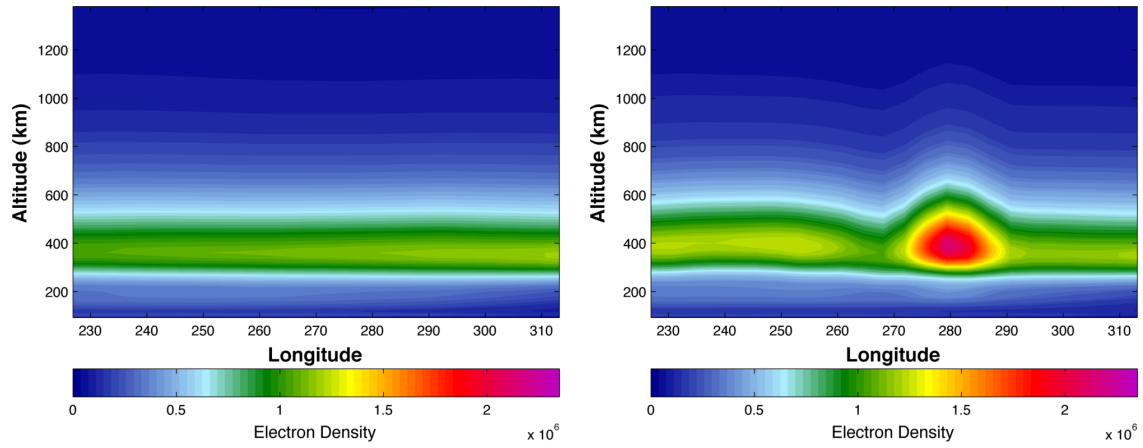
Each of these next cases has its own significant variation from the 3 previous cases and will shed additional light on GAIM-GM's abilities to create accurate TEC maps during geomagnetic storming, beginning with Case 4.

The motivation for this case is illustrated in Figure 33, which shows a sequence of GAIM-GM vertical density profiles from Case 1 for 1945 UT. Figure 33(a) is a specification with zero data assimilation, Figure 33(b) is a specification with the AFWA+100 grid, and Figure 33(c) gives the difference between the two. GAIM-GM correctly recreated the plasma enhancement in the SED layer from 200 – 600 *km*, but inaccurately increased electron densities in the rest of the vertical column when it should have left them alone. In other words, it put the SED exactly where the F₂ peak is climatologically expected to be. This raised the question: how well can GAIM-GM reproduce the vertical profile of a SED if the enhanced densities do not fall within the climatological boundaries of the F₂ peak?

To answer that question, a special high-altitude SED was designed. It used the same IFM background but the SED layer was set at 500 – 1000 *km* and all densities within this layer were enhanced by a factor of 4. Densities in the layer from 90 – 500 *km* were depleted by a factor of 2 to simulate the base of the SED being lifted (Figure 34(a)). Slant TEC measurements were taken using the AFWA+100 grid and loaded into the modified version of GAIM-GM, which was done to give the model the best chance of accurately reproducing the SED.

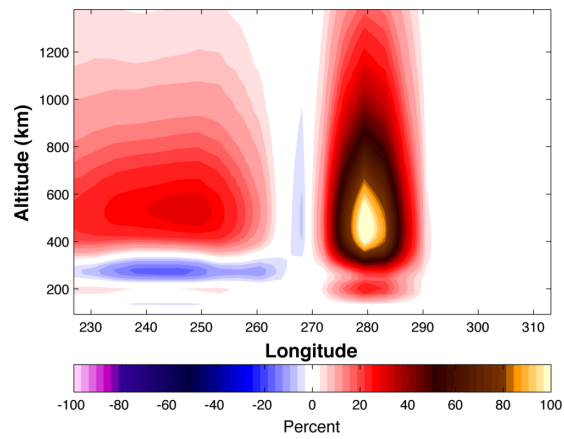
The results are shown in Figure 34(b). GAIM-GM only lifted the base of the SED about 50 *km* above the background, specifying it near 350 *km* instead of at 500 *km*. In the SED core GAIM-GM reached a maximum density of 1.09×10^6 *electrons/cm*⁻³, compared to the maximum of 3.34×10^6 *electrons/cm*⁻³ in the IFM.

This highlights one of the shortcomings of the Gauss-Markov version of GAIM, which presently does not include the horizontal winds nor low-latitude electric fields



(a) Zero Stations

(b) AFWA+100



(c) Density difference (b minus a)

Figure 33. Motivation for Case 4, taken from Case 2 vertical density profiles at 40° N latitude. Shown are 1945 UT specifications for: (a) GAIM-GM vertical profile with zero stations, (b) GAIM-GM vertical profile with AFWA+100 stations, and (c) the difference between the two. Note that GAIM-GM increased electron densities throughout the entire vertical column and not just in the 200 – 600 km SED layer

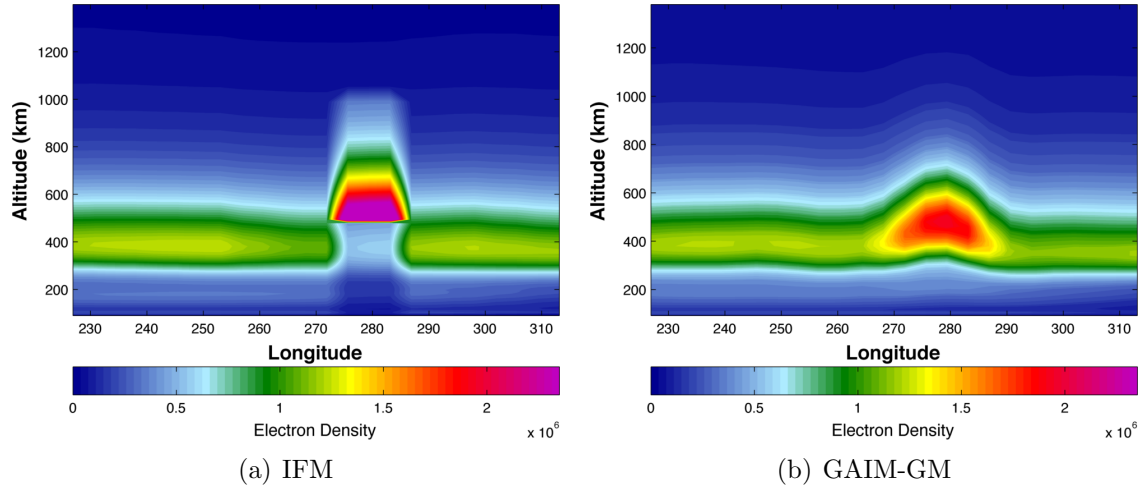


Figure 34. GAIM-GM electron density reproduction of the high altitude synthetic SED, using the AFWA+100 grid at 1945 UT. Both latitude slices were taken at 40° N. Note how GAIM-GM did not accurately capture the vertical profile of the SED

necessary to capture the vertical profile of the SED (*Scherliess, 2011*). A physics-based version of GAIM is currently under development at USU and is expected to significantly improve the 3-D plasma density reconstruction (*Scherliess, 2004*).

4.7 Case 5: Reduced Time Constant

The Time Constant determines how long ingested data are retained in GAIM-GM as density perturbations. The default Time Constant is 5 and causes perturbations from assimilated data to be held in GAIM-GM’s density perturbation matrix for 5 hours before being relaxed to zero. The purpose of the Time Constant is to retain ionospheric features detected by observations and propagate them over data sparse areas. For this case the modified version of GAIM-GM was run with the AFWA+400 grid and the Time Constant was reduced to 1. The results were then compared to those from Case 2.

Reducing the Time Constant caused the greatest effects off the western coast of CONUS and Mexico. Figure 35 is a difference plot at 1945 UT between Case 2-E

and Case 5 TEC specifications, where Case 2-E was subtracted from Case 5. The blue shading west of the Pacific Ocean coastline indicates that there was 4 – 7% less TEC in this area when the Time Constant was reduced. This is because the higher-value perturbations over CONUS, introduced from slant TEC data, were relaxed from the density perturbation matrix before they could propagate very far from their originating GPS ground stations. Smaller TEC differences also occurred over the mainland in the lee of dense GPS ground station areas.

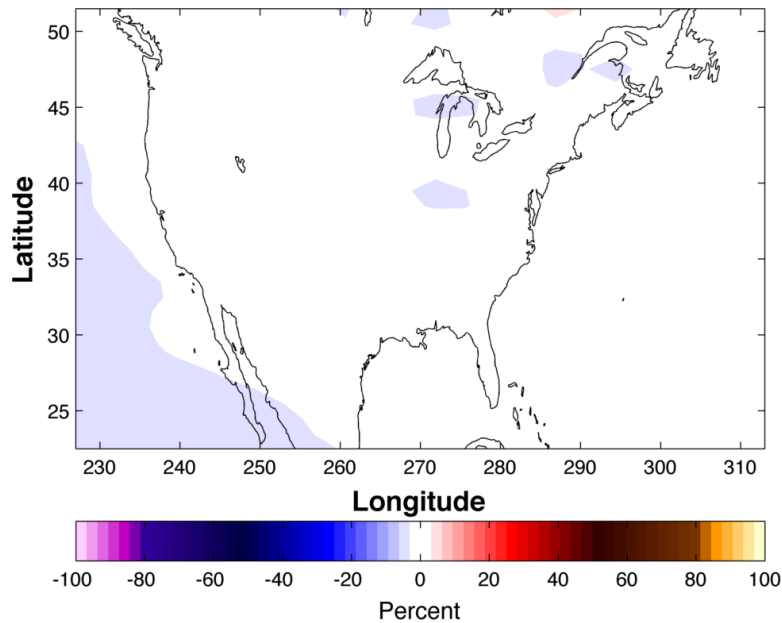


Figure 35. TEC difference at 1945 UT caused by lowering the Time Constant from 5 to 1 with the AFWA+400 grid in the modified version of GAIM-GM. The blue, negative difference areas occurred where plasma perturbations moved from areas of dense GPS station coverage to areas of sparse (or no) GPS station coverage and relaxed out of the model solution before drifting very far downstream

Removing these density perturbations from the model after just 1 hour instead of 5 gave a significant boost to the entire grid’s skill score. The average skill score for the entire map over the 1800 – 2145 UT storm period increased by 9.3 points, while the SED-only domain saw an increase of 4.4 points. Figure 36 shows the time-

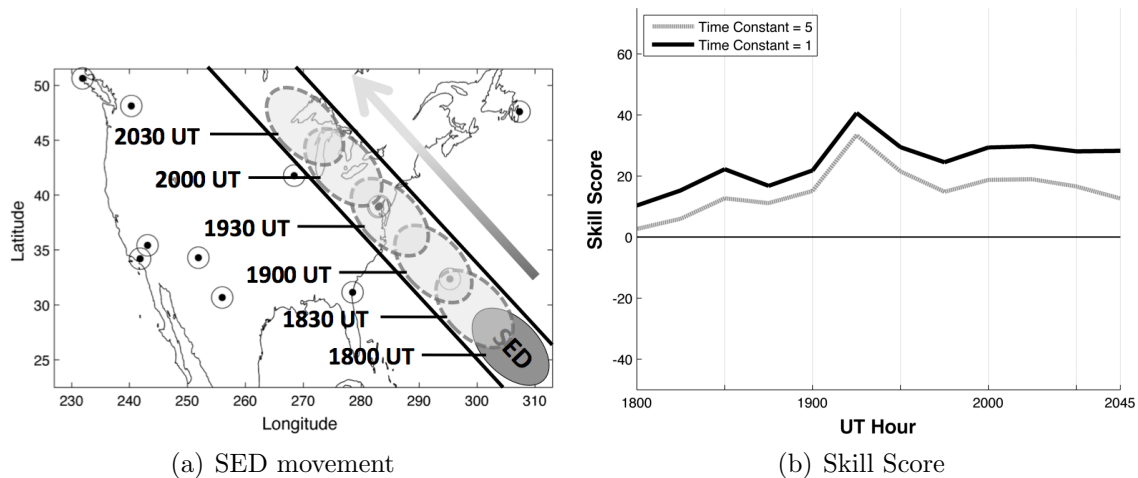


Figure 36. Skill scores for the entire map, using the AFWA+400 grid in the modified version of GAIM-GM. A trajectory plot of the synthetic SED’s movement is shown in (a). The sharp increase in scores at 1915 UT occurred as the SED moved onshore and over more ground receivers

dependent skill score improvement for the entire grid alongside a diagram of the SED’s trajectory. The difference between scores is slightly larger at the end of the storm period, most likely due to less high-density SED perturbations advecting downstream into GPS station-sparse areas. A summary of average skill scores for all three domains is presented in Table 12.

Table 12. Summary of Case 5 average skill scores. Standard deviations are given in parenthesis to the right of each score

Domain	Time Constant = 5	Time Constant = 1
Entire map	15.4 (7.8)	24.7 (8.1)
SED only	31.0 (21.7)	35.4 (17.5)
Outside SED	7.7 (7.9)	18.9 (10.2)

4.8 Case 6: Simulated Bad Data at One Station

Thus far the modified version of GAIM-GM (which trusts data more) has shown overall higher skill scores than normal version of GAIM-GM. However, all slant TEC

measurements used so far have been carefully controlled and relatively error-free since they are artificial data. The objective of this case was to deliberately introduce erroneous data into GAIM-GM and determine how it affected the model's accuracy.

The AFWA+100 grid was used for this case. Freeport, Ohio, a GPS ground station which resides directly in the SED's path, was selected to give bad data to GAIM-GM for day 172. Every slant TEC measurement was deliberately reduced by a factor of 4 to simulate corrupt data, which in reality could result from things such as uncalibrated instrumentation, broken sensors, or interference from nearby microwave radiation sources, among other things.

Figure 37 shows the percentage TEC difference at 1945 UT caused by introducing the bad data. This figure was created by subtracting the AFWA+100 grid output with good data (see Case 2-C) from the Case 6 output which include the bad station. The bad data caused TEC depletions as high as 9% over the Appalachian Mountains and into the Tennessee River Valley, and a TEC increase of up to 10% over the lower Great Lakes. Note that the effects of the bad data were not mitigated by the dozen other stations in the region that provided good data.

Examining the entire grid's skill score over the course of the day reveals interesting behavior. Note in Figure 38 that bad data at Freeport caused three negative skill score spikes at 1345 UT, 1745 UT, and 2145 UT. The 1345 UT skill score decrease was also seen to a lesser extent in the good data model run (dashed line) and coincided with a large TEC gradient from the Appleton Anomaly moving over the CONUS East Coast. All three negative skill score spikes due to bad data (solid line) were unexpectedly greater than 25 points.

The skill score maps in Figure 39 shed light on the cause of one of the skill score decrease. On the left is the 1730 UT skill score map and on the right is the 1745 UT map. A large area of negative skill scores appeared over the lower right corner of

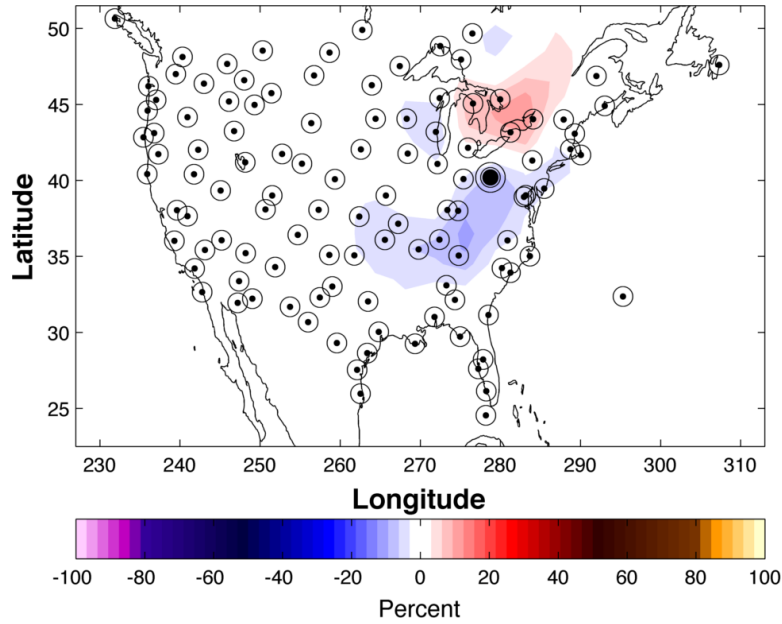


Figure 37. TEC difference in the modified version of GAIM-GM at 1945 UT caused by bad data from one GPS ground station. Small circles represent 111 stations with good data while the large black circle over Ohio is a station with deliberately degraded slant TEC data (reduced by a factor of 4). Note the far-reaching effects despite the dozens of good data sources in the region. The Time Constant was 5

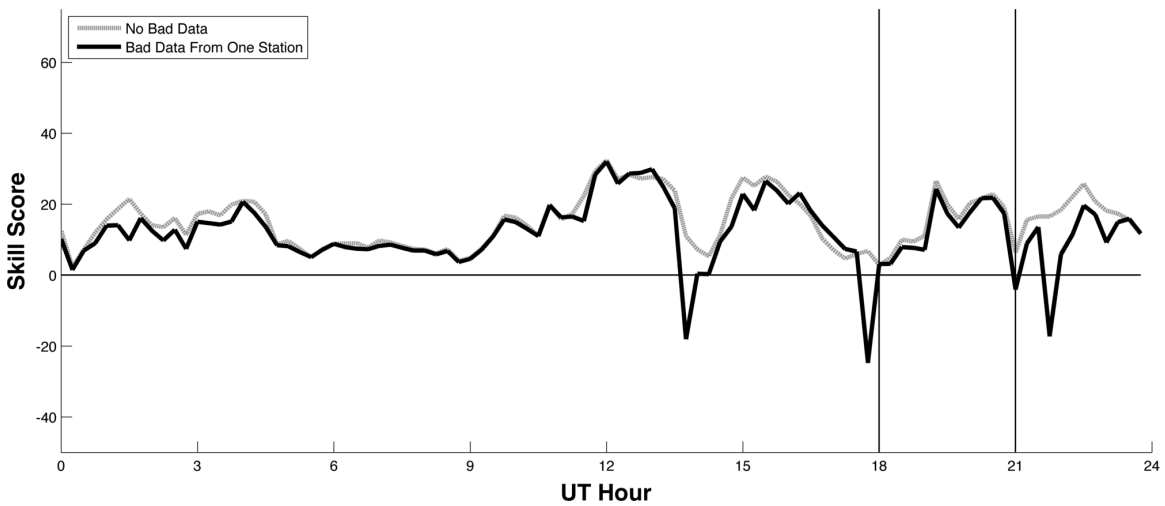


Figure 38. Skill score for the entire map, comparing the AFWA+100 grid with good data to the AFWA+100 grid where one station's data were reduced by a factor of four to simulate erroneous data. The modified version of GAIM-GM was used. The storm period is defined by the two vertical asymptotes. Note the three sudden drops in skill score in the latter half of the day due to ingestion of bad data

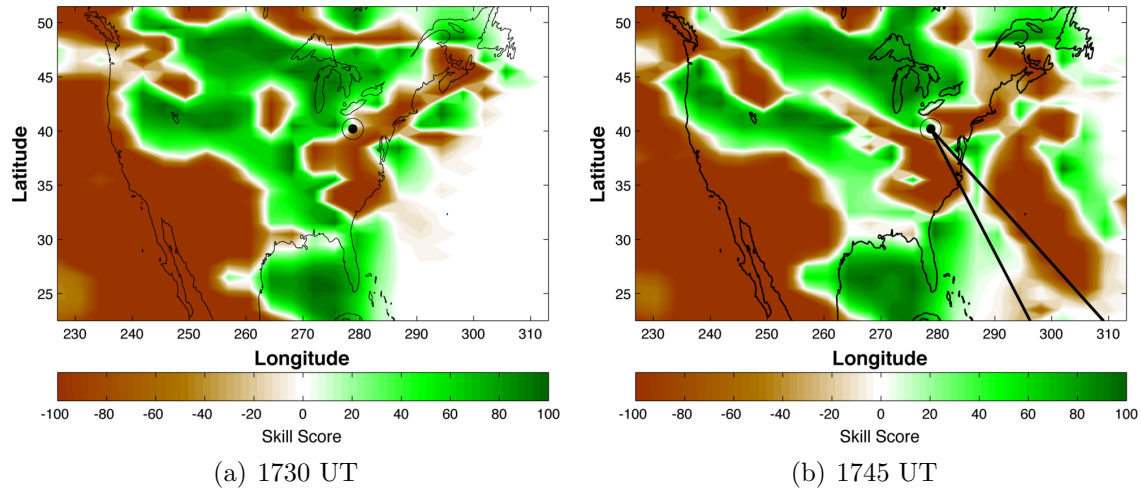


Figure 39. Time-dependent skill score maps showing the sudden appearance of a large area of negative skill scores over the Atlantic Ocean. The modified version of GAIM-GM was run using the AFWA+100 list where data from one station over Ohio was purposely degraded (slant TEC reduced by a factor of 4). The area of abruptly lower skill scores was caused by degraded low-angle slant TEC measurements as two satellites over the mid-Atlantic Ocean came the Ohio station’s view, indicated by the black lines

the map at 1745 UT as two GPS satellites over the mid-Atlantic Ocean moved into Freeport’s view, providing two new, degraded slant TEC measurements. This scenario could happen dozens of times per day in reality, which is why AFWA currently does not use this modified version of GAIM-GM that blindly trusts data. The normal version of GAIM-GM is designed to reject obviously wrong observations (*Scherliess et al.*, 2006) and would not have assimilated the bad data from Freeport.

Table 13 gives the average skill scores during the 1800 – 2145 UT storm period for all three map domains. Bad data from FREO caused the entire map to lose 1.9 points, the SED region to lose 2.4 points, and everything outside the SED to lose 2.8 points. It was interesting that bad data from 1% of the stations could reduce the entire map’s skill score by 12% when modified GAIM-GM was used.

Table 13. Summary of Case 6 average skill scores. Standard deviations are given in parenthesis to the right of each score

Domain	All good stations	One bad station
Entire map	15.4 (7.6)	13.5 (7.5)
SED only	21.2 (18.3)	18.8 (18.4)
Outside SED	15.4 (7.3)	12.6 (9.2)

4.9 Case 7: Reversed Ideal 21 Grid

This case examined how the specific placement, not quantity, of GPS ground stations affected GAIM-GM TEC maps. Two artificial station grids were compared: 1) the Ideal 21 grid and 2) a left-to-right reversed version of the Ideal 21 grid, hereafter called the Reversed Ideal 21 grid.

A visual comparison of TEC results at 1945 UT for each grid is presented in Figure 40, where Figure 40(a) used the Ideal 21 grid and Figure 40(b) used the Reversed Ideal 21 grid. The SED was resolved much better by the reversed Ideal 21 grid because of the SED's specific path in relation to the GPS receivers. The Reversed Ideal 21 grid attained a maximum TEC value in the SED region of 89.3 TEC units at 1945 UT, compared to only 55.8 TEC units attained by the Ideal 21 grid (note that the synthetic SED maximum was 111.4 TEC units).

Figure 41(a) shows the exact path of the SED through both grids, where the small black circles represent Ideal 21 grid stations and the large red circles are Reversed Ideal 21 grid stations. To its right in Figure 41(b) are the time-dependent skill scores for the entire map. Scores significantly improved with the reversed Ideal 21 grid, especially prior to 1930 UT when the SED was still over the ocean.

The average skill scores for all domains are given in Table 14. All areas saw improvements, with the largest gains (16.5 point improvement) occurring for the SED-only domain. This case demonstrated that 21 well-placed land and sea GPS receivers had a 13.5 point skill score improvement over the 12 AFWA ground receivers.

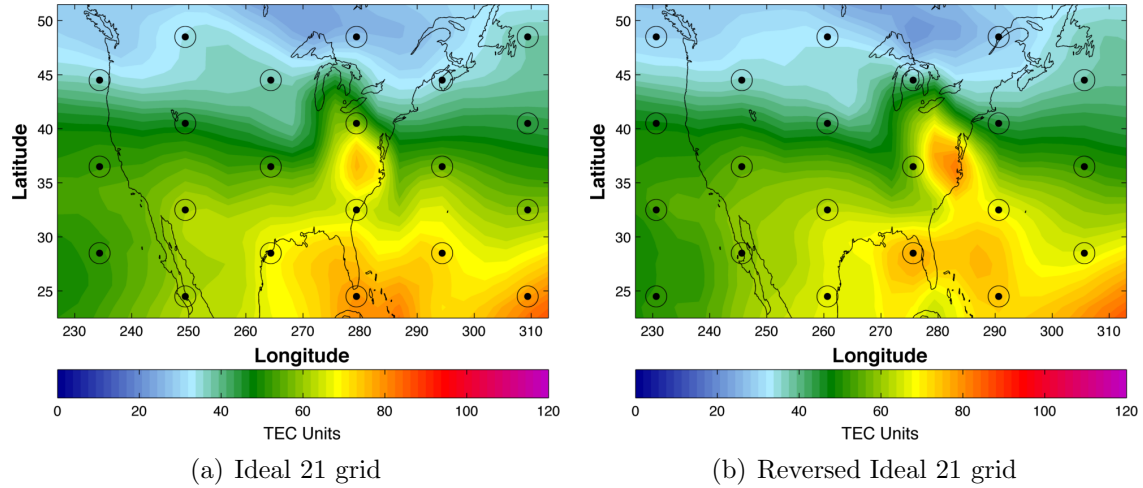


Figure 40. GAIM-GM TEC maps at 1945 UT using (a) the Ideal 21 grid and (b) a left-right reversed Ideal 21 grid. The modified version of GAIM-GM was used. By simply adjusting the arrangement of GPS ground stations (and without changing the average distance between stations), the SED was reproduced more accurately

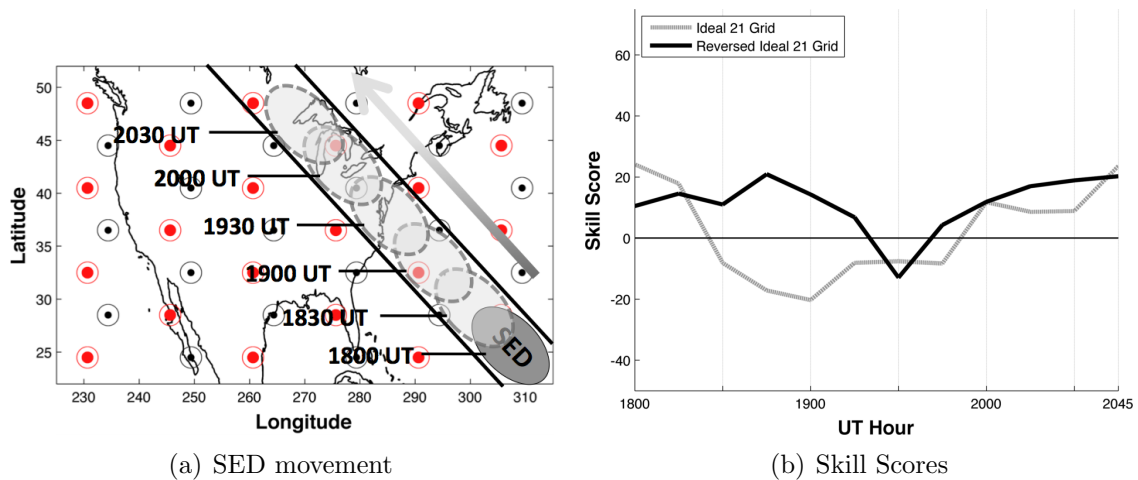


Figure 41. Skill scores for the entire map, comparing the Ideal 21 grid to the Reversed Ideal 21 grid. As a reference, both grids are superimposed on the SED movement plot in (a). The small black circles denote the Ideal 21 grid and the large red circles denote the Reversed Ideal 21 grid. The Reversed grid's station locations were more favorable for this SED's specific trajectory, resulting in largely improved skill scores

Table 14. Summary of Case 7 average skill scores. Standard deviations are given in parenthesis to the right of each score

Domain	Ideal 21 grid	Reversed Ideal 21 grid
Entire map	2.1 (15.5)	13.5 (9.2)
SED only	-3.9 (25.4)	12.6 (15.0)
Outside SED	8.7 (11.8)	11.5 (12.0)

4.10 Case 8: Normal GAIM-GM with Depleted IFM

Geomagnetic storms often cause TEC increases such as SEDs, but they can also cause TEC depletions in other areas outside SEDs due to complex electric field and upper atmosphere dynamics (*Foster, 1993*). The objective for this case was to duplicate the storm shown in Figure 12 by depleting IFM background densities in areas outside the SED. For example, note the TEC depletions east and west of the historic SEDs in Figures 12 and 13.

Using the historic SED specifications as a pattern, all densities above 30° N latitude in the IFM background were depleted by a factor of 4, except for those in the synthetic SED. Slant TEC measurements were then taken in the normal fashion using the CORS grids and ingested by normal GAIM-GM. An example of the depleted IFM background TEC with the imposed SED at 1945 UT is shown in Figure 42(a), while Figures 42(b) through 42(f) give the GAIM-GM TEC specifications using the five CORS grids.

Note in Figure 42 that the TEC across the entire map changed very little once the amount of ground stations exceeded the AFWA+30 point. Additionally, note the green-colored ridge of higher TEC values along the eastern edge of the map where GAIM-GM lacked the data to reproduce the lower background densities. This ridge can be seen in Figure 43, which shows 1945 UT electron density vertical cross-sections at 40° N latitude for the synthetic SED in IFM, compared to the GAIM-GM specifications using the AFWA and AFWA+30 grids.

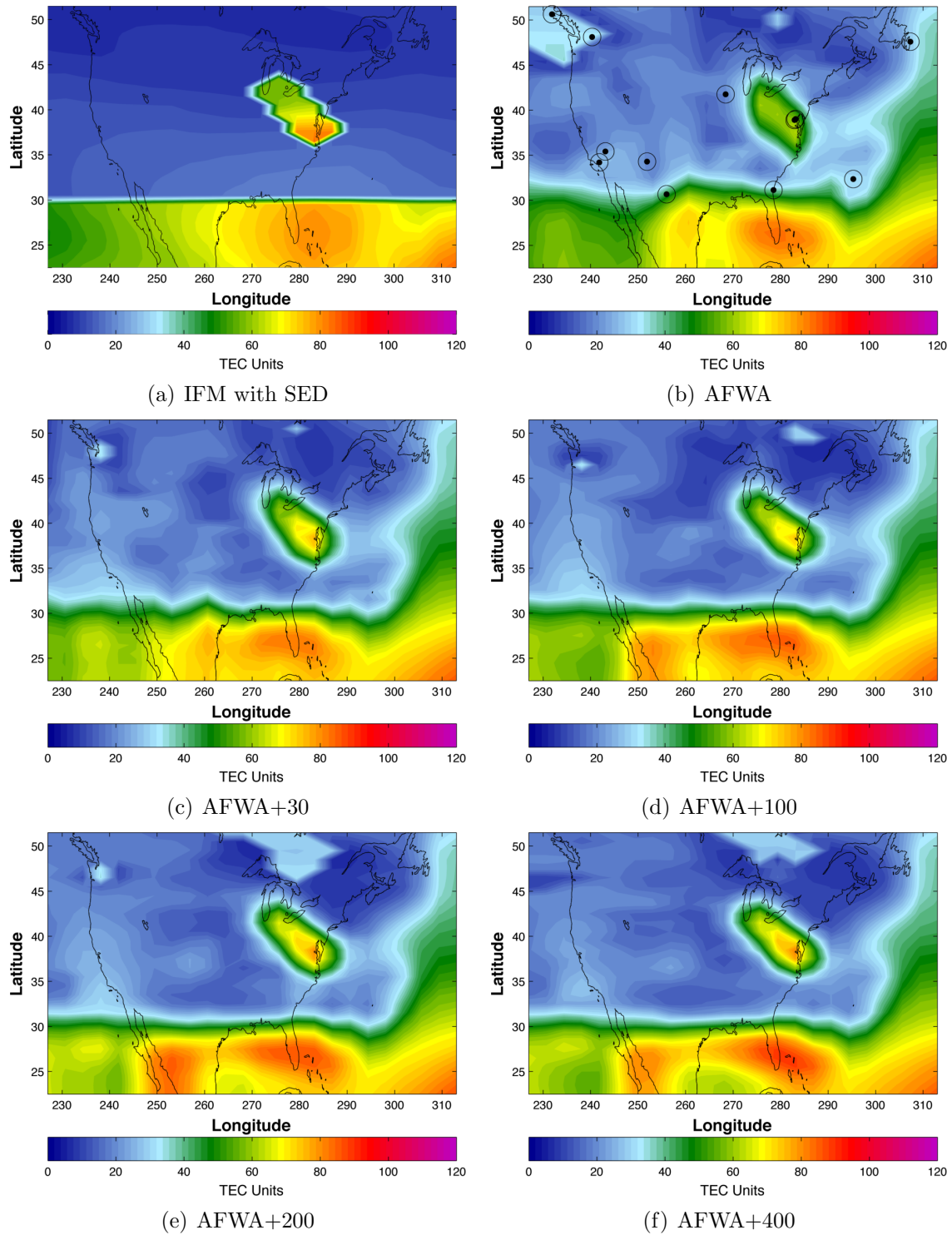


Figure 42. GAIM-GM TEC reproduction of the synthetic SED at 1945 UT, using GPS slant TEC data from the CORS grids. The synthetic SED in the depleted IFM background is shown in (a) as a reference and the 12 AFWA ground stations are plotted as black circles in (b)

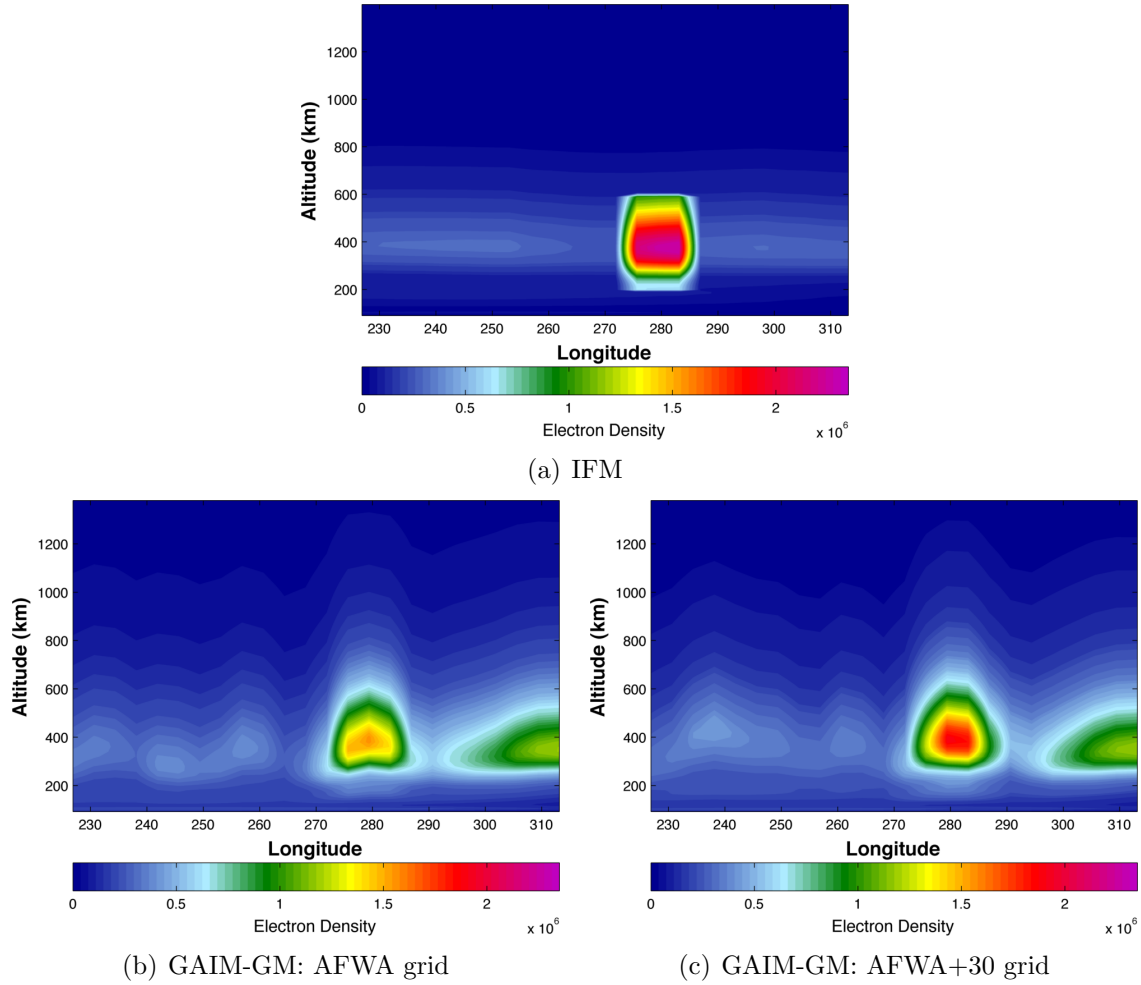


Figure 43. IFM and GAIM-GM electron density vertical profiles at 1945 UT. Latitude slices at 40° N are shown for the IFM background (a), AFWA grid output (b) and AFWA+30 grid output (c)

In the IFM, the maximum density of the SED core was 2.29×10^6 *electrons/cm⁻³*, whereas for the AFWA and AFWA+30 grids it was 1.56×10^6 *electrons/cm⁻³* and 1.90×10^6 *electrons/cm⁻³*, respectively. Electron density profiles for the AFWA+100, AFWA+200, and AFWA+400 grids were similar to Figure 43(c) and are not shown.

Skill scores for the SED-only domain, along with a trajectory plot of the SED, are shown in Figure 44. Unlike the relatively smooth curves of Figure 26(c) from Case 1, which did not have a depleted IFM, these scores fluctuated sharply with each time step. This pattern was explained in Case 2 as resulting from very low RMSEs for the

AFWA grid whenever the SED was directly over an AFWA station. As expected, the skill scores improved as station counts increased.

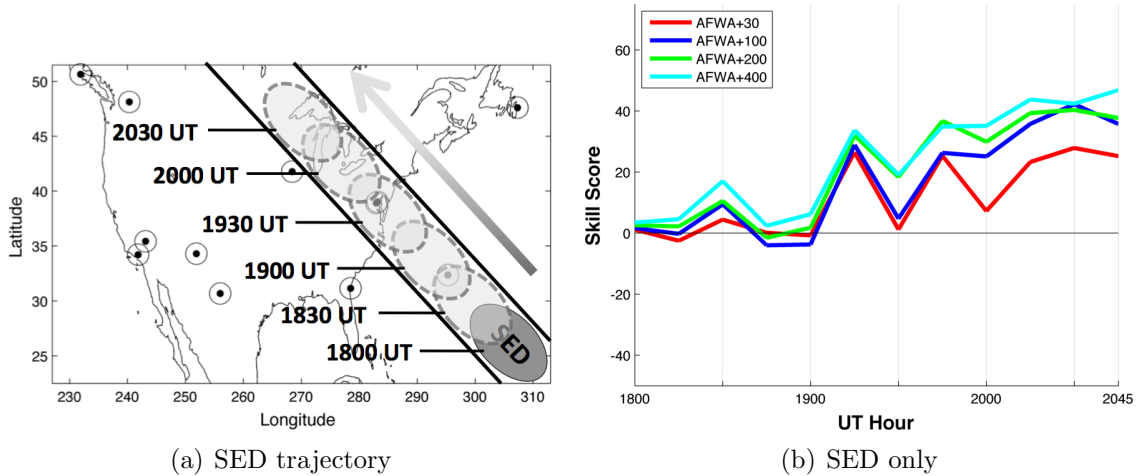


Figure 44. SED skill scores over the entire map for each of the CORS grids during the storm period from 1800 – 2045 UT. The trajectory of the SED is shown in (a) as a reference. Scores above 0 indicate the grid was more accurate at reproducing the IFM background than the AFWA grid, while scores below 0 indicate worse accuracy

Table 15 lists the average skill scores during the 1800 – 2045 UT storm period for the three domains. The zero station scores were extremely low due to the large difference between the depleted IFM background and GAIM-GM’s internal IFM background. This re-emphasizes the advantage that GAIM-GM has over the IFM during geomagnetic storming due to data assimilation. Skill scores increased in every domain as more stations were added, with the greatest improvements seen in the SED-only domain. With respect to the entire map, going from 30 extra stations to 400 extra stations only caused a 2.7 point skill score increase.

Table 15. Summary of Case 8 average skill scores. Standard deviations are given in parenthesis to the right of each score

Domain	No stations	AFWA +30	AFWA +100	AFWA +200	AFWA +400
Entire map	-77.4 (14.7)	7.1 (2.1)	7.8 (2.1)	8.1 (2.3)	9.9 (2.3)
SED only	-9.8 (18.3)	11.6 (12.7)	16.8 (17.1)	20.8 (16.8)	24.1 (17.1)
Outside SED	-81.8 (46.5)	7.2 (9.6)	7.7 (8.6)	7.8 (8.0)	9.4 (8.8)

4.11 Case 9: Reduced Time Constant with Depleted IFM

This case tested the effects of reducing the Time Constant in normal GAIM-GM with a depleted IFM background for all densities above 30° N latitude. As mentioned in Case 5, the purpose of the Time Constant is to retain ionospheric features detected by observations and propagate them over data sparse areas. Recall that Case 5 showed how reducing the Time Constant to 1 raised skill scores (i.e. reduced the errors) for all areas of the map. Skill scores were not available for this case because comparing the AFWA grid to itself results in a skill score of zero (see Equation 8), so MAEs were used instead.

The TEC difference caused by lowering the Time Constant is shown in Figure 45. Note that this difference was much greater than that seen in Figure 35 from Case 5. Because the slant TEC measurements through the depleted IFM background were so different from GAIM-GM’s internal IFM background, the resulting perturbations were also much larger. Removing those perturbations after just 1 hour instead of 5 naturally caused the large TEC differences. Another item to note is that the areas of positive and negative differences nearly balanced each other out, leading to the small average MAE differences listed in Table 16. Overall there was very little change in the storm period’s average MAE other than a 2.8 TEC unit improvement for the SED-only domain.

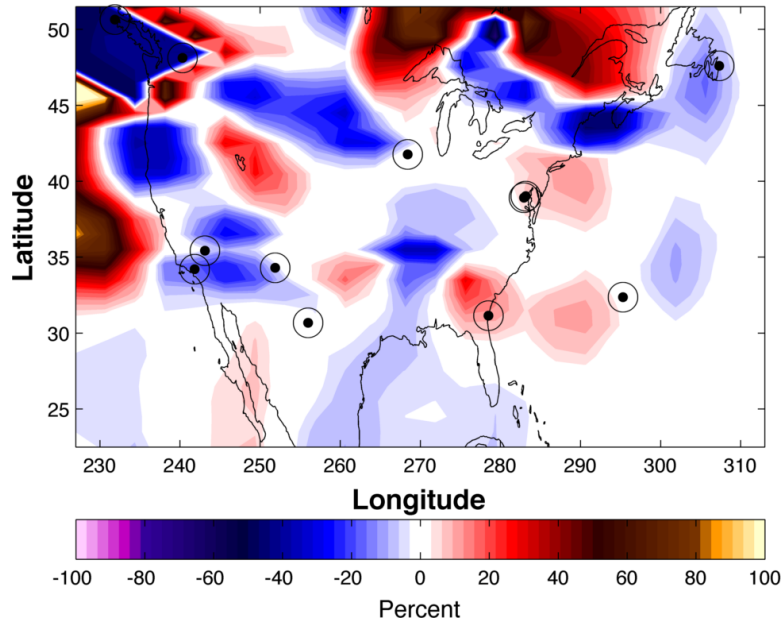


Figure 45. TEC difference at 1945 UT caused by lowering the Time Constant from 5 to 1 for the AFWA grid. All background IFM densities above 30° were depleted by a factor of 4 prior to slant TEC piercing, therefore these large percentage differences equate to relatively small TEC unit differences. Note that most of the differences occurred downstream of the GPS ground stations

Table 16. Summary of Case 9 average MAEs (TEC units). Standard deviations are given in parenthesis to the right of each score

Domain	Time Constant = 5	Time Constant = 1
Entire map	12.3 (1.9)	12.3 (1.7)
SED only	15.4 (10.4)	12.6 (9.6)
Outside SED	11.9 (3.6)	11.9 (3.6)

4.12 Case 10: Elevation Mask Raised to 45°

The final case in this project examined how changing the GPS station Elevation Mask affected the accuracy of GAIM-GM TEC specifications. For all nine previous cases the Elevation Mask was set to 15° , meaning slant TEC measurements would only be taken between a GPS satellite and ground station if the satellite was at least 15° above the horizon, from the station's reference frame. In this case the Elevation Mask was raised to 45° , significantly narrowing the field of view for every station.

Slant TEC measurements were then taken using the AFWA grid. As with the two prior cases, the normal version of GAIM-GM was used and the IFM background was depleted above 30° N latitude by a factor of four. The Time Constant was reset to its default value of 5.

Figure 46 shows the outcome of this scenario by comparing its results to electron density and TEC maps at 1945 UT from Case 8-A. The central column gives the 15° Elevation Mask GAIM-GM specifications from 8-A while the right column gives the 45° results. Perhaps the most striking feature is seen in Figure 46(c), where there is a circular region of low TEC (about 30 TEC units) directly over the Bermuda GPS receiver. With higher look angles, there were fewer long-path slant TEC measurements taken near the Earth’s surface to help expand Bermuda’s influence on the surrounding region. The same phenomenon was seen over southern CONUS where higher TEC ridges appeared to wrap around the periphery of GPS ground stations, creating a tunnel vision effect due to the reduced field of view.

Average MAEs for this case are given in Table 17, which indicates that the MAE for the entire map only increased by 2.3 TEC units, or approximately 19%. This error would be expected to decrease if a higher density GPS station grid were used and the fields of view were able to overlap.

Table 17. Summary of Case 10 average MAE (TEC units). Standard deviations are given in parenthesis to the right of each score

Domain	Look angle = 15°	Look angle = 45°
Entire map	12.3 (1.9)	14.6 (2.8)
SED only	26.6 (10.4)	29.3 (11.9)
Outside SED	11.9 (3.6)	14.1 (4.4)

Table 18 compares the number of data ingested by GAIM-GM for 45° and 15° Elevation Masks. When the Elevation Mask was raised to 45° the average amount of

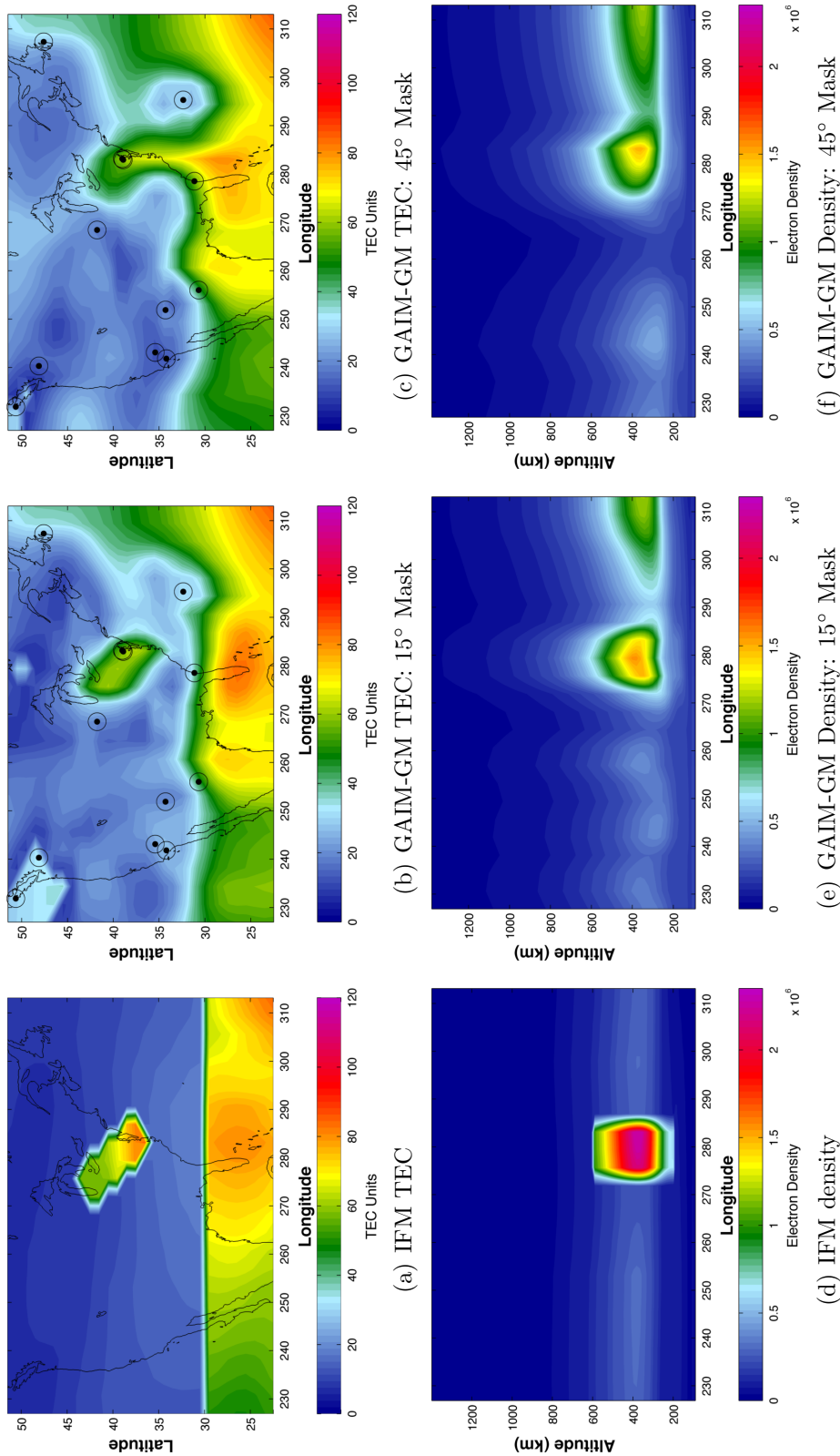


Figure 46. TEC and electron density vertical profiles in GAIM-GM, using the AFWA grid. The left column shows the IFM backgrounds that GAIM-GM was recreating, which had been depleted by a factor of 4 above 30° N latitude. The central column shows GAIM-GM output using the default 15° Elevation Mask. The right column shows GAIM-GM output using a 45° Elevation Mask

ingested data per time step decreased by 55%. Surprisingly this had relatively little effect on the average MAE for the storm period of 1800 – 2045 UT.

Table 18. Number of slant TEC measurements assimilated by GAIM-GM using the AFWA grid and varying Elevation Masks, in the normal version of GAIM-GM

Time (UT)	Elevation Mask = 45°	Elevation Mask = 15°
1800	45	77
1815	44	76
1830	40	71
1845	43	76
1900	36	79
1915	35	77
1930	42	73
1945	43	77
2000	45	75
2015	45	82
2030	44	80
2045	43	76

V. Conclusions and Recommendations

5.1 Chapter Overview

This chapter consists of two sections. The first section summarizes the results from using GAIM-GM to reproduce a synthetic SED with varying numbers of GPS ground stations and for several different model configurations. The second section presents recommendations for future research with the GAIM-GM model.

5.2 Conclusions

The accuracy of TEC maps produced by GAIM-GM varied considerably, based on both amount and distribution of available GPS ground stations. Using skill scores as a basis for accuracy, Figure 47 summarizes GAIM-GM's performance in reproducing the IFM background with the imposed synthetic SED. Scores are given for three domains: 1) entire map; 2) SED-only; and 3) area outside the SED. Note that these scores are the averaged, time-dependent skills scores for each grid during the 1800 – 2045 UT storm period.

Model runs using slant TEC measurements from a network of CORS (Figure 47(a)) showed TEC skill score improvements of 13.1 points for the entire map when 30 ground stations were added to the existing AFWA network. Increasing the number of stations beyond 30 provided less than 1 point of improvement for the entire map. However, skill scores for the SED-only domain continued to improve as stations were added and reached a score of 24.1 with 400 extra stations. Skill scores for all areas outside the SED simultaneously declined at about the same rate. Similar skill score trends for the entire map and SED-only domain (Figure 47(d)) were observed when the IFM background was depleted by a factor of 4 above 30° N latitude, although scores for areas outside the SED did improve 2.2 points with 400 extra stations.

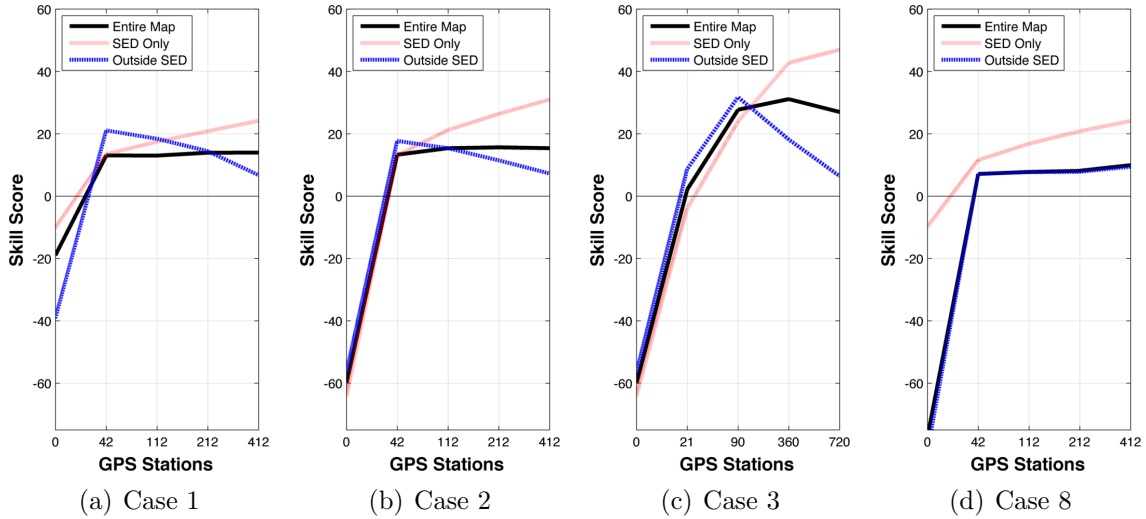


Figure 47. GAIM-GM skill score summaries for the 4 most important cases, which are: (a) normal GAIM-GM with CORS grids; (b) modified GAIM-GM with CORS grids; (c) modified GAIM-GM with Ideal grids; and (d) normal GAIM-GM with CORS grids and depleted IFM background;

CORS grids in the modified version of GAIM-GM performed on average 10% better for the entire grid, 21% better for the SED-only domain, and 15% worse for everything outside the SED (see Figure 47(b)), compared to the normal version of GAIM-GM. Although the improvements for the entire grid and SED-only domain were impressive, it must be emphasized that the data in this research were quality-controlled and only had 5,7% uncertainty. When slant TEC data at one GPS ground station in the SED’s path were deliberately degraded (75% error introduced), skill scores for the entire map dropped an average of 12%. Because of the negative effects even a small amount of bad data can cause, the modified version of GAIM-GM should not be used operationally as a stand-alone model. However, it would be advantageous to use it alongside the normal version of GAIM-GM in ensemble fashion, giving AFWA access to potentially superior specification as long as data fidelity is monitored.

Tests with the Ideal grids in modified GAIM-GM (Figure 47(c)) demonstrated that strategically placing ground GPS receivers yielded significant improvements in

accuracy. An evenly distributed grid of 90 artificial stations yielded skill scores of 27.1 for the entire map, 23.9 for the SED-only domain, and 31.8 for everything outside the SED. Those scores are 80%, 13%, and 106% higher than their counterpart scores using the AFWA+100 grid in modified GAIM-GM. It was also found that low-density ground station grids were highly dependent upon the trajectory of the SED. The Ideal 21-station grid initially scored -3.9 for the SED-only domain, but reversing the grid from left to right (without altering station spacing) raised the score to 12.6 by placing more ground stations in favorable locations to observe the SED.

The significant accuracy advantages of the Ideal grids could be realized if ocean-borne GPS receivers were added to AFWA's network. One possible avenue is to deploy GPS receivers on naval vessels, either on U.S.-owned military ships or on commercial vessels via a contractor. Oil rigs are also potential sites, although they would not provide as broad a reach from the mainland. Buoys might not be a viable option without a way to correct for the constant altitude fluctuations that ocean waves would cause to the receiver's position (recall that the GPS receiver's coordinates must be precisely known).

In addition to altering the number and location of ground GPS receivers, adjusting the Time Constant affected the accuracy of GAIM-GM TEC maps. Reducing the Time Constant from 5 to 1 caused GAIM-GM to relax density perturbations sooner and had the greatest effects downstream of data-rich areas. Skill scores in the modified version of GAIM-GM increased by an average of 9.3 for the entire grid, 4.4 for the SED-only domain, and 11.2 for everything outside the SED. In normal GAIM-GM there were large localized TEC differences for the entire grid, but negligible overall reduction of errors. Average MAEs for the SED-only domain decreased by 3.6 TEC units (a 10% improvement in MAE) because GAIM-GM propagated fewer low-density upstream perturbations into the SED.

Lowering the Time Constant in the operational GAIM-GM will yield accuracy improvements in some cases but degradations in others. With the Time Constant set to 1, short-lived features or those that have poleward velocity components would not be overly skewed to the west, and therefore GAIM-GM would have improved precision. Conversely, long-lived ionospheric features that propagate zonally westward, especially over data-sparse regions, would not be captured as well with a Time Constant of 1. Given that AFWA currently uses a low-density GPS station grid over CONUS, there would be little operational advantage in lowering the Time Constant.

Changing the Elevation Mask also affected GAIM-GM's performance. Raising the angle from the default 15° to 45° with the AFWA grid effectively narrowed each GPS ground station's field of view and limited the amount of available slant TEC observations. The average TEC MAE increased by 16% for all areas as a result of this tunnel vision effect, indicated poorer model performance.

One limitation of GAIM-GM uncovered during this research was that, although it typically reproduced TEC with good accuracy, it could not correctly specify the electron density vertical profile of a high-altitude synthetic SED. It appeared that GAIM-GM tended to reconstruct the height of the ionosphere F_2 peak based on climatology. Because the test only used slant TEC measurements, it is unclear whether those data alone provided inadequate information for resolving the SED profile, or if it was entirely due to the limitations of the Gauss-Markov model. Assimilating ionosonde and *in situ* DMSP data into GAIM-GM could potentially supply the altitude-specific electron density information needed for GAIM-GM to accurately specify the SED. It is recommended that Case 4 be repeated with these additional data types.

Based on all results, there are three recommendations for the number of ground GPS receivers AFWA should employ over CONUS to help ensure reliable TEC correction maps during geomagnetic storming. These numbers consider the balance between

accuracy over the entire grid and accuracy for the SED-only domain. For a network using existing CORS sites, the optimal number is ~ 110 GPS receivers. If availability of data or economic considerations preclude using that amount, the number could be lowered to ~ 40 and still provide significant improvements over the current 11-station AFWA network. If the Ideal grid were attainable and GPS receivers could be evenly situated over land and sea, the recommended number would be ~ 90 .

Finally, note that these results were obtained from very specific sets of data, under carefully controlled scenarios, and that the synthetic observations were taken at GAIM-GM's highest allowable cadence of 15 minutes. Because real slant TEC data are subject to many uncertainties (instrument calibration, sensor errors, etc.) and are not always available every 15 minutes, results using real data in GAIM-GM may vary from those presented here.

5.3 Recommendations for Future Work

Questions raised during this research could provide several avenues for future study on SEDs and their effect on geo-location accuracy. These include repeating some of the most interesting cases but under different conditions, such as: 1) running the Ideal grids in normal GAIM-GM instead of the modified version of GAIM-GM; 2) conducting tests with the saturated Ideal 720 grid to determine why it gave skill scores lower than the Ideal 360 grid; 3) testing Time Constant changes in sparser grids, such as the AFWA+30 and AFWA+100 grids; 4) running more scenarios with simulated bad data to determine why reduced slant TEC values over Freeport caused counter-intuitive TEC increases over the Great Lakes; and 5) recreating a high-altitude SED using DMSP and ionosonde data, as mentioned in the previous section.

It is highly recommended that these suggested studies, or any similar studies, take advantage of historical SED specifications in GAIM-GM and use an actual GAIM-

GM density background instead of an IFM background for slant TEC piercing. Recall that the synthetic SED in this project was basic construct representing a single propagating patch of enhanced plasma, precisely imposed onto an IFM background. This simple yet effective storm feature could be made even more realistic and dynamic by adopting the actual GAIM-GM historical recreation of a SED as the density background, and then taking slant TEC measurements through it using a modified version of *SlantTEC.m*. With the necessary MATLAB[®] utilities already pioneered by AFIT, research could commence almost immediately.

Additionally, the same cases presented here could be repeated using smaller GPS station increments, such as 10, 20, 30, 40, and 50. Given the cost of GPS data vs. economic realities, it is extremely likely that additions to the AFWA station network will come in small increments, perhaps even one station at a time. A methodical study of SED climatology to identify regions where GPS receivers are needed most, followed by testing in GAIM-GM, is recommended. This would prioritize which GPS ground stations to acquire next and would be tremendously valuable to AFWA and space weather forecasting in the coming years.

Appendix A. The Global Positioning System (GPS)

The GPS is a U.S. government-built system consisting of three segments: 1) space segment; 2) user segment; and 3) control segment. The space segment is operated and maintained by the U.S. Air Force and is composed of a constellation of 32 satellites orbiting at approximately 20,200 *km* with an orbital period of 12 hours. Each satellite transmits two signals, L1 and L2, at microwave frequencies. The L1 frequency is 1575.42 *MHz* and transmits the Standard Positioning Service signal, which can be used worldwide by anyone without restrictions or charges. The L2 signal is broadcast encrypted at 1227.60 *MHz* and is used by the U.S. military and its allies' militaries, as well as other select agencies approved by the U.S. Government (*Dana, 2010*).

Figure 48 shows the orbital tracks of all 32 GPS satellites over a 24-hour period. Note how the orbital inclination prevents overflight of the poles but still offers ample coverage for the mid-latitudes where SEDs frequently occur.

The user segment consists of the GPS receiver. At any given time there are five to eight satellites with direct lines-of-sight to a user at any point on earth, although linkage is only needed with four satellites in order to determine the user's three-dimensional geo-location. Three satellites are used to determine the latitude, longitude, and elevation of the receiver while the fourth satellite corrects the time offset in the receiver's clock. Time correction is necessary so that the receiver can precisely measure the time delays of the other three satellites' signals. If the receiver equipment contained its own atomic clock, perfectly synchronized with the GPS constellation, it would only need three satellites for a location fix.

The third segment is the control segment, which composed of the Master Control Facility located at Schriever Air Force Base, Colorado and a worldwide monitoring network of GPS ground tracking stations. The control segment performs a number of vital functions: 1) monitors and maintains the satellites in their proper orbits

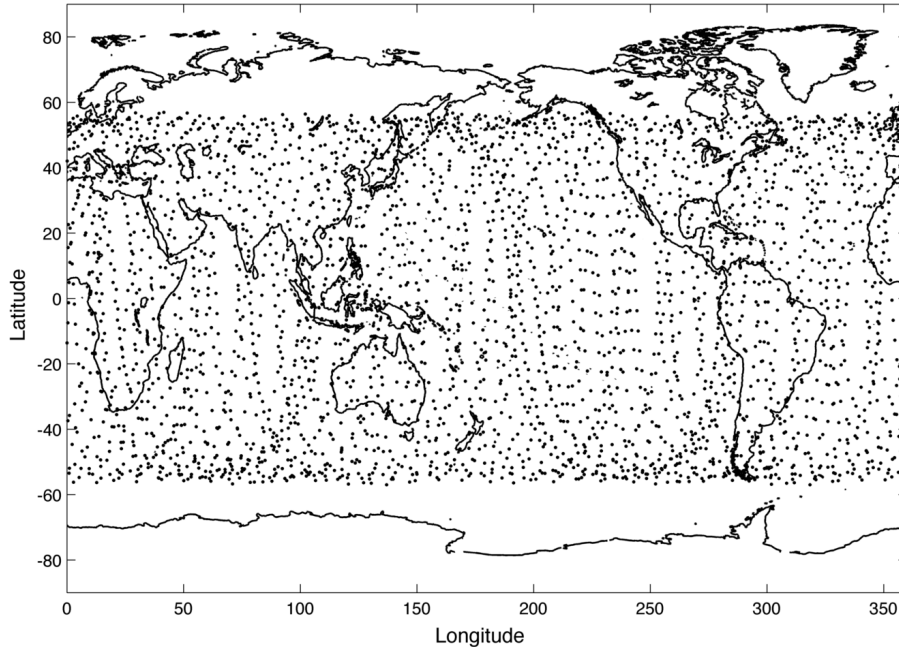


Figure 48. Orbital tracks for all 32 GPS satellites over the course of one day, at 15-minute time steps. The orbital inclination of 55° prevents overflight of the polar regions

through occasional command maneuvers; 2) adjusts the satellites' clocks; 3) tracks the satellites; 4) uploads updated navigational data; and 5) maintains the health and status of the satellite constellation. There are currently more than 360 active stations in the International Global Navigation Satellite System Service (IGS) tracking network (*International Global Navigation Satellite System Service*, 2011). Closer to CONUS, the National Geodetic Survey (NGS) manages a network of over 1900 Continuously Operating Reference Stations (CORS) throughout the U.S., its territories, and a few foreign countries (*National Geodetic Survey*, 2011). Figure 49 shows the CORS network over the CONUS area.

In most cases the ionosphere is a hindrance to radio transmission between GPS satellites and ground stations (*Ondoh and Marubashi*, 2001). At the same time, although GPS signals were not intended specifically for ionospheric monitoring, they can be used for ionospheric research. GPS ground stations contribute to studies of the

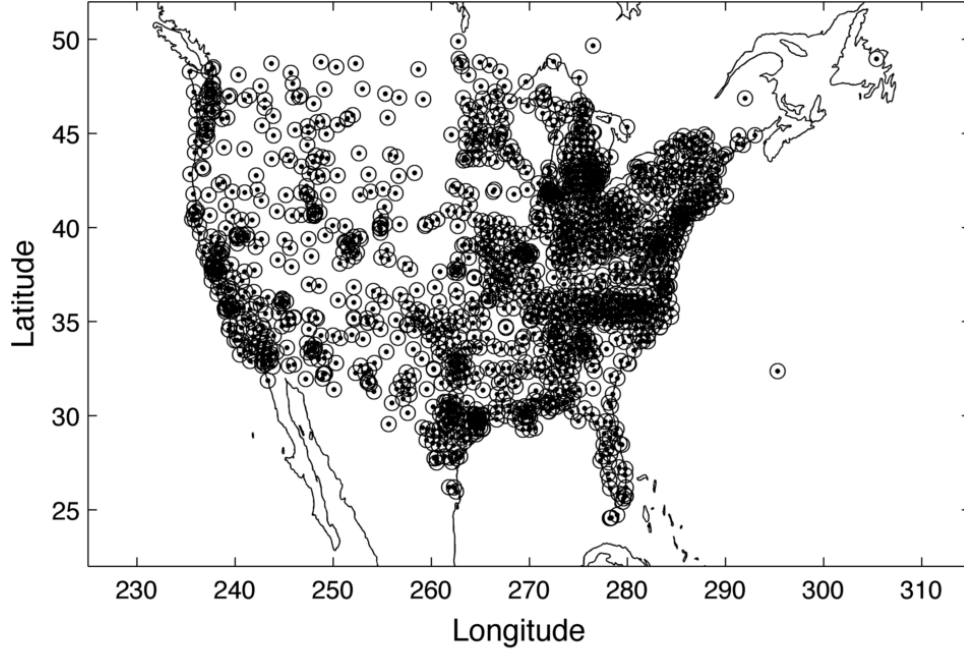


Figure 49. Continuously Operating Reference Stations (CORS) network over CONUS. There are 1920 stations shown here, with the majority located over the eastern U.S.

ionosphere by calculating slant TEC values, which are integrated electron densities along the path between GPS satellites and the ground stations. The development of the calculation presented here closely mirrors that given by *Ondoh and Marubashi* (2001) and involves measuring the *time delay difference* δt between the L1 and L2 signals received at the station:

$$\delta t = \Delta t_2 - \Delta t_1 \quad (10)$$

The variables Δt_1 and Δt_2 correspond to L1 and L2 and represent the amount of *group delay* imposed on a radio signal of frequency f_1 or f_2 . Generically this is:

$$\Delta t = \frac{e^2}{8\pi^2 m_e \epsilon_0 f^2} \int_s n ds \quad (11)$$

where the constants are listed in Table 19. The integral represents the integrated

electron density over the propagation path length (from satellite to ground):

$$\int_s nds = N_T \quad (12)$$

where N_T is the *TEC* along the path length. To solve for the TEC, Equations (11) and (12) are substituted into Equation (10), resulting in:

$$\delta t = \frac{e^2}{8\pi^2 m_e \epsilon_0} \left(\frac{1}{f_2^2} - \frac{1}{f_1^2} \right) N_T \quad (13)$$

Finally, the values of the constants in Table 19 are inserted into Equation (13):

$$N_T = 2.85 \times 10^{25} \delta t \text{ [electrons/m}^2\text{]} \quad (14)$$

From Equation (14) the slant TEC can be easily calculated for any given amount of group delay.

Table 19. Slant TEC equation constants

Symbol	Name	Value
e	Elementary charge	$1.6022 \times 10^{-19} \text{ C}$
m_e	Static electron mass	$9.1094 \times 10^{-31} \text{ kg}$
ϵ_0	Permittivity of free space	$8.8542 \times 10^{-12} \text{ F/m}$
f_1	L_1 signal frequency	1575.42 MHz
f_2	L_2 signal (P code) frequency	1227.60 MHz

Appendix B. AFWA 12th Station

The original list of GPS ground stations used by AFWA for running GAIM-GM contained 59 global stations, 11 of which were located in the CONUS assimilation region (see Table 3). This list was provided courtesy of AFWA and identified all sites which had provided slant TEC measurements to GAIM-GM during the month of February 2011. The actual number of stations used changes slightly from month-to-month, based on the availability of data (*Reich*, 2011). For example, during May 2011 GAIM-GM used 77 stations from around the globe, which were 18 more than the number used in February.

Because the AFWA list has so few GPS ground stations over CONUS, there are data-sparse areas which prevent accurate specifications of the ionosphere via slant TEC measurements. Large scale features might be big enough to blanket a few GPS ground stations, but small scale features may be partially or fully unresolved if they fall inconveniently between widely separated stations. Conversely, a small feature might pass directly over an isolated GPS ground station and cause GAIM-GM to correlate the feature's density into the surrounding grid squares' density solution, effectively smearing the feature over an extended area where it should not exist.

Consider the two TEC maps in Figure 50. On the left is a GAIM-GM historical specification of the 20 November 2003 SED. On the right is an IFM specification with an imposed synthetic SED. The large surface area of enhanced TEC in the real SED covers nearly the bottom third of the map. Large Latitude Correlations and Time Constants would favor the real SED in a data sparse environment (like the AFWA grid) by spreading enhanced densities over areas lacking ground stations, creating a more accurate specification. With the synthetic SED, the aim is to minimize the amount of smearing caused by the Latitude Correlation and Time Constant, so the best path is one through a corridor of stations that will resolve all edges of the SED.

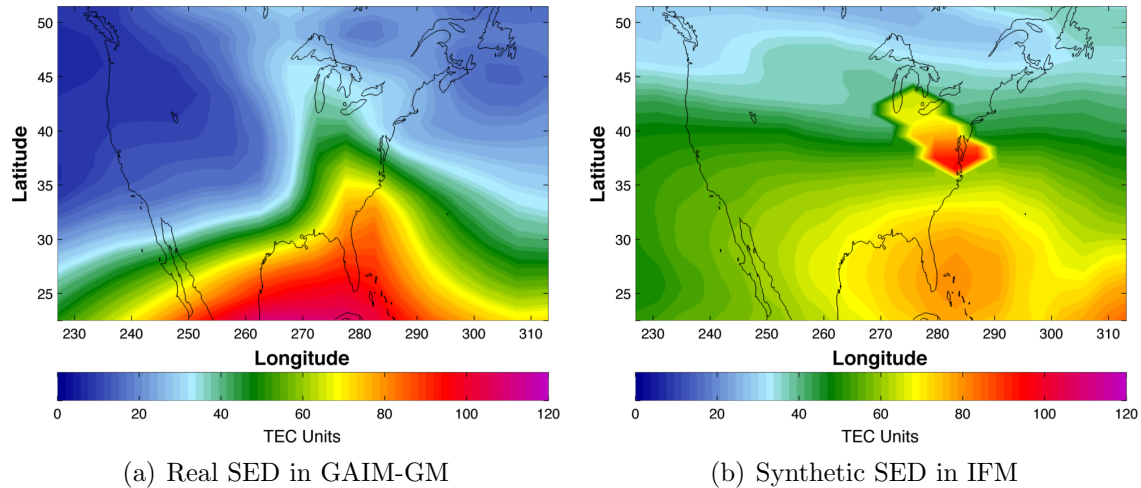
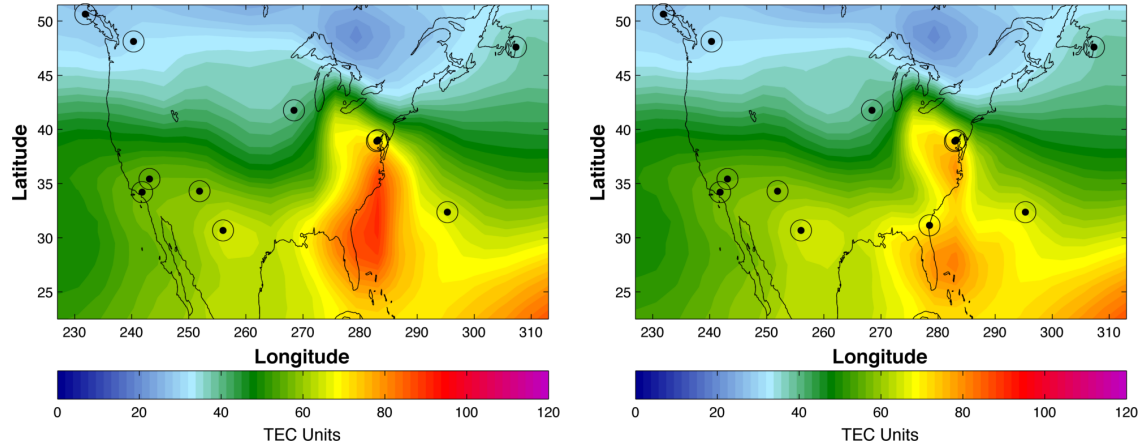


Figure 50. Historical depiction of an SED in GAIM-GM (left), versus a synthetic SED (right). The synthetic SED’s small profile make it a challenging target for slant TEC measurements over sparsely populated GPS ground station networks

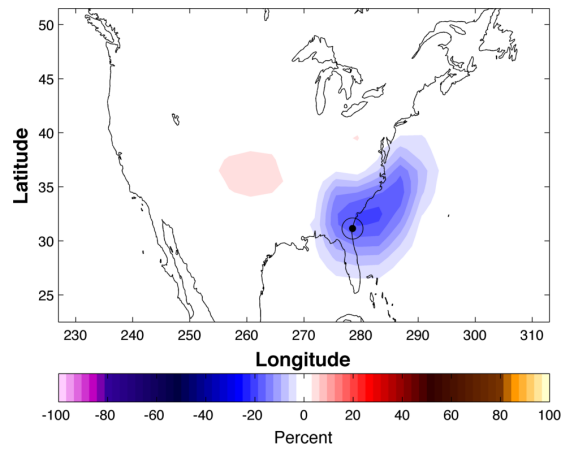
In the case of the original 11-station AFWA grid, the synthetic SED happens to pass directly over two GPS stations in Maryland as it moves onshore. Figure 51(a) shows the GAIM-GM TEC map for the 11-station AFWA grid. Note that there are no other stations immediately to the south which can help resolve the southern edge of the SED. Consequently the Kalman filter continues to propagate enhanced densities detected earlier by the Bermuda GPS station, while correlating the SED values latitudinally to the south. This results in the SED being specified grossly out of proportion. However, if a station is added along the lower East Coast (see Figure 51(b)), GAIM-GM detects the true values that should exist over that area and significantly firms up the solution, reducing the false TEC values by over 20%.

These results in Figure 51 powerfully illustrate how adding just one station to fill the gap in a data-sparse region can significantly improve GAIM-GM TEC results. They additionally reveal the disadvantage that this synthetic SED’s trajectory levies on the 11-station AFWA grid and show how the extra station over Georgia creates a fairer playing field for the numerous cases conducted during this project.



(a) 11 station list

(b) 12 station list



(c) Percent TEC difference

Figure 51. Differences in GAIM-GM TEC specifications due to the addition of a 12th GPS ground station over Georgia. (a) illustrates how station sparsity can cause GAIM-GM to spread perturbations into regions well beyond the SED. (b) shows the correction provided by the extra ground station. The difference between the two TEC specifications, shown in (c), is about 20% over the new station

Appendix C. Slant TEC Assimilation Per Time Step in GAIM-GM

A GPS slant TEC measurement consist of the integrated electron densities along the path between a GPS satellite and a ground receiver. Because each GPS satellite is continuously emitting its electromagnetic signal, it can reach hundreds of GPS ground receivers at a time as it orbits the Earth. Figure 52 illustrates the signal locks between GPS satellites and the AFWA grid at 1945 UT, where each line connecting a satellite (triangle) to a ground stations (circle) represents the signal path along which a slant TEC measurement is taken and later ingested by GAIM-GM.

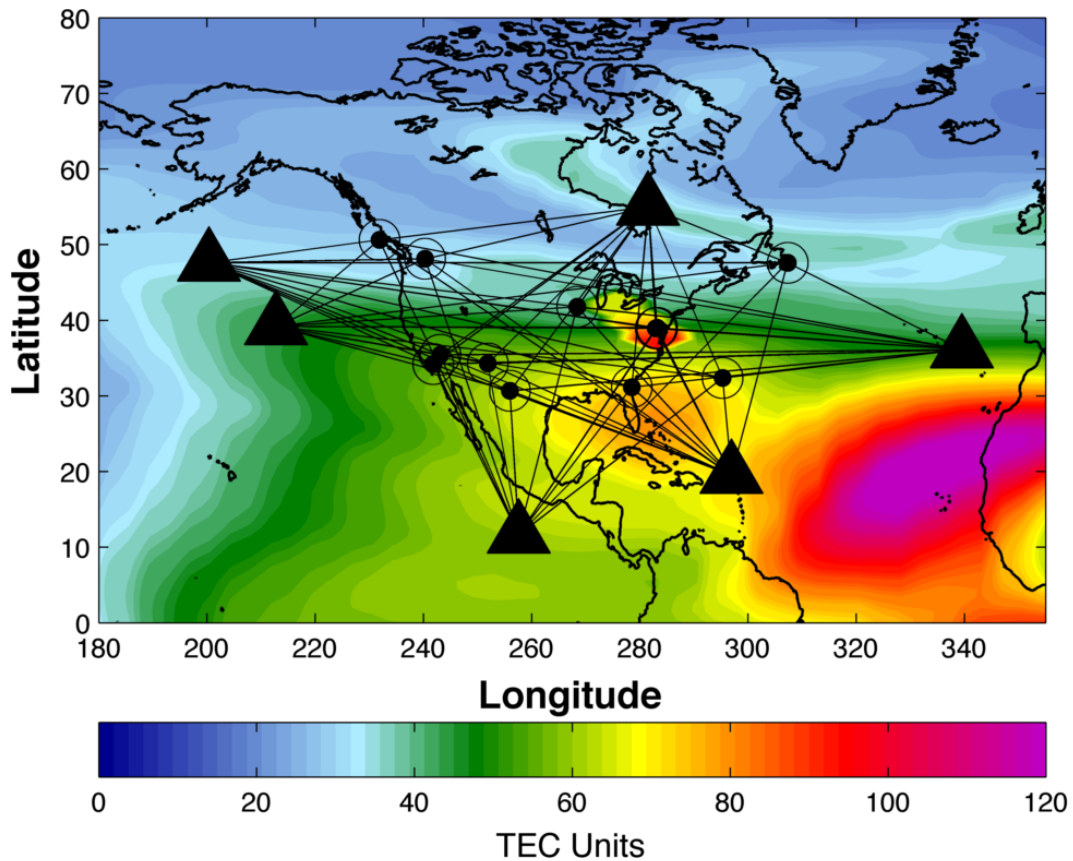


Figure 52. Slant TEC paths through IFM background to AFWA ground stations at 1945 UT. Triangles represent GPS satellites and circles are the ground stations. The exact number of slant TEC measurements for this time step was 300 (not all slant paths are shown). The SED can be seen over the U. S. East Coast

Table 20 lists the number of data ingested by GAIM-GM at each 15-minute time step during the storm period, according to the grid type and number of stations used. This information is available in all GAIM-GM NetCDF output files. The number of slant TEC observations increased linearly as station number increased, with two exceptions. First, the amount of data assimilated for the AFWA+400 station grid were omitted because the actual amounts listed in the NetCDF files were incorrectly listed in the 60-70 range. The results in Chapter V show there were clearly many more data assimilated per time step. The second exception is that fewer data were assimilated from the Ideal 720 grid than from the Ideal 360 grid. This suggests that GAIM-GM might reach data saturation even before observations are available for every model grid square, but future testing is needed to verify this assumption.

Table 20. Slant TEC measurements ingested by GAIM-GM per GPS ground station distribution. Note that slant TEC counts for the AFWA+400 distribution were not available in the GAIM-GM output. This table pertains to the modified GAIM-GM version that trusts data more

Time (UT)	CORS grids					Ideal grids			
	AFWA	+30	+100	+200	+400	21	90	360	720
1800	73	284	766	1458	–	130	549	2201	2031
1815	71	272	743	1417	–	125	524	2122	1984
1830	66	254	710	1370	–	119	499	2018	1798
1845	71	265	723	1397	–	119	510	2049	1860
1900	74	279	761	1469	–	128	538	2140	2042
1915	72	266	731	1411	–	127	525	2117	1972
1930	70	252	689	1318	–	115	497	1993	1644
1945	72	261	705	1342	–	123	517	2054	1733
2000	71	273	747	1422	–	130	535	2125	1865
2015	76	282	761	1446	–	129	544	2173	1905
2030	77	273	737	1398	–	129	533	2140	1908
2045	72	260	699	1329	–	123	512	2071	1869

Bibliography

- Baker, D. N., et al., The National Academic Press, Severe Space Weather Events – Understanding Societal and Economic Impacts Workshop Report, 2008.
- Coster, A., J. Foster, P. Erickson, and F. Rich, Regional GPS mapping of storm enhanced density, Proceedings of the 14th International Technical Meeting of the Satellite Division of The Institute of Navigation, 2001.
- Crustal Dynamics Data Information System, <http://cddis.nasa.gov>. 28 May, 2011.
- Dana, P. H., The geographer's craft project, Department of Geography, University of Colorado at Boulder, CO., <http://www.colorado.edu/geography/gcraft/notes/gps/gps.html>. 26 May, 2010.
- Decker, D. T., and L. F. McNamara, Validation of ionospheric weather predicted by Global Assimilation of Ionospheric Measurements (GAIM) model, *Radio Science*, 42, 2007.
- Duchon, C. E., Lanczos filtering in one and two dimensions, *Journal of Applied Meteorology*, 18, 1979.
- Dyrud, L., A. Jovancevic, A. Brown, D. Wilson, and S. Ganguly, Ionospheric measurement with GPS: Receiver techniques and methods, *Radio Science*, 43, 2008.
- Federal Aviation Administration, <http://www.faa.gov>. 22 June, 2011.
- Foster, J. C., Storm time plasma transport at middle and high latitudes, *Journal of Geophysical Research*, 98, 1993.
- Foster, J. C., P. J. Erickson, A. J. Coster, J. Goldstein, and F. J. Rich, Ionospheric signatures of plasma tails, *Geophysical Research Letters*, 29, 2002.
- Foster, J. C., A. J. Coster, P. J. Erickson, F. J. Rich, and B. R. Sandel, Stormtime observations of the flux of plasmaspheric ions to the dayside cusp/magnetopause, *Geophysical Research Letters*, 31, 2004.
- Foster, J. C., W. Rideout, B. Sandel, W. T. Forrester, and F. J. Rich, On the relationship of SAPS to storm-enhanced density, *Journal of Atmospheric and Solar-Terrestrial Physics*, 69, 2006.
- Foster, J. C., et al., Multiradar observations of the polar tongue of ionization, *Journal of Geophysical Research*, 110, 2005.
- Hyndman, R. J., and A. B. Koehler, Department of Econometrics and Business Statistics, Monash University, VIC, Australia, 2005.

- International Global Navigation Satellite System Service, <http://igsceb.jpl.nasa.gov>. 6 May, 2011.
- Jenniges, J., Sensitivity analysis of empirical parameters in the Ionosphere-Plasma-sphere Model, M. S. thesis, Air Force Institute of Technology, Wright-Patterson AFB, 2011.
- Kelley, M. C., M. N. Vlasov, J. C. Foster, and A. J. Coster, A quantitative explanation for the phenomenon known as storm-enhanced density, *Geophysical Research Letters*, *31*, 2004.
- Murphy, A. H., Skill scores based on the mean square error and their relationship to the correlation coefficient, *Monthly Weather Review*, *116*, 1988.
- National Geodetic Survey, <http://geodesy.noaa.gov/CORS>. 6 May, 2011.
- National Geophysical Data Center, <http://www.ngdc.noaa.gov>. 11 May, 2011.
- Nava, O. A., Analysis of plasma bubble signatures in the ionosphere, M. S. thesis, Air Force Institute of Technology, Wright-Patterson AFB, 2011.
- Ondoh, T., and K. Marubashi, *Science of Space Environment*, Ohmsha, Ltd., Chiyoda-ka, Tokyo, Japan, 2001.
- Perrone, L., and G. De Franceschi, Solar, ionospheric and geomagnetic indices, *Annali Di Geofisica*, *41*, 1998.
- Prolls, G. W., *Physics of the Earth's Space Environment*, Springer, Berlin, Germany, 2004.
- Reich, J. P., Air Force Weather Agency, Personal Correspondence, 2011.
- Rosen, N., WAAS Technical Memorandum, *Tech. Rep. DR 93*, William J. Hughes Technical Center, 2010.
- Scherliess, L., Development of a physics-based reduced state Kalman filter for the ionosphere, *Radio Science*, *39*, 2004.
- Scherliess, L., Utah State University, Logan UT, Personal Correspondence, 2011.
- Scherliess, L., R. W. Schunk, J. J. Sojka, D. C. Thompson, and L. Zhu, Utah State University Global Assimilation of Ionospheric Measurements Gauss-Markov Kalman Filter model of the ionosphere: Model description and validation, *Journal of Geophysical Research*, *111*, 2006.
- Schunk, R., and A. Nagy, *Ionospheres*, Cambridge University Press, Cambridge, UK, 2009.

- Schunk, R. W., and L. Scherliess, Global Assimilation of Ionospheric Measurements (GAIM), *Radio Science*, 39, 2004.
- Schunk, R. W., J. J. Sojka, and J. V. Eccles, Expanded Capabilities for the Ionospheric Forecast Model, *Tech. Rep. AFRL-VS-HA-TR-98-0001*, Air Force Research Laboratory, 1997.
- Schunk, R. W., L. Scherliess, and D. C. Thompson, Ionosphere data assimilation: Problems associated with missing physics, submitted to IAGA Book Aeronomy of the Earth's Atmosphere and Ionosphere, 2010.
- Sojka, J. J., D. C. Thompson, L. Scherliess, R. W. Schunk, and T. J. Harris, Assessing models for ionospheric weather specifications over Australia during the 2004 Climate and Weather of the Sun-Earth-System (CAWSES) campaign, *Journal of Geophysical Research*, 112, 2007.
- Space Environment Corporation, Ionospheric Forecast Model User Manual, 2002.
- Thompson, D. C., L. Scherliess, J. J. Sojka, and R. W. Schunk, The Utah State University Gauss-Markov Kalman filter of the ionosphere: The effect of slant TEC and electron density profile data on model fidelity, *Journal of Atmospheric and Solar-Terrestrial Physics*, 68, 2005.
- Thompson, D. C., L. Scherliess, J. J. Sojka, and R. W. Schunk, Plasmasphere and upper ionosphere contributions and corrections during the assimilation of GPS slant TEC, *Radio Science*, 44, 2009.
- U.S.–Canada Power System Outage Task Force, final Report on the August 14, 2003 Blackout in the United States and Canada: Causes and Recommendations, 2004.
- Zhu, L., R. W. Schunk, G. Jee, L. Scherliess, J. J. Sojka, and D. C. Thompson, Validation study of the Ionosphere Forecast Model using the TOPEX total electron content measurements, *Radio Science*, 41, 2006.

Vita

Captain Lindon Steadman was born in Murray, Utah. After graduating from Spanish Fork High School in 1998, he studied Meteorology at the University of Utah. He graduated with honors with a Bachelor of Science Degree in Meteorology in May 2005. At the same time, he commissioned into the United States Air Force as a distinguished graduate through the Reserve Officer Training Corps, Detachment 850, at the University of Utah.

Captain Steadman's initial assignment upon commissioning was to Euro-NATO Joint Jet Pilot Training at Sheppard AFB, TX. His second assignment was to the 15th Operational Weather Squadron in July 2006 where he served as Senior Duty Officer and then as Flight Commander. In January 2010, he entered the Graduate Applied Physics program, School of Engineering, Air Force Institute of Technology to obtain a Master's Degree in physics with a specialization in space weather. Upon graduation, Captain Steadman will be assigned to the 2nd Weather Squadron and serve at Detachment 2, the Sagamore Hill Radio Solar Observatory in Massachusetts.

REPORT DOCUMENTATION PAGE

Form Approved
OMB No. 0704-0188

The public reporting burden for this collection of information is estimated to average 1 hour per response, including the time for reviewing instructions, searching existing data sources, gathering and maintaining the data needed, and completing and reviewing the collection of information. Send comments regarding this burden estimate or any other aspect of this collection of information, including suggestions for reducing this burden to Department of Defense, Washington Headquarters Services, Directorate for Information Operations and Reports (0704-0188), 1215 Jefferson Davis Highway, Suite 1204, Arlington, VA 22202-4302. Respondents should be aware that notwithstanding any other provision of law, no person shall be subject to any penalty for failing to comply with a collection of information if it does not display a currently valid OMB control number. **PLEASE DO NOT RETURN YOUR FORM TO THE ABOVE ADDRESS.**

1. REPORT DATE (<i>DD-MM-YYYY</i>) 15-09-2011		2. REPORT TYPE Master's Thesis		3. DATES COVERED (<i>From — To</i>) Jan 2010 — Jul 2011	
4. TITLE AND SUBTITLE Effect of Storm Enhanced Densities on Geo-Location Accuracy Over CONUS				5a. CONTRACT NUMBER	
				5b. GRANT NUMBER	
				5c. PROGRAM ELEMENT NUMBER	
6. AUTHOR(S) Capt Lindon H. Steadman				5d. PROJECT NUMBER	
				5e. TASK NUMBER	
				5f. WORK UNIT NUMBER	
7. PERFORMING ORGANIZATION NAME(S) AND ADDRESS(ES) Air Force Institute of Technology Graduate School of Engineering and Management (AFIT/EN) 2950 Hobson Way WPAFB OH 45433-7765				8. PERFORMING ORGANIZATION REPORT NUMBER AFIT/GAP/ENP/11-S03	
9. SPONSORING / MONITORING AGENCY NAME(S) AND ADDRESS(ES) Air Force Weather Agency 101 Nelson Drive Offutt AFB, NE 68113 DSN 271-0690, COMM 402-294-0690 Email: 2syosdor@offutt.af.mil				10. SPONSOR/MONITOR'S ACRONYM(S) AFWA	
				11. SPONSOR/MONITOR'S REPORT NUMBER(S)	
12. DISTRIBUTION / AVAILABILITY STATEMENT APPROVED FOR PUBLIC RELEASE; DISTRIBUTION UNLIMITED.					
13. SUPPLEMENTARY NOTES					
14. ABSTRACT Storm enhanced densities (SEDs) are ionospheric plasma enhancements that disrupt radio communications in the near-Earth space environment, degrading the Global Positioning System (GPS) and other key technologies. Accurate GPS/total electron content (TEC) correction maps produced by ionosphere models can mitigate degradations from SEDs. An artificial SED was created and ingested via slant TEC measurements into the Global Assimilation of Ionospheric Measurements Gauss-Markov Kalman Filter Model to determine how many ground GPS receivers are needed to produce reliable GPS/TEC correction maps over the continental United States during geomagnetic storming. It was found that 110 well-positioned GPS receivers produced the best overall TEC accuracy, although significantly improved accuracy was still achieved if 40 or more receivers were used. Furthermore, receiver positioning had a greater impact on TEC accuracy than the number of receivers used. It was also found that TEC accuracy for the SED region increased at the expense of TEC accuracy everywhere else on the map.					
15. SUBJECT TERMS Ionosphere, Ionosphere Forecast Model, Global Assimilation of Ionospheric Measurements Gauss-Markov Kalman Filter Model, Space Weather					
16. SECURITY CLASSIFICATION OF:			17. LIMITATION OF ABSTRACT	18. NUMBER OF PAGES	19a. NAME OF RESPONSIBLE PERSON
a. REPORT	b. ABSTRACT	c. THIS PAGE			Lt Col Ariel O. Acebal, AFIT/ENP
U	U	U	U	112	19b. TELEPHONE NUMBER (<i>include area code</i>) (937) 255-3636, x4518; ariel.acebal@afit.edu